Na prawach rękopisu

POLITECHNIKA WROCŁAWSKA
WYDZIAŁ MECHANICZNO-ENERGETYCZNY

Raport serii PRE nr …./2019

Thermodynamic and technological optimization of complex cryogenic insulation systems

Valentina Venturi

Praca doktorska

Promotor: prof. dr hab. inż. Maciej Chorowski

Wrocław, 2019

Acknowledgements

I would like first of all to express my gratitude to doct Vittorio Parma, my CERN supervisor, and prof Chorowski for giving me the opportunity of spending these three years exploring a field new for me: especially Vittorio for his advices and assistance in keeping my progress on schedule in his CERN section and prof Chorowski for the academic support from Wroclaw University of Science and Technology. I would like to thank doct Torsten Koettig for his daily immense patience in the cryogenics laboratory at CERN and doct Jarolsaw Polinski for being my academic supervisor and precious guide as the person that could understand my position better than anyone else. Thanks to Luca Bottura, Miguel Jimenez and Michael Benedict for making this collaboration possibleand thanks to Philippe Lebrun and Laurent Tavian for their suggestions.
A big appreciation goes to all the CERN cryolab team also for the big patience, for the knowledge transferred to me and the good laughs: Johan Bremen, Laetitia Dufay-Chanat, Agostino Vacca, Patricia Borges de Sousa, Mario Xavier, Florian Noly, Jean-Luc Carpano, Sebastien Prune. A big thank to Jaakko Murtomäki for the moral and technical support during the PhD. A thank to Federico Zampolini, Claudio Kotnig and Ireneu Pla for the mathematical help, to Aleksander Kopczynski and Agnieszka Piotrowska for being my polish references, to Wesley Johnson for his precious tips on boil-off measurements. A thank goes to the Kindergarten officemates, and my colleagues, especially Alain Bastard, Edward Andrews, Arnaud Vand Craen and Yann Leclerq. Thank to Joanna Liberadzka and her multi functionality (cryogenics expert, Polish translator for this thesis) and the other Cernoises de l'Ambience: Anne-Laure Lamure (vacuum expert), Farah Hariri and Emelie Nilsson, which are my closest CERN friends. A big thank to Paola Catapano and Kassandra Klaritsch for helping me a lot in weak moments.
Grazie mille anche ai miei genitori Manu e Tino e la mia famiglia e amici in Italia.

Abstract

Future accelerators like the Future Circular Collider (FCC) [24] under study at CERN, will be considerably larger than the Large Hadron Collider (LHC) [18] presently in operation, with consequently increasing demands for cryogenically efficient cryostat solutions. With a cold mass surface exposed estimated to be five times higher than the one of LHC, the insulation solution of the cryostat will be critical for its operating costs. Multilayer Insulations Systems (MLI) remain the technology of choice for large accelerators. MLI are used in cryogenic or space application in presence of good vacuum and their main function is cutting radiation heat transfer. They are composed of several reflective layers made of a thin insulation material core and a reflective coating like aluminium. Layers are kept separated by low conductivity material spacers ensuring the minimum contact. MLI blankets offer a very good compromise between thermal performance and cost-effectiveness. Thermal design solutions for cryostats can employ different combinations of intermediate thermal shields operating at intermediate temperatures between the cold mass temperature and the ambient temperature, with optimally chosen MLI solutions. The temperature at which the thermal shield operates is the key parameter to determine the total power of refrigeration needed in the cryostat for the static heat loads. The total refrigeration power during operation is the sum of the cooling power of the thermal shield and the cooling power of the cold mass. This latter depends on the performances of MLI at different thermal screen temperatures. Data in literature is scarce though for MLI performance at 4.2 K when operating with a thermal shield kept between 60 K and 20 K. Therefore, a dedicated test program for the qualification of MLI samples was done at CERN, exploring different MLI configurations with a shielding radiative heat from $20 - 60$ K to 4.2 K and with residual gas pressures between 10^{-7} and 10^{-4} mbar. The experimental campaign on MLI performances was performed with a boil-off cryostat provided by Wroclaw University of Science and Technology. The system was previously used for experiments involving the temperature range $300 - 77$ K therefore it has been modified for a use with liquid helium. The blankets were prepared with an original methodology for the control of their layer density. This thesis work shows all the steps done for further optimizing the experimental set-up that brought to the measurement of different systems and all in different degraded vacuum conditions too. The mathematical approaches to predict the MLI performances and the optimization of the temperature of an active cooled screen for FCC are presented as well. The results of the experimental campaign show that MLI insulation performance does not improve significantly when the hot boundary is kept below $45 - 50$ K. The collected data is used in an exergy approach aiming at finding the minimum refrigeration power vs thermal screen temperature. The resulting optimal temperature for operating the thermal screen is found to be 53 K and the refrigeration power for the FCC cryostat corresponding to this point is 6 W/m.

Streszczenie

Przyszłe akceleratory, jak studiowany w CERNie Future Circular Collider (FCC) [24], będą znacząco większe niż obecnie działający Wielki Zderzacz Hadronów (ang. Large Hadron Collider - LHC [18]) z konsekwentnie rosnącymi potrzebami na efektywne kriogenicznie rozwiązania kriostatów. Pięć razy większa niż w LHC powierzchnia tzw. „zimnej masy", czyni izolację kriostatów krytycznym parametrem wpływającym na koszty eksploatacji. Superizolacja (ang. Multilayer Insulation Systems - MLI), czyli system izolacji wielowarstwowej, pozostaje najczęściej wybieraną technologią w przypadku dużych akceleratorów. Jest używana w kriogenice i przestrzeni kosmicznej, gdzie jej główną funkcją jest znaczące ograniczenie wymiany ciepła przez promieniowanie w wysokiej próżni. MLI składa się z od kilku do kilkudziesięciu cienkich warstw izolującego materiału pokrytego wysoce refleksyjnym aluminium. Materiał oddzielający warstwy aluminium ma możliwie niską przewodność termiczną, ograniczającą wymianę ciepła pomiędzy warstwami. Technologia MLI stanowi dobre optimum wydajności termicznej i nakładów finansowych. Projekty kriostatów mogą zawierać różne warianty ekranów radiacyjnych o temperaturach pomiędzy temperaturą pokojową, a temperaturą zimnej masy, z optymalnie dobraną izolacją wielowarstwową. Temperatura ekranu radiacyjnego jest kluczowym parametrem determinującym moc chłodzenia w stanie ustalonym. Całkowita moc chłodzenia kriostatu jest sumą mocy koniecznej do utrzymania ekranu w ustalonej temperaturze oraz mocy koniecznej do schłodzenia zimnej masy, która z kolei zależy od skuteczności MLI na ekranie. W literaturze fachowej niewiele jest badań opisujących efektywność zastosowania MLI na ekranie o temperaturze w przedziale od 20 K do 60 K, przy temperaturze zimnej masy 4.2 K. Z tego powodu w CERNie stworzony został program kwalifikacji izolacji wielowarstwowej MLI w różnych konfiguracjach, ograniczających promieniowanie cieplne między ekranem o temperaturze $20\,\mathrm{K} - 60\,\mathrm{K}$ a zimną masą o temperaturze 4.2 K w próżni degradowanej od 10^{-7} mbar do 10^{-4} mbar. Badania zostały przeprowadzone w CERNie na kriostacie zapewnionym przez Politechnikę Wrocławską. Kriostat ten, uprzednio zaprojektowany dla temperatur $77 - 300\,\mathrm{K}$, został zmodyfikowany do pracy w temperaturze ciekłego helu. Płachty MLI przygotowano zgodnie z oryginalną metodologią dla kontrolowanej gęstości warstw. Niniejsza praca pokazuje wszystkie kroki modyfikacji stanowiska eksperymentalnego wykonane w celu przeprowadzenia pomiarów różnych konfiguracji MLI przy różnych ciśnieniach gazu rezydualnego, jak również podstawy modelu matematycznego zbudowanego do oszacowania efektywności MLI oraz optymalizacji temperatury aktywnie chłodzonego ekranu dla FCC. Wyniki kampanii pomiarowej pokazują, że skuteczność MLI nie poprawia się znacząco gdy cieplejsza ze stron ma temperaturę niższą niż $45 - 50\,\mathrm{K}$. Zebrane dane są używane w celu egzergetycznego oszacowania minimalnej mocy chłodzenia dla FCC w funkcji temperatury ekranu termicznego. Wynikająca z powyższego oszacowania optymalna temperatura ekranu jest równa 53 K, a odpowiadająca jej moc chłodzenia wynosi $6\,\mathrm{W/m}$.

Contents

List of Figures

List of Tables

1 Introduction

1.1 Cryogenics in the LHC and Future Circular Collider

Cryogenics and its applications are a growing industry, its use has grown in several fields like aerospace, medical for example in MRI imaging, fuel transport and storage, food transport, material technologies and accelerators. The need of optimization of thermal insulation systems is very important for the thermodynamic cost of low-temperature refrigeration especially when considering large scale applications.

The Large Hadron Collider (LHC) at CERN is a 27 km long machine cooled down at 1.8 K. It allows scientist to do a large number of discoveries in particle physics by colliding particles with energies up to 14 TeV. Besides the aim of the research, many innovative technologies are being developed during the years in order to achieve the construction and operation of accelerators. on its trajectory is through electric and magnetic fields mainly by using radio-frequency cavities and electromagnets. Particle like protons are kept inside an evacuated pipe and accelerated in either linear or circular accelerators. The need of very high electric and magnetic fields requires the use of super conductive materials, materials which at a certain temperature loose their DC electrical resistivity and allow for very low losses. The first observation in superconductivity was performed by the Dutch physicist H. K. Onnes [23] during some experiments with mercury in 1911. Nowadays the most used superconductive material in LHC magnets is the Niobium-Titanium alloy and it is present in many parts of the accelerator. The most numerous big component of the LHC are dipole magnets, able to keep the particle beam in circular orbit by means of a 8.3 or 8.6 T bending magnetic field applied on it. The so-called critical surfaces of a superconductor defining the limit temperature, current density and magnetic field for which the material behaves as a superconductor, is shown for Niobium Titanium (NbTi)in figure 1. It is possible to see that the material show superconductivity below 10 K. The coil can be operated with certain limits of current density and magnetic field in order to remain in superconductive state. In order to achieve the required low temperatures the magnets are kept in a bath of helium in superfluid state at 1.9 K for the whole length. Other cryogenic systems are present in a typical cross section of the collider such as a cooled thermal shield, to avoid direct thermal radiation from ambient, kept at an optimal level of temperature. A cooled beam pipe, the beam screen, which is protecting the cold mass from the dynamic heat loads coming from the beam presence and the current-lead cooling system is transferring the electric power to the magnet from ambient to cold temperatures.

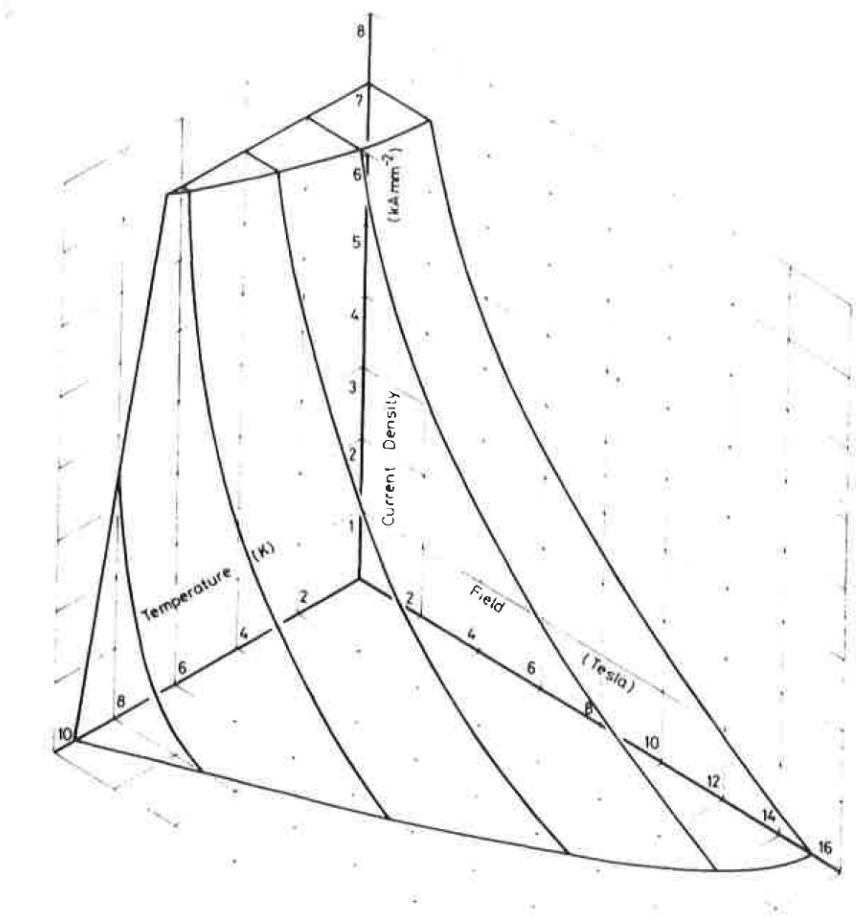

Figure 1: Critical surface for Niobium-Titanium showing the boundary in 3D between the normal conductivity and the superconductivity of the material. [21]

The cryogenic distribution system of a circular collider is shown in figure 2, [15]. Colliders are normally build underground because of the big irradiations created during operation and in order to be as far away from noises caused by human presence.

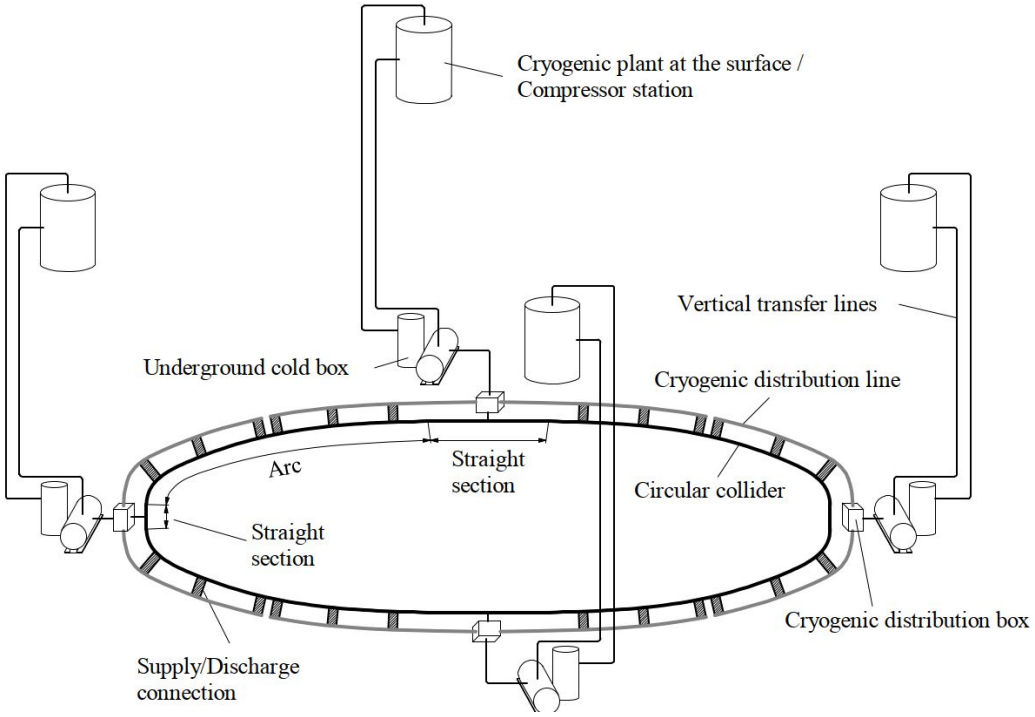

Figure 2: General cryogenic distibution system for a collider [15]

In order to extend the research conducted with the LHC, scientist are working on a new bigger collider, measuring 100 km circumference, the Future Circular Collider (FCC), where more powerful magnets will allow for collision energies in the order of 100 TeV, much higher than the current 14 TeV reached with LHC. The FCC will further accelerate beams coming from LHC, see figure 3.

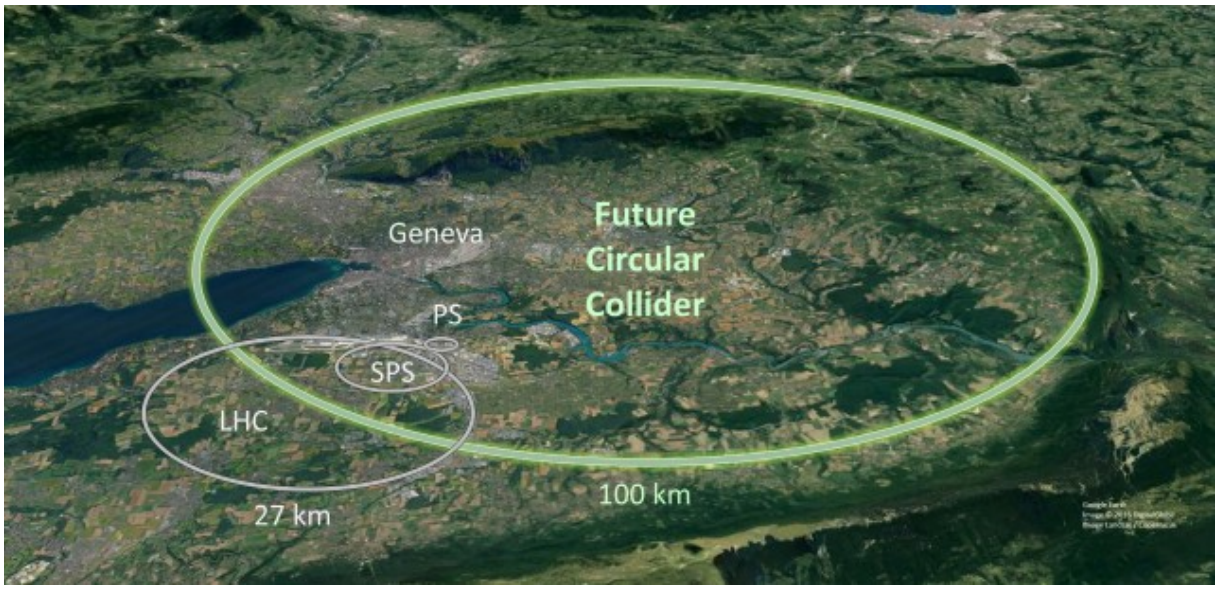

Figure 3: The Future Circular Collider in the context of CERN accelerator complex, CERN picture

The general configuration of the FCC is shown in figure 4: the cryogenic distribution system with the 10 plants covering the whole 100 km. Each plant provides the cryogenics for one of the eight long sectors (around 10 km long) or for two of the four short sectors (around 6 km long). The single sectors can contain 79 (long sector) or 37 (short sector) half cells. The typical half cell structure is shown in figure 5.

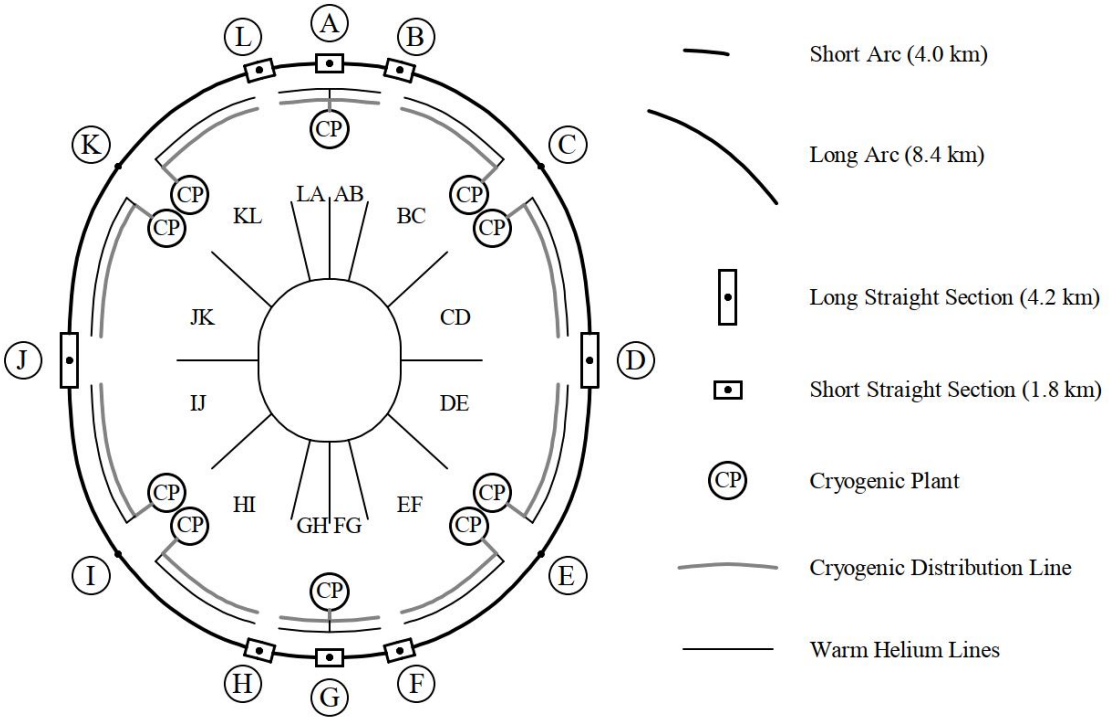

Figure 4: FCC cryogenic layout [15]

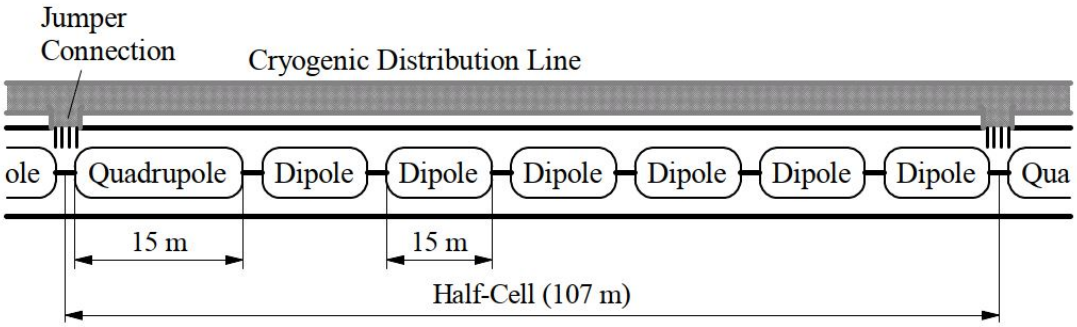

Figure 5: Schematics of the FCC hal cell layout [15]

The dipoles are the most numerous components of the collider, in LHC there were 1232 units. Being the LHC's dipole design very satisfactory, it was decided to start the design of the FCC cryostat from a similar baseline for FCC.

1.2 Dipole configuration for LHC and FCC

The cross section of a dipole magnet of the LHC is shown in figure 6. In the center of the structures there are two beam pipes, kept at very high vacuum in the order of 10^{-10} mbar, allowing for the beam not to interact with any particle. Inside the pipe is the beam screen, kept at $4.5 - 20\,\mathrm{K}$. The beam pipe is surrounded by the niobium titanium coils. Non-magnetic collars around the coils keep them in position during operation. Outside there is an iron yokes. The whole structure described is called cold mass and it is immersed in a bath of pressurized superfluid helium at 1.9 K.

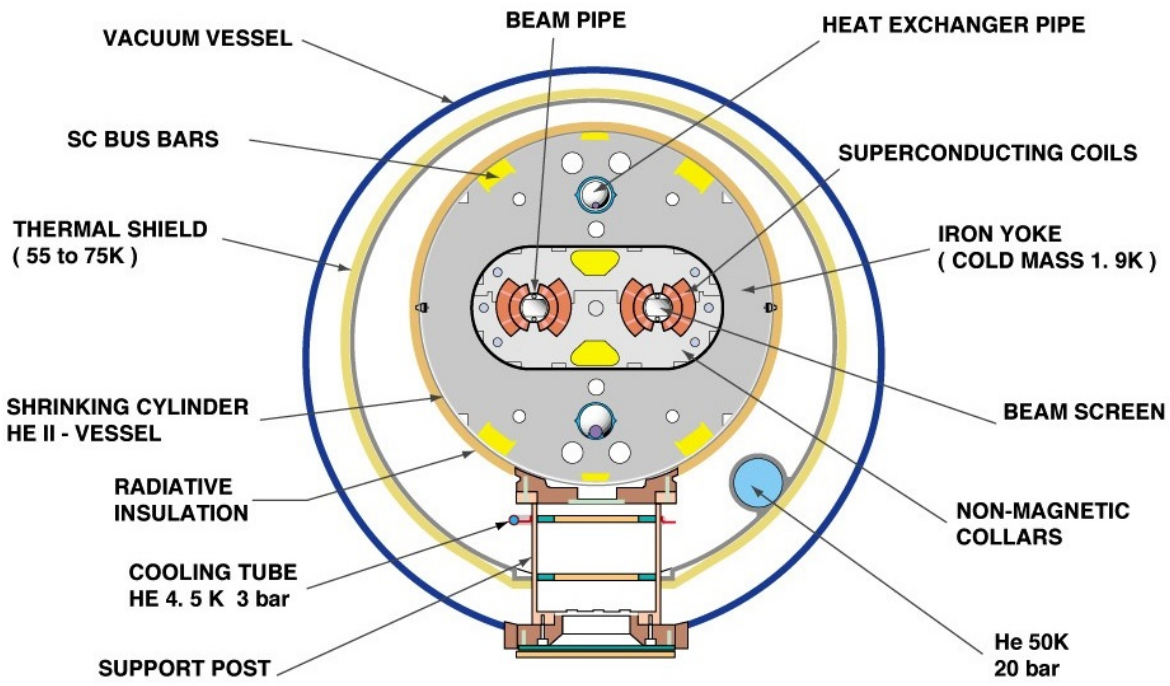

Figure 6: Cross section of a LHC dipole magnet showing the cold mass kept at 1.9 K including the beam pipes, the coils and the yokes; the thermal shield cooled by gaseous helium at 50 K, the vacuum vessel; the support post made of G10 and thermally in contact with the thermal shield and a helium tube kept at 4.5 K to minimize solid conduction [4].

Superfluid helium shows a peak of heat capacity at its superfluid transition temperature and a very low viscosity allowing for a very efficient heat transfer and thermal stability. The heat is extracted through a heat exchanger pipe on the top of the coils containing saturated helium at 1.86 K.
The cold mass just described has to be well insulated from room temperature for high efforts to be made for helium refrigeration at 1.8 K. The way this is done is through a vacuum vessel where convection is minimize and one intermediate stage where heat is intercepted at a temperature of 50 K through an aluminium shield. The aluminium shield and the cold mass are thermally protected with a series of aluminized reflective foils called Multi-Layer Insulation (MLI).

The schematics of the typical LHC dipole cooling system is shown in figure 7.

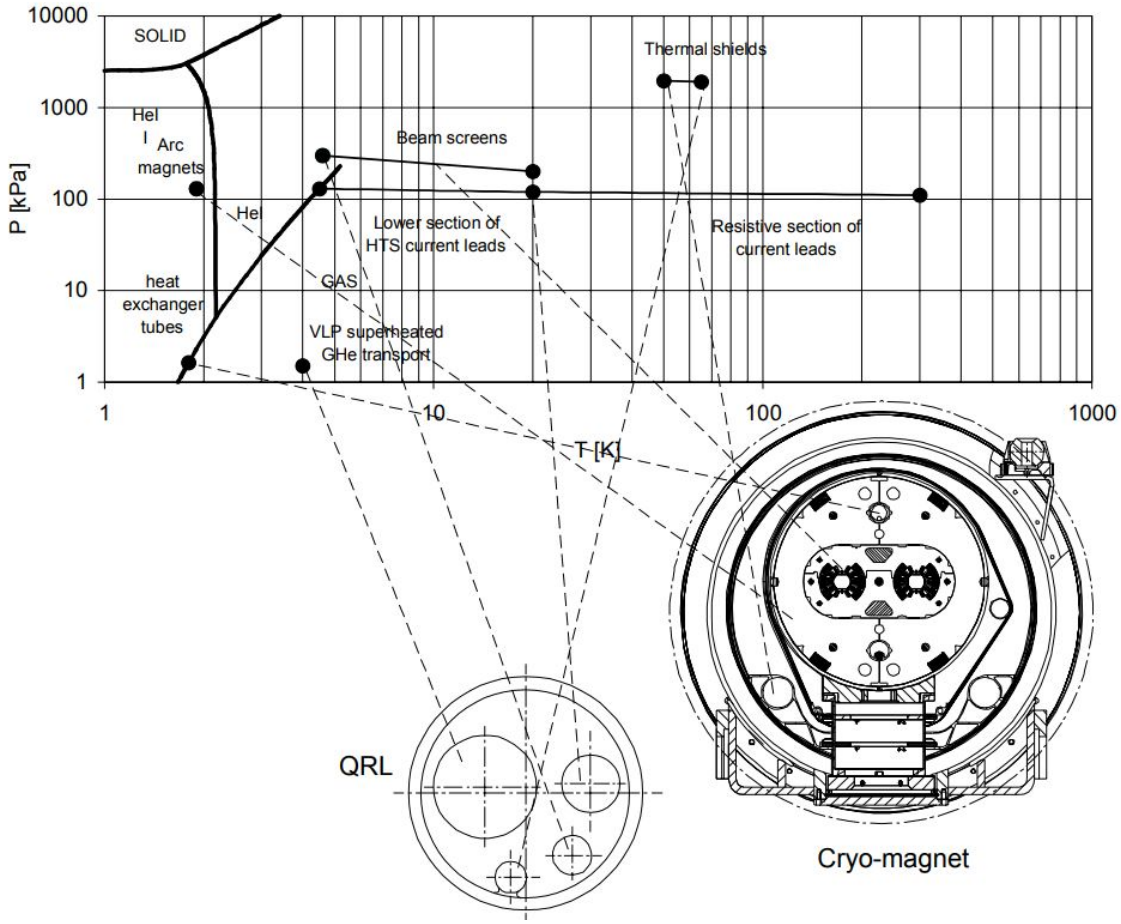

Figure 7: Thermodynamic state of helium in LHC cryogenics system [22]

The possibility of placing a second thermal screen between the screen at $50-70\,\mathrm{K}$ and the cold mass in order to further reduce the heat flux to the cold mass Ihas been investigated in the past [25]. After a technical-economic analysis based on numerical parameters drawn from the existing data of the LHC and a simplified numerical model on heat transfer, it was concluded that a thermal screen at $4.5\,\mathrm{K}$ would be un-economical for the LHC operating conditions on a period of operation of ten years. The literature is in fact scarce when such a model has to be built because the heat transfer performances from the thermal shield at 40-60 K to the cold mass were not yet measured at the time LHC was being designed.

Concerning FCC dipole cryostat, a possible configuration of the cross section is shown in figure 8. The configuration is very similar to the LHC with one main difference: the cooling circuit for the beam screen is kept at $40-60\,\mathrm{K}$, which makes it possible to unify it with the shield cooling. Helium flows at $50\,\mathrm{bar}$, a choice due to the limited size of the supply and return lines respecting the increased arch length and the very big refrigeration capacities for the system beam-screen thermal-shield.

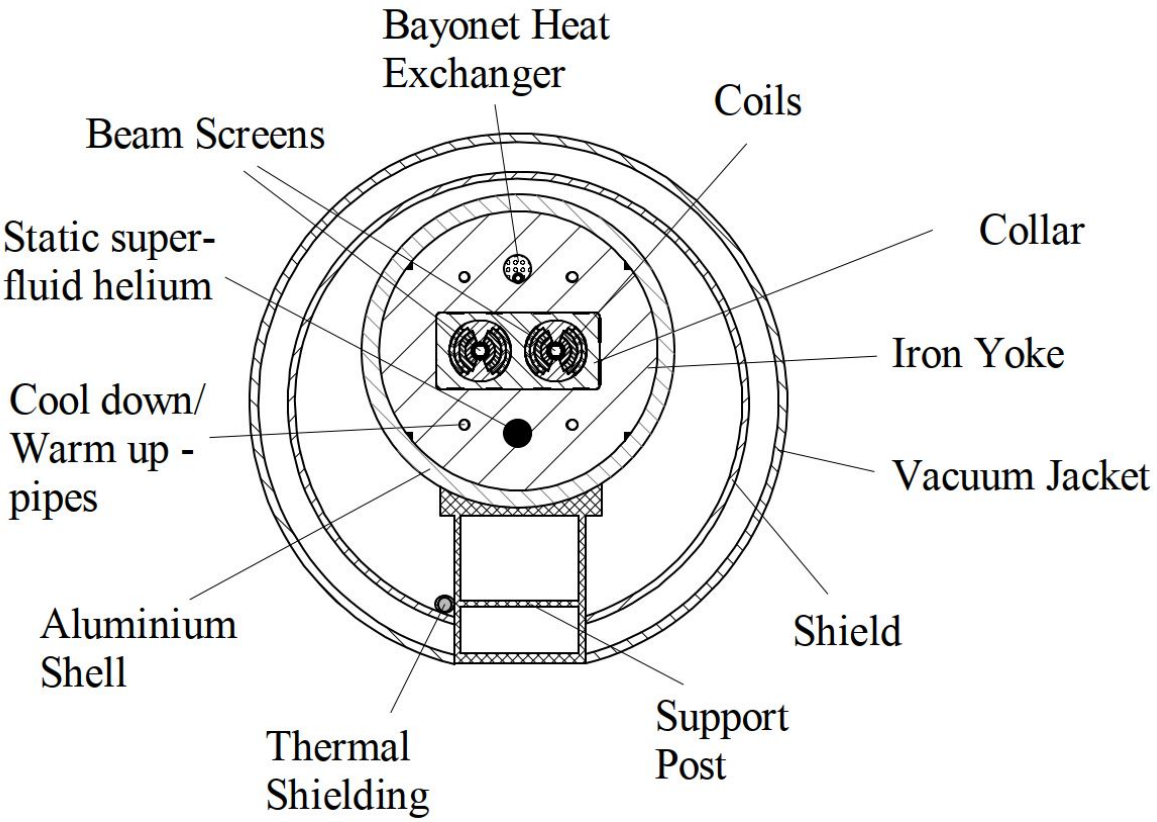

Figure 8: Schematics of the Future Circular Collider cryostat preliminary design [15]

1.3 Motivations

When comparing the expected thermal performances of the FCC with the ones of LHC per linear meter it is possible to realize that the static heat loads on the cold mass are 3 times higher: 0.84 W/m compared to the 0.28 W/m, see Table 1 [20], [15]. Considering then the length of the two colliders, the total heat results in 9 times higher for the 100 km long ring.

Property	**HERA**	**TEVATRON**	**LHC**	**FCC**
Centre-of-mass energy	0.95 TeV	2 TeV	14 TeV	100 TeV
Circumference	6.3 km	6.5 km	27 km	100 km
Static heat loads (including distribution)	2.24 W/m @ 40 - 80 K	2.15 W/m @ 85 - 90 K	5.5 W/m @ 50 - 75 K	9.3 W/m @ 57 - 61 K
	0.17 W/m @ 4.4 K	0.14 W/m @ 4.6 K	0.085 W/m @ 4.6 - 20 K	–
	–	–	0.28 W/m @ 1.9 K	0.84 W/m @ 1.9 K
Dynamic heat loads	0.14 W/m @ 4.4 K	0.11 W/m @ 4.6 K	0.7 W/m @ 4.6 - 20 K	62.2 W/m @ 40 - 57 K
	–	–	0.15 W/m @ 1.9 K	0.8 W/m @ 1.9 K
Minimal required cooling power (Carnot)	0.19 MW	0.14 MW	2.88 MW	60.42 MW
Ratio of minimal required cooling powers to extract dynamic heat loads and to extract static heat loads	0.46	0.50	0.60	2.95

Table 1: Heat load estimation for FCC cryostats and comparison with LHC

The static heat load on the cold mass comes from the support posts and the external ambient temperature. Understanding how to improve the design of the insulation system to reduce the thermal heat load coming from the external ambient is the aim of this work. The need of an optimization of the insulation is a must for a project of such dimensions. The approach is done by considering the configuration of the main dipole cryostat with a single thermal screen, the solution adopted for the LHC, and the total exergy produced which should be minimized [38]. Considering the schematics in figure 9, the total exergy ΔE is the sum of the one correlated to the cold mass and the one correlated to the thermal screen in ideal refrigeration, see equation (1.3.1) and (1.3.2):

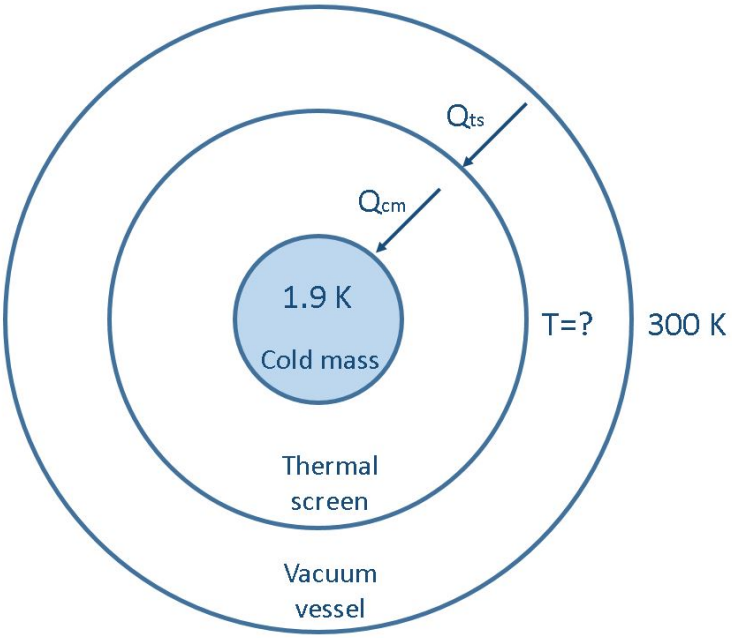

Figure 9: Schematics of head load coming from the external ambient to the thermal screen and from thermal screen to the cold mass

$$\Delta E = \Delta E_{ts} + \Delta E_{cm} \tag{1.3.1}$$

$$\Delta E = (Q_{ts} - Q_{cm}) \cdot (\frac{T_{amb}}{T_{cm}} - 1) + Q_{cm} \cdot (\frac{T_a}{T_{ts}} - 1) \tag{1.3.2}$$

The real refrigeration electrical power needed is higher than the total exergy of the system, see equations (1.3.3) and (1.3.4):

$$P_{ref} = \frac{\Delta E}{\eta(T)} \tag{1.3.3}$$

$$\eta(T) = \frac{COP_{Carnot}}{COP_{Real}} \tag{1.3.4}$$

where $\eta(T)$ is the efficiency with relation to Carnot. The COP_{real} is the coefficient of performance, indicator of the efficiency of the refrigerator system, defined by the ratio between the cold capacity to the driving power. Its value is normally lower than the Carnot efficiency, the COP_{Carnot}, defined as the ratio between the cooling power and the ideal driving power using the Carnot equation.

The total refrigeration power for the static loads found can be described by equation (1.3.5):

$$P_{ref} = Q_{cm} \cdot (\frac{T_{ts}}{T_{cm}} - 1) \cdot \frac{1}{\eta_{cm}(T_{cm})} + Q_{ts} \cdot (\frac{T_{amb}}{T_{ts}} - 1) \cdot \frac{1}{\eta_{ts}(T_{ts})} \tag{1.3.5}$$

Where P_{ref} is the total refrigeration power in W needed in steady state per linear meter of cryostat. Q_{cm} is the heat to be extracted from the cold mass at 1.9 K in Watts and it depends on the temperature of the thermal screen and its infrared properties, the quality of the vacuum and the efficiency of the insulation system protecting the cold mass. The value of Q_{cm} for different outer boundary temperatures is mostly estimated and it's difficult to find experiments done in order to find its value for outer temperatures below 77 K. The main work of the thesis is to find the values by conducting a series of experiments to complete the thermal model on MLI performances at low temperatures. T_{ts} is the temperature of the thermal screen in KK and T_{cm} is the temperature of the cold mass in K, and η_{cm} is the efficiency with respect to the Carnot efficiency for cooling down helium at 1.9 K. The second term of the equation considers the power Q_{ts} to be extracted from the thermal screen in Watts where T_{amb} is the ambient temperature in K, and η_{ts} is the s the efficiency with respect to the Carnot efficiency for cooling down helium at the temperature T.

For the 1.9 K and 40 K temperature evels, values for η_{cm} and η_{ts} equal to 0.18 and 0.42 are respectively considered in FCC cryogenic studies [15], [11], [31].
For the 4.2 K, another interesting working point (liquid helium at ambient pressure) the efficiency with respect to the Carnot efficiency was measured to be 0.27, [32].

In figure 10 some data are collected for the real efficiency of refrigerators at different temperatures [28].

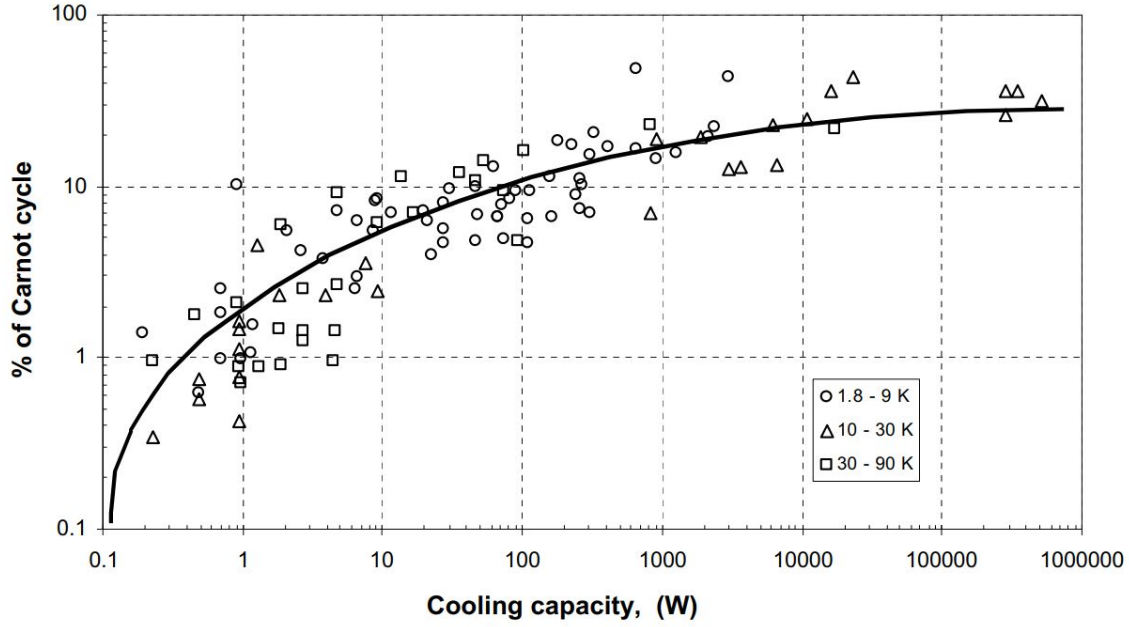

Figure 10: Real efficiency for cryogenic coolers

1.4 Multilayer Insulation Systems

1.4.1 General description

MLI systems (figure 11 and 12) are formed by blankets of several reflective layers kept separated by a low density thermal insulation material. They are the most efficient insulations in cryogenic applications and they are widely since decades in very low temperatures applications. MLI systems are still considered one of the best choice among other kind of insulation systems in high vacuum, see figure 13.

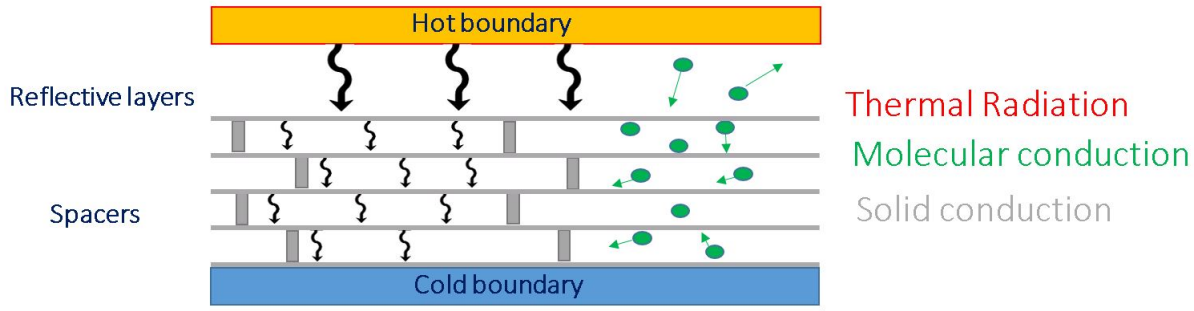

Figure 11: Schematics of a multilayer insulation systems: MLI is paced around the cold part to protect it from external heat. At low temperatures vacuum is used and the heat is transferred through thermal radiation, residual molecular conduction and solid conduction through the spacers.

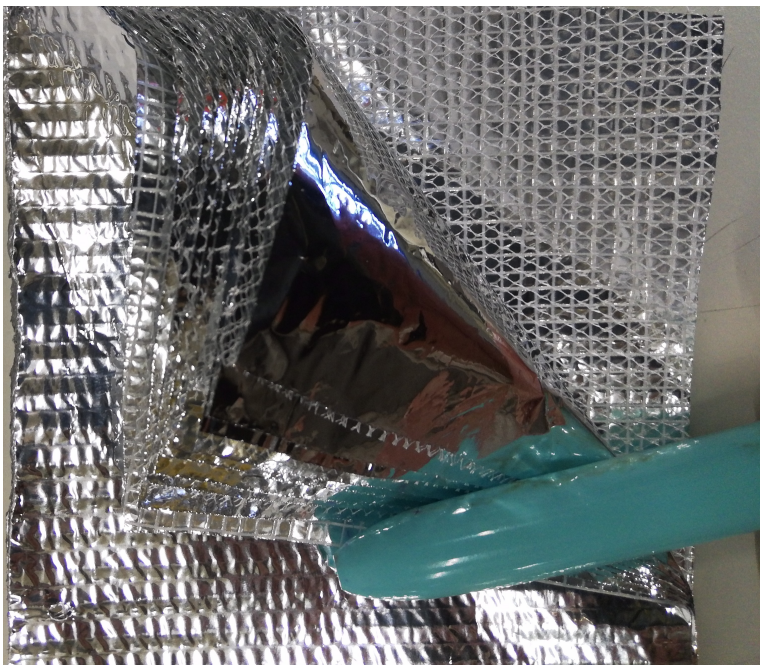

Figure 12: Example of MLI system: the reflective layers of aluminized Mylar®are interleaved by a net of polyester spacer. Typically the layers number in a blanket are from 10 to 30

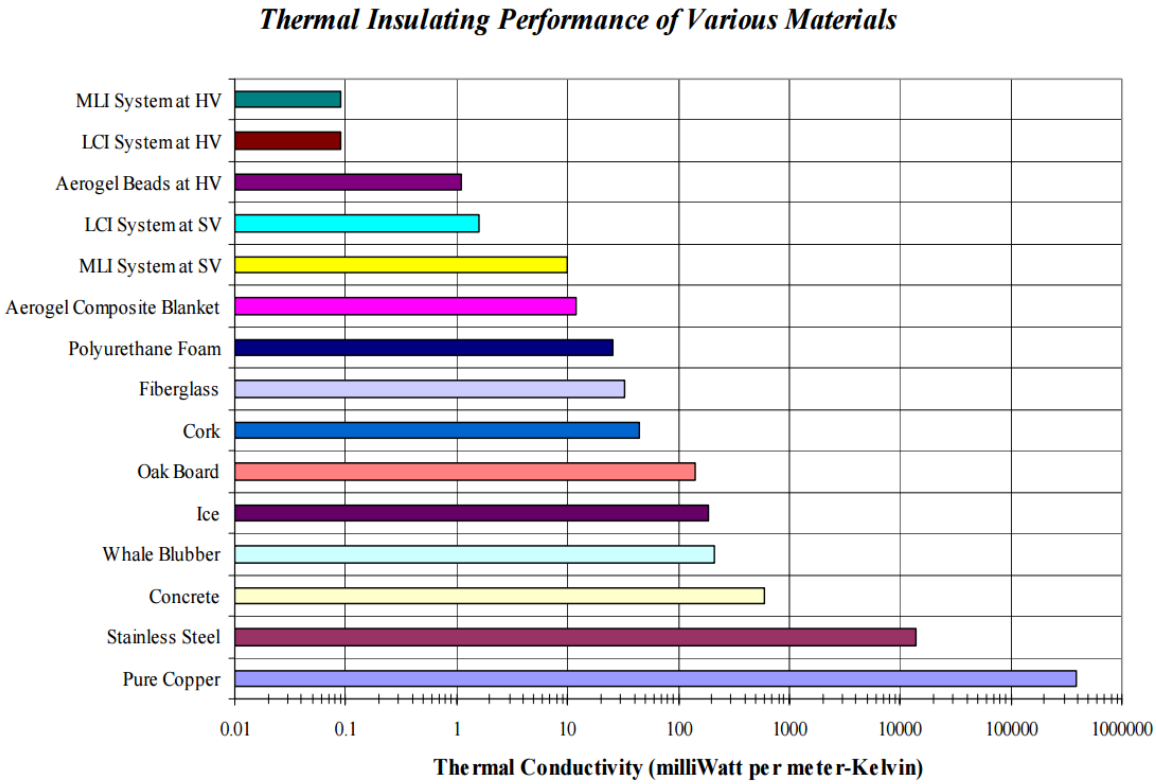

Figure 13: Thermal conductivities of various materials: MLI systems in high vacuum show the best insulation performances [14].

Compared to other insulation systems, the MLI found a wide application not only for their outstanding performances but also because it is very versatile and easy to be used.

MLI used at CERN for the LHC are composed of highly reflective thin layers made of a 6 μm thick Mylar foil coated by physical vapour deposition with a thin aluminium film (400 Å). Layers are kept separated by spacers of low conductivity material (polyester net). In order to get the best performance from an insulation system and minimize all the type of residual heat transfer, it is necessary to create a vacuum to eliminate as much as possible convection. The gas molecules escape the MLI blankets through small holes produced in the layers. Being not possible to create a perfect vacuum a part of the heat transfer will remain, due to the presence of residual molecules. The residual gas molecular conduction becomes important in MLI because the distance between the layers is usually comparable with the mean free path of the gas molecules. It will be shown analytically in chapter 1.4.2, that for n reflective layers with the same emissivity parallel to each other and to the heat flux the heat transfer through radiation in the system is ideally reduced to a factor of N+1. By adding layers though, the heat transfer starts to increase because the layers need to be kept separate by spacers, and the solid conduction at some number of layers starts to prevail. Some nets of low thermal conductivity material are used as spacers. The most used are polyester nets, glassfiber or silk. Despite they are scrims, they represent a thermal bridge and the major cause of heat inleaks in application such

as the LHC cryostats, where the high vacuum allows for low molecular conductions.

1.4.2 Heat transfer through MLI

MLI systems are normally used to protect low temperature objects already in a vacuum environment. Above a certain limit of vacuum, typically 10^{-5} mbar , molecular conduction starts to play a role in heat transfer. Being made by low emissivity reflective layers, the MLI objective is the one of cutting thermal radiation heat transfer as much as possible. Thermal radiation for ideally perfect emissive layers with no transmittance, is reduced by N-1 times, where N is the number of layers. The layers should not touch each other in order to avoid conduction at interfaces. The best solution found up to now is the use of spacers made of low density materials like glass fiber foils or polyester tulle.

1.4.3 Conduction through the MLI spacers

Inside the MLI the contribution of the solid conduction through the spacers in contact with the reflective layers has to be considered. This latter can be described by Fouriers law, see equation (1.4.1).

$$\dot{q} = -k \cdot A \cdot \nabla T \tag{1.4.1}$$

Where $\dot{q}$ is the local heat flux density in W/m^2, k is the thermal conductivity in W/(mK), A is the cross sectional area of contact between spaces and reflective layers in m^2 and ∇ T is the thermal gradient in K/m. Despite the heat by conduction is easy to be described in a mathematical formulation, in MLI application it is very difficult to determine its value because of the difficulty in determine the thermal contact between the layers and the spacers, the complex geometry of the spacers and the temperature of each layer. Many mathematical models are reported in literature aiming at predicting the conduction through MLI, some are described in chapter 1.5.4.

1.4.4 Radiant heat transfer

Radiation heat transfer takes place by means of electromagnetic radiation energy emitted by bodies because of their temperature. The energy is emitted because of the electronic changes in electronic configurations of atoms or molecules and the energy varies with the wavelength. The thermal radiation takes places at a wavelength between 10^{-1} and 100 μm. This range includes part of UV, full range of visible light and infra-red region in the electromagnetic spectrum.

A black body is an ideal body that absorbs all incident radiation and does not reflect it, a perfect emitter. It is convenient to introduce this kind of body as a reference for real bodies. For each temperature of a black body, the heat emitted in $W/(m^2\mu m)$ can be plotted versus wavelength and it follows a Plank law (1.4.2), see figure 14.

$$E_{b\lambda} = \frac{C_1}{\lambda^5 \cdot (exp\frac{C_2}{\lambda \cdot T} - 1)} \tag{1.4.2}$$

Where C_1 and C_2 are constants, λ is a particular wave length of the emissive spectrum.

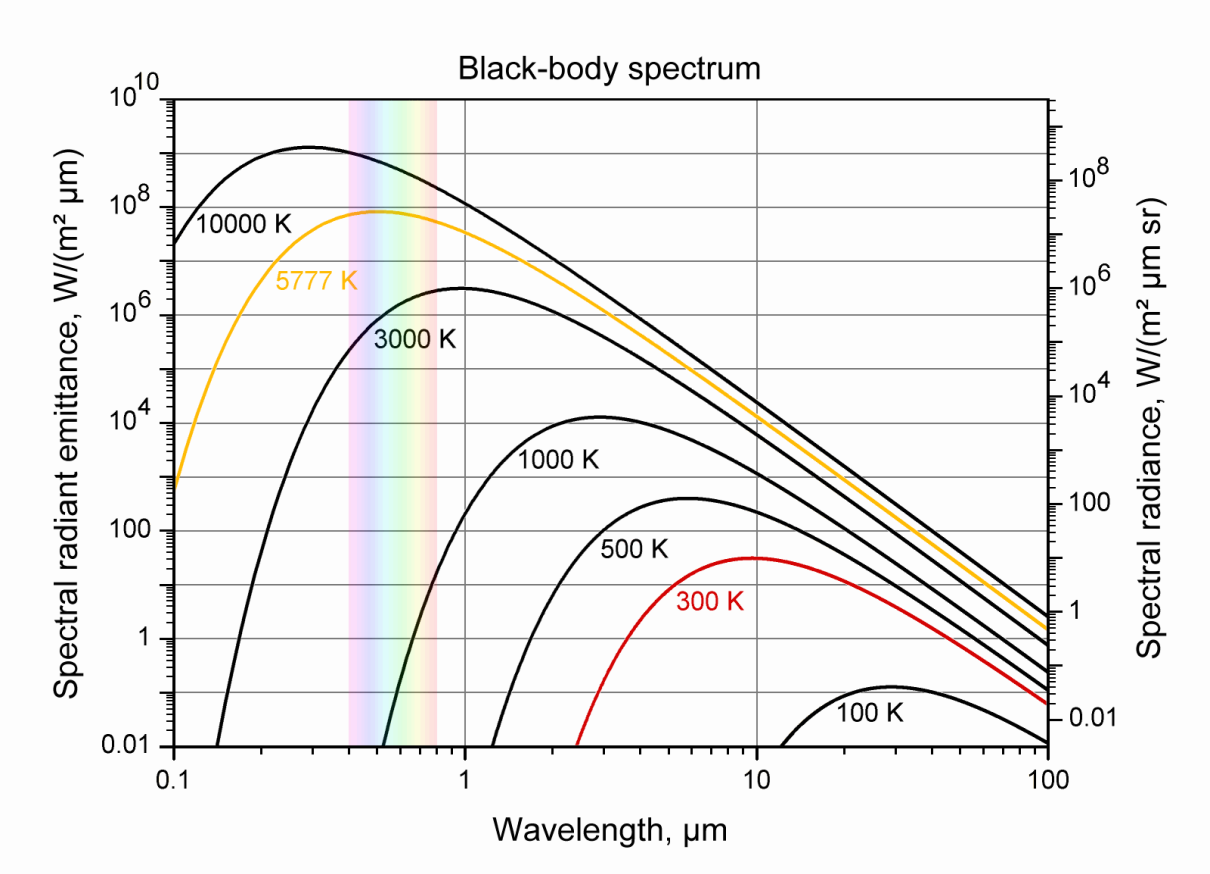

Figure 14: Black-body spectrum for temperatures between 300 K and 10000 K [43]

If integrating Plank's equation from zero to infinite, the total power per squared meter emitted by the black body is found. The integration results in a simple formula called Stefan-Boltzmann law, see equation (1.4.3)

$$E_b = \sigma \cdot T^4 \tag{1.4.3}$$

Where E_b is the spectral black body emissive power for all the spectrum per m^2 and σ is the Stefan-Boltzmann constant equal to 6.67^{-8} $Wm^{-2}K^{-4}$.

A real body does not behave like a black body because only a fraction of its energy is emitted, the property called emissivity, varying from zero to 1, is important for thermal application in vacuum.

When incident electromagnetic radiation intercepts a real body, part of the energy is reflected, part of it is transmitted and part of it is absorbed (while for the black body all

of it is absorbed). Reflectivity, absorptivity and transmittivity are material properties dependent on the body temperature and, ranging from 0 to 1. Their sum is equal to 1.

A type of body that can approximate reality is called a grey body. This particular body is defined as a body whose absorptivity doesn't vary with temperature or wavelength of incident radiation. Thermal radiation problems can be addressed as electrical analogy. When energy balance is done between two surfaces, the geometrical configuration of the surfaces plays an important role. The way this can be taken into account is defined as the viewing factor. The viewing factor F_{12} is the fraction of energy exiting an isothermal surface 1 that impinges directly on surface 2. The viewing factor is calculated considering figure 15.

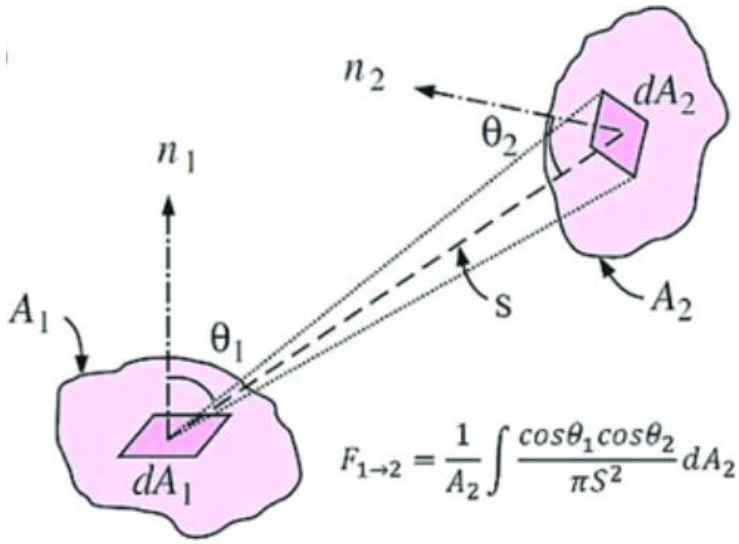

Figure 15: Viewing factor definition [37].

If considering two infinite parallel surfaces the viewing factor equals to 1. The thermal radiation energy balance between these two can be described by equation (1.4.4).

$$\dot{q_{12}} = \frac{\sigma \cdot A \cdot (T_1^4 - T_2^4)}{\frac{1}{\epsilon_1} + \frac{1}{\epsilon_2} - 1} \tag{1.4.4}$$

Where $\dot{q_{12}}$ is the heat flux in W/m^2, σ is the Stefan Boltzmanns constant, T_1 and T_2 are the temperature of the two surfaces and ϵ_1 and ϵ_2 are the emissivities of the two surfaces.

If in between the two surfaces N layers of same emissivity are placed, the model describing the radiation heat transfer can be reduced to equation (1.4.5):

$$\dot{q_{12}} = \frac{\sigma \cdot A \cdot (T_1^4 - T_2^4)}{(\frac{1}{\epsilon_1} + \frac{1}{\epsilon_2} - 1)(N+1)} \tag{1.4.5}$$

1.4.5 Gas conduction

The gas trapped in the MLI blankets could play a big role in the heat exchange above a certain level. Residual gas conduction, can be described by different models for different regimes of the flow [36]. The viscous regime appears when the mean free path λ of the molecules (average distance travelled by a molecule between collisions) is much smaller than the distance between the two surfaces it travels from and to. In this case the gas can be considered as a media with certain conductivity and the heat transfer does not depend on the pressure. In the other case the molecules bounce directly between the objects and the regime is called molecular conduction. A transition regime is present when the ratio between the mean free path and the characteristic length of the system, also called Knudsen number) is between 0.01 and 1.

The mean free path is described by equation (1.4.6):

$$\lambda = \frac{k \cdot T}{\sqrt{2} \cdot d^2 \cdot \pi \cdot P} \tag{1.4.6}$$

Where k is the Boltzmann constant equal to 1.380649^{-23} J/K, T is the temperature of the gas in K, d is the diameter of the particles in m and P is the gas pressure in Pa.

In molecular regime, for parallel surfaces, the heat flux by gas conduction can be described as in equation (1.4.7):

$$\dot{q} = \frac{\alpha_0}{4} \cdot \frac{\gamma + 1}{\gamma - 1} \cdot (\frac{2R}{\pi MT})^{\frac{1}{2}} \cdot p \cdot (T_2 - T_1) \tag{1.4.7}$$

Where α_0 is an averaged accommodation coefficient, which is normally used in absence of detailed gas-surface interaction models. It is a measure of the efficiency of the thermal energy interchange occurring when a particle hits a surface. It can be expressed as the combination of the accommodation coefficient describing the molecules-wall energy exchange and the surface area affected. In case there are different values of areas and accommodation coefficients, α_0 can be described as the average of the two coefficients α_1 and α_2 see equation (1.4.8), γ is the ratio of specific heats for helium gas in kJ $kg^{-1}K^{-1}$, R is the universal gas constant in J/mol, M is the molecular mass in kg/mol, p the pressure in Pa. α is the accommodation coefficient which depends on gas species, on the temperature and the geometry of the surfaces A_1 and A_2 [36].

$$\alpha_0 = \frac{\alpha_1 \cdot \alpha_2}{\alpha_1 + \alpha_2 \cdot (1 - \alpha_2) \cdot \frac{A_1}{A_2}} \tag{1.4.8}$$

α_1 and α_2 are dependent on the temperature of the gas.

where α is described in equation (1.4.9):

$$\alpha = \frac{T_i - T_e}{T_i - T_w} \tag{1.4.9}$$

where T_i is the temperature in K of the incident molecule, T_e the temperature in K of the emitted or reflected molecule, and T_w is the temperature in K of the wall.

As the temperature of the molecule is very difficult to be determined, an approximate expression can be used for the accomodation coefficient [10] for a range of temperature from 0.25 K to 300 K, see equation (1.4.10).

$$\alpha = 1.23e^{\frac{-T}{20}} + 8.34 \cdot 10^{-4}T \tag{1.4.10}$$

For regimes in which the mean free path of the molecules is smaller than the distance between the walls, the heat is conducted through the continuum gas.

The conductivity for helium in case of the continuum regime can be expressed [40]as in equation (1.4.11).

$$k = 3.83 \cdot 10^{-3}T^{0.65} \tag{1.4.11}$$

The thermal conductivity k doesn't depend anymore on the pressure but only on the temperature.

1.4.6 Parameters influencing the heat transfer through MLI

Heat transfer through MLI can significantly change depending on various parameters. An important parameter is the residual gas pressure between layers. In the most used kind of multilayer insulation blanket, in fact, the mean free path of residual molecules is much bigger than the typical distance between layers, and the molecular regime occurs. The molecular conduction can have a significantly high contribution in the heat transfer at residual pressures higher than 10^{-4} Pa, while if vacuum can be kept at levels below the 10^{-5} Pa, the residual pressure does not influence any more the heat transfer in a relevant way, see Chapter 1.5.3. In cases of very high vacuum the optical state of the layers surfaces plays an important role and also the solid conduction between layers. In this case the parameter influencing the performance is the packing density (or the number of layer per unit length) meaning a direct influence on the mechanical pressure exerted between the layers and the spacers. The more the MLI is packed, the more thermal bridges are likely to be created and the worse the performance of the insulation system. The number of layers per unit length, also called packing density, is also something that needs to be studied before an application is designed. While adding up layers is reducing the thermal radiation heat transfer, the addition of more layers could create a mechanical contact if the space is limited, which will enhance heat transfer by conduction.

1.5 Review of literature

The first concept of multilayer insulation comes from Sweden and dates back to 1951, the year in which P. Peterson first demonstrated that MLI could improve the thermal performances of any other existing insulation system, by an order of magnitude [5].

The literature on MLI is quite heterogeneous and it is not always easy to compare two results. Several values of performance are found for the same kind of blakets apparently at the same conditions. But not always the conditions of the tests are the same. NASA has produced several documents with recommendation on how to perform tests on MLI performances, being the results in literature very different between each others [9], [2], [1]. MLI application is also a very delicate procedure in which parameters such as the packing density could be strongly influenced.

A bibliographic study has been conducted and experimental data collected together. An excel file has been produced for identifying the main results and comparison between different experiments. Then results are collected in different categories (see figure 16 as an example for temperature profiles over a blanket between 300 K and 77 K).

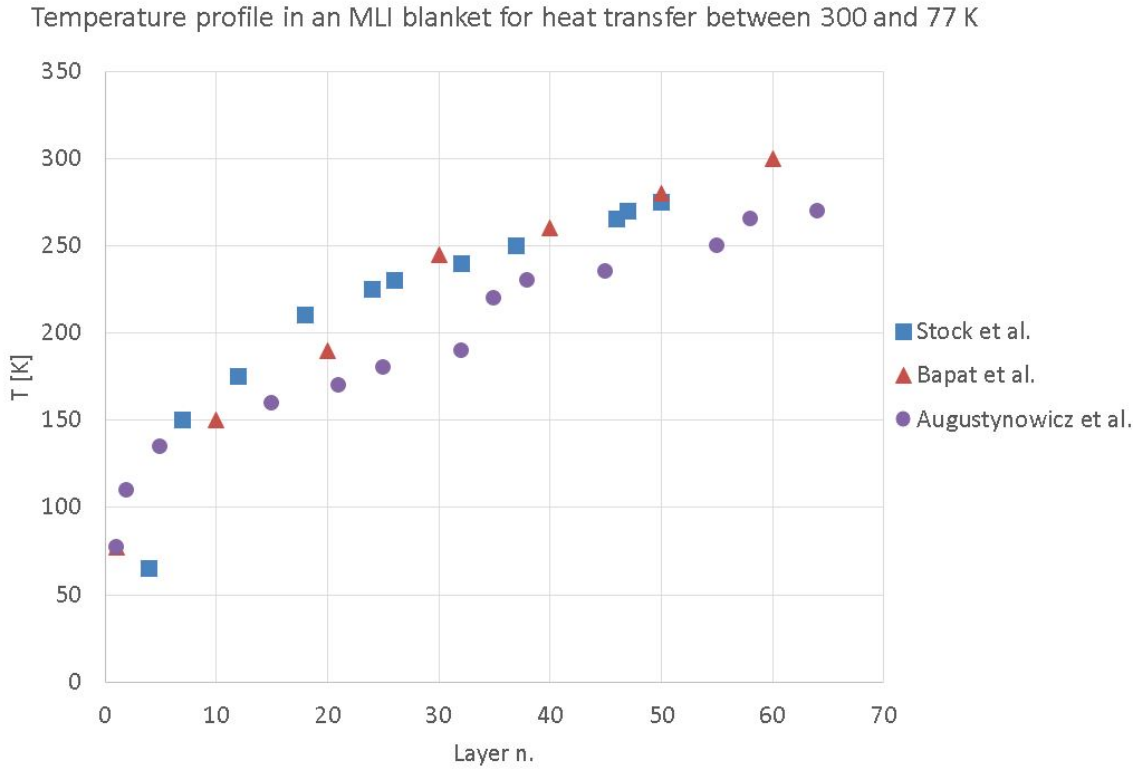

Figure 16: Temperature profile of MLI layers for experiments [33], [34], [30].

1.5.1 Experiments with different layer densities

Many results are shown as function of the layer density or packing density. This parameter is defining how many layers are present per unit length and the bigger the number the bigger chance that solid conduction is playing a very important role in the blanket. The data on layer density influence on the heat flux between 300 K and 77 K is quite abundant. Despite the similar residual pressures at which experiments have been performed, the results are also quite different for samples with the same number of layers and similar residual pressure. This confirms that the packing density is not only a very important

parameter, but also a very difficult parameter to be set in an experiment. For this reason quite some attention was devoted to the methodology to obtain the desired layer density in a reproducible way (see figure 17).

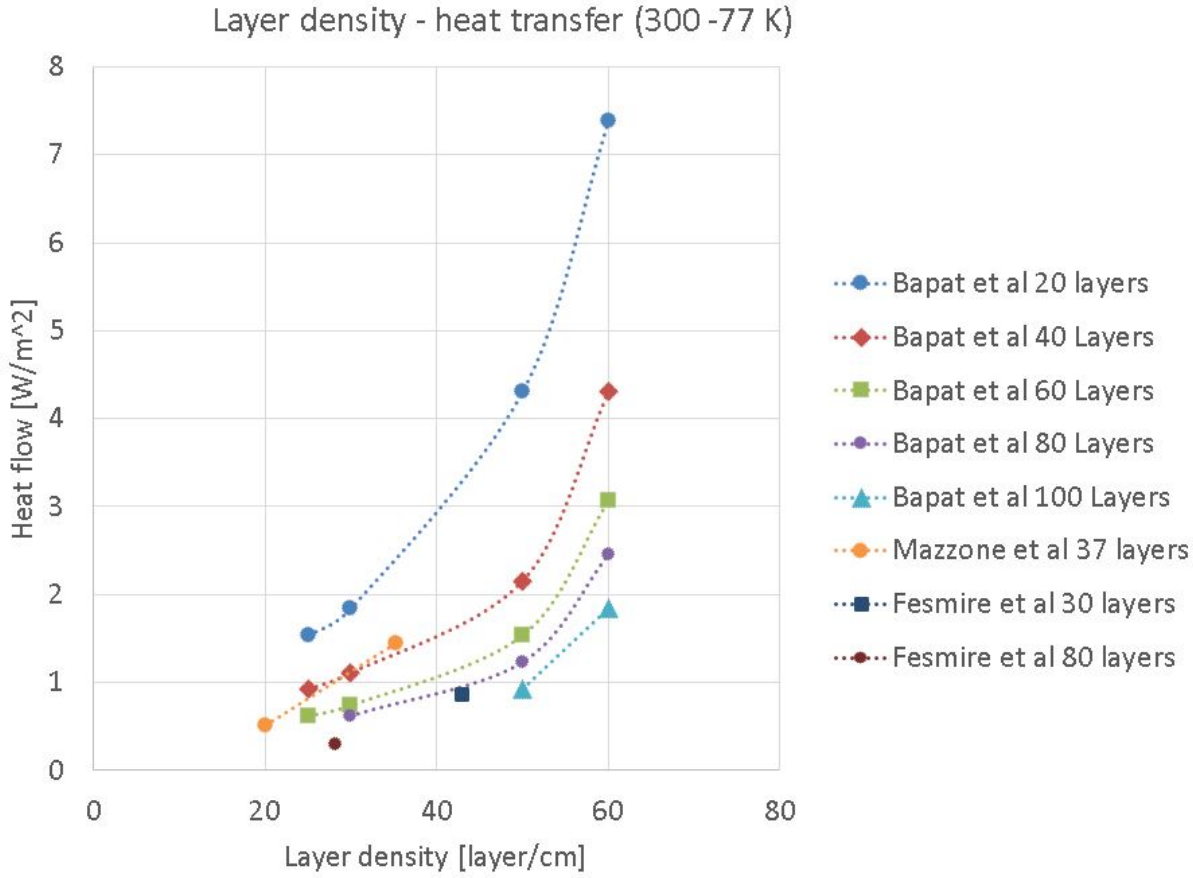

Figure 17: Heat flux and layer density: 300 K - 77 K [34], [16], [13]

1.5.2 Experiments with different number of layers

Concerning the number of layers, it seems that the number of layers improves the performance of the MLI up to 20 layers in the 300 K - 77 K. Then the increase of layers at fixed layer densities does not improve the performance significantly (see figure18).

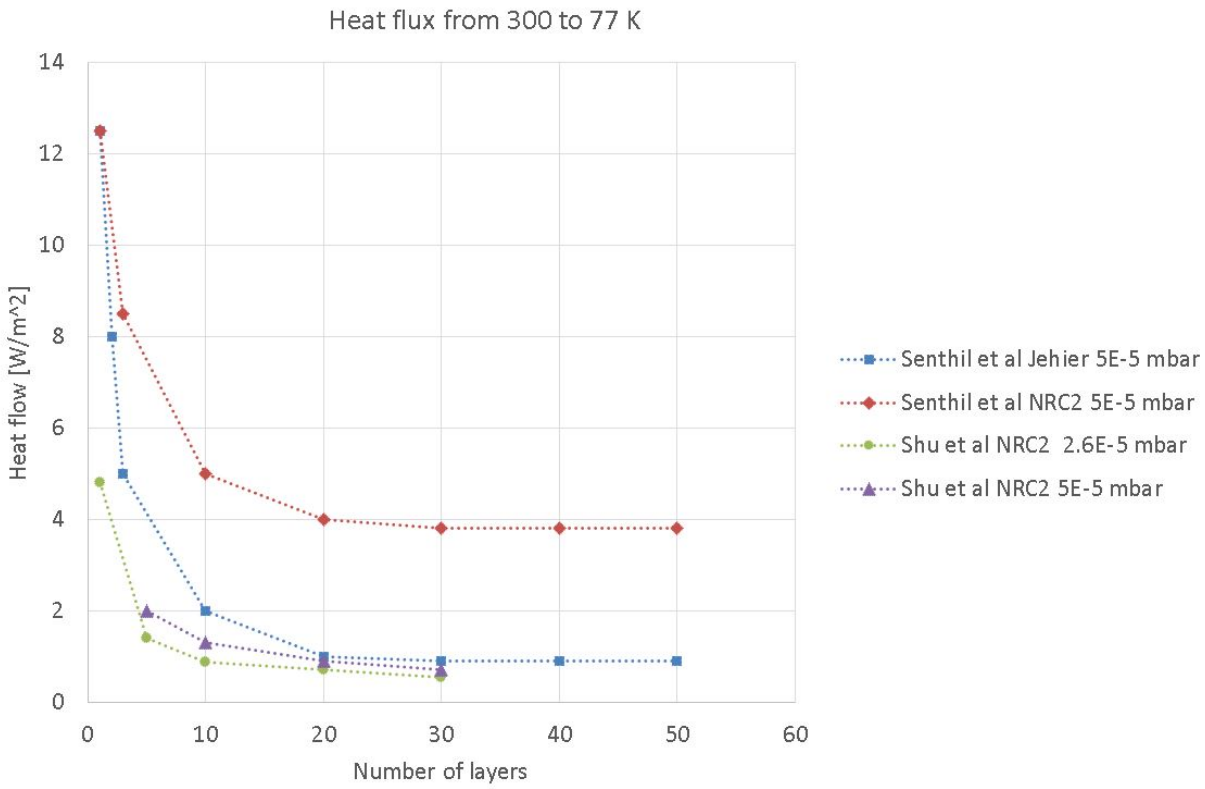

Figure 18: Heat flux and number of layers: 300 K - 77 K [29], [3]

The trend looks similar in the case of 77 K - 4.2 K where space limitations are present and such to influence the layers density at high number of layers, the performance start to decrease as the packing density is also influenced if too many layers are used (see figure 19).

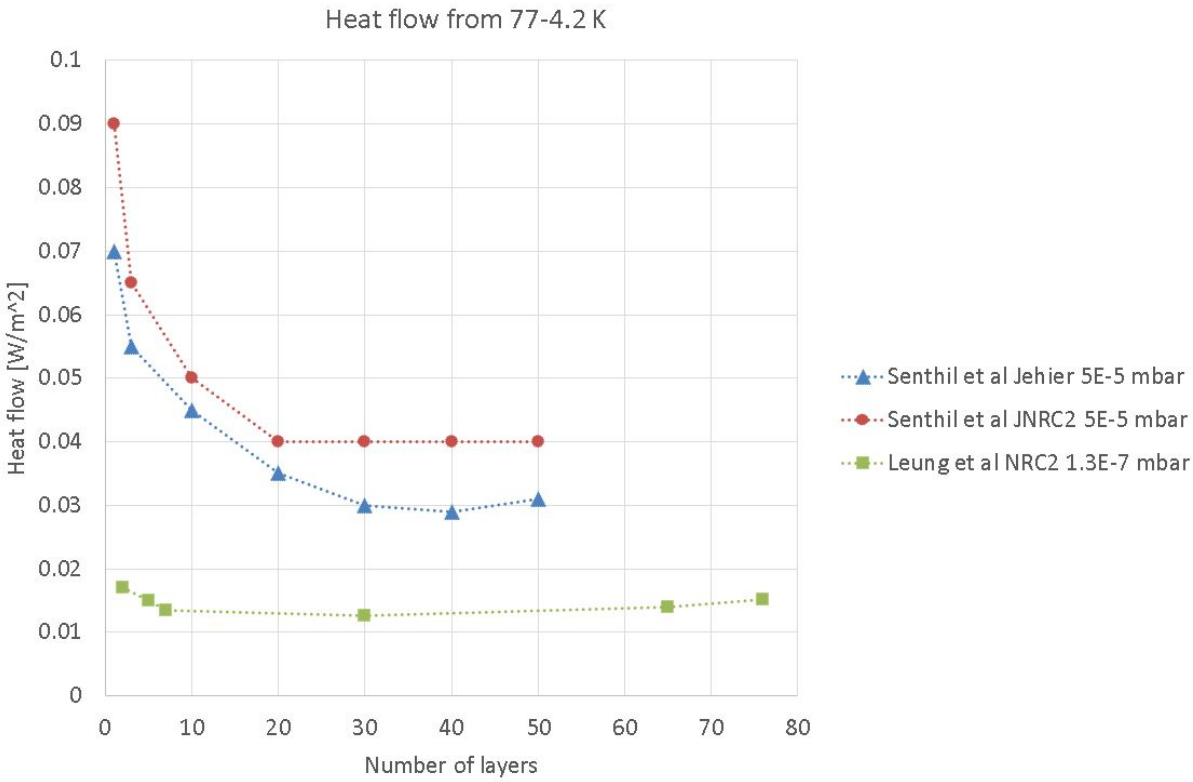

Figure 19: Heat flux and n of layers: 77 K -4.2 K [3], [7], [26], [39]

1.5.3 Experiments with different residual gas pressure

Results for residual pressure influence on the heat flux are showing a linear decrease of heat flux with residual pressures of up to the range of some few mPa. Some results are shown in figure 20 and 21 for different ranges of temperature.

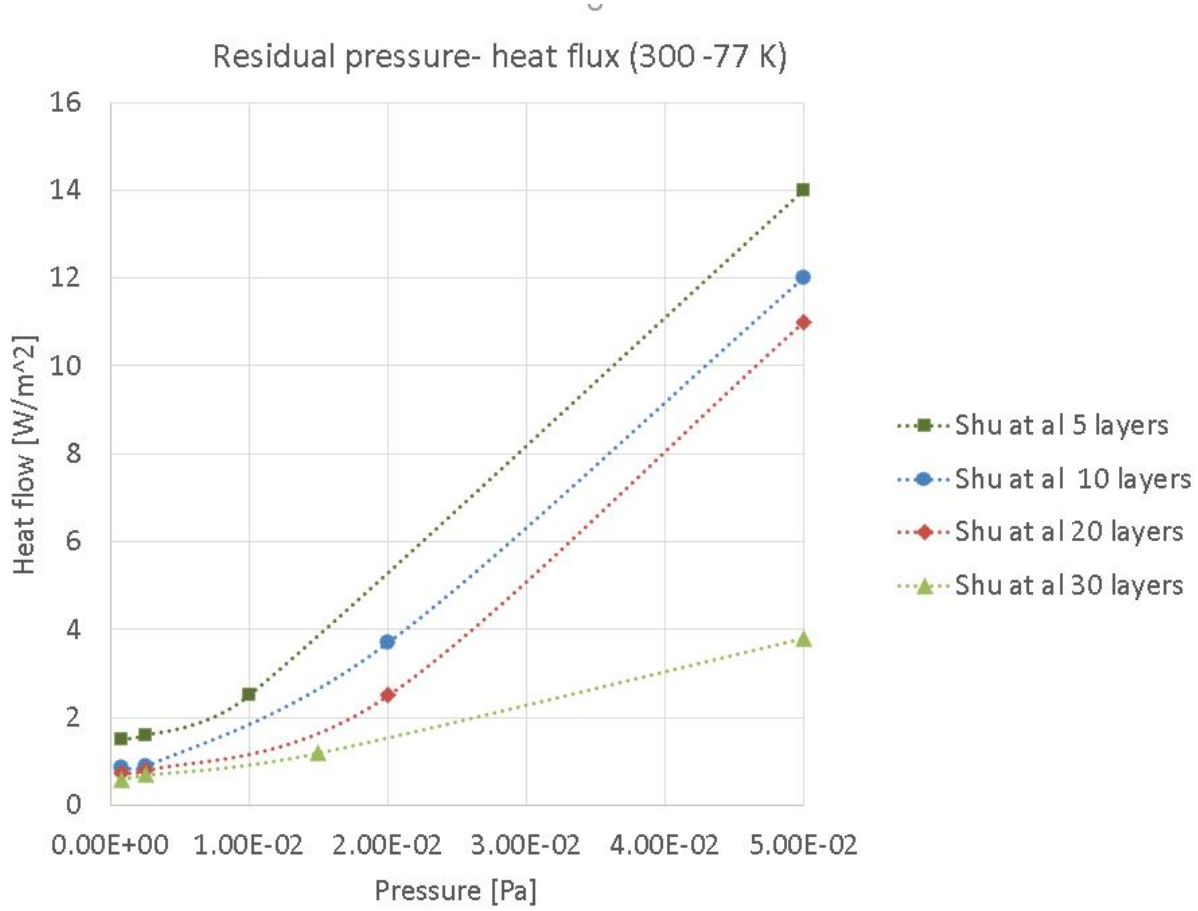

Figure 20: Heat flux and residual presure: 300 K -77 K [29].

The residual pressure plays mainly a role in the heat transfer when above 1×10^{-5} mbar

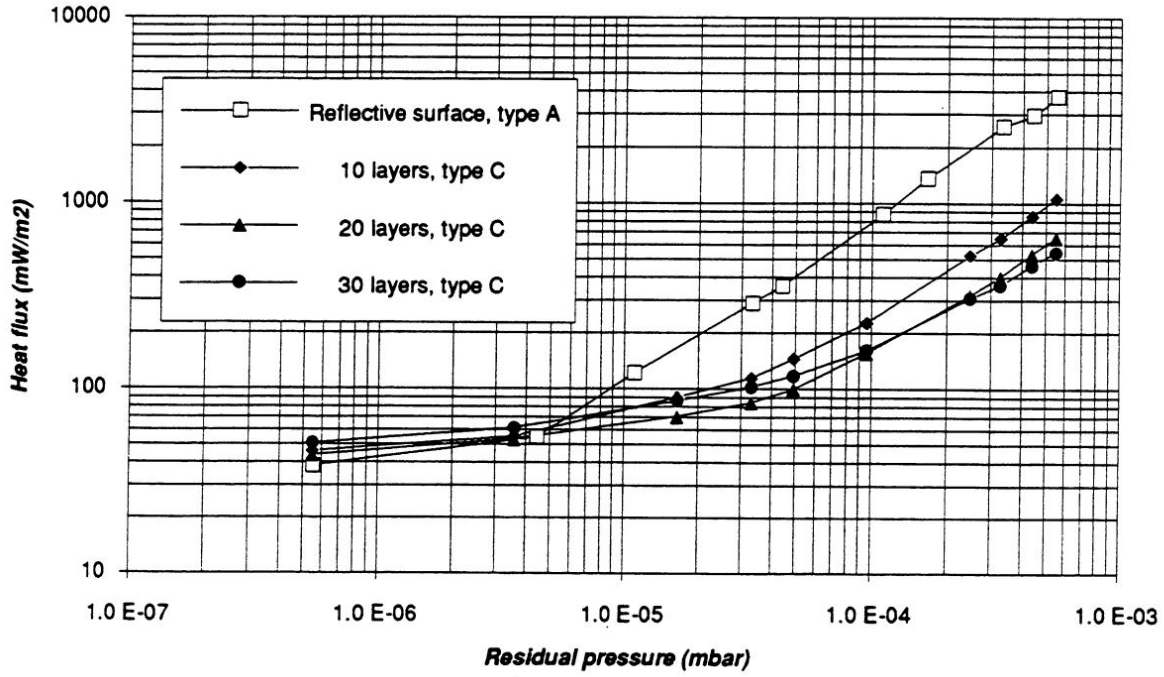

Figure 21: Heat flux and residual presure: 77 K -4.2 K [26].

1.5.4 Mathematical models developed for MLI system heat transfer

Many mathematical formulations have been written in order to fit the results obtained by the experiments on MLI performance. The abundance of semi-empirical mathematical models confirms the difficulty in reproducibility of results and the big influence of the testing apparatus and the handling of the specimens. A summary of some mathematical models can be found in [35] [17].

2 Doctoral thesis and scope of the dissertation

The thesis goal is to find the optimal temperature for the thermal shield used in FCC in order to minimize the refrigeration power required during operation. The size of the project is such to require the need of experimental data in order to complete the refrigeration power equation (5.2). In figure 22 a schematic approach of the problem is shown: a generic configuration of the FCC cryostat composed by a cold mass, a thermal screen and a vacuum vessel. The heat load on the cold mass is coming by the thermal screen, the heat load on the thermal screen is coming from ambient. The total power of refrigeration required during operation is equal to the sum of the refrigeration power needed in order to keep the cold mass at 1.8 K and the thermal screen at its temperature. The refrigeration power can be plotted in function of the thermal screen temperature. The exergetic approach reveals a minimum in the refrigeration power for a certain value of the screen temperature, considering the heat loads and their Carnot efficiencies. The

value of the heat load on the cold mass depends on the kind of insulation used and its performance. Cold masses in accelerators are generally protected by multilayer insulation systems MLI (described in chapter 1.4. The literature data available for the efficiency of multilayer insulation system is only available for temperatures between 77 K and 4.2 K, see literature review in chapter 1.5. Not many data exist for performance at temperatures lower than 77 K. For completing the model for refrigeration power, experimental data are required at lower temperatures for MLI performance in order to determine the real value of heat on the cold mass. A dedicated test campaign was done at CERN to get data on MLI performance to 4.2 4.2 K from temperatures in the rage $20-60$ K. The experimental results are done for different temperatures but also different MLI configurations, like number of layers and packing density described in 1.4.6 and different levels of vacuum.

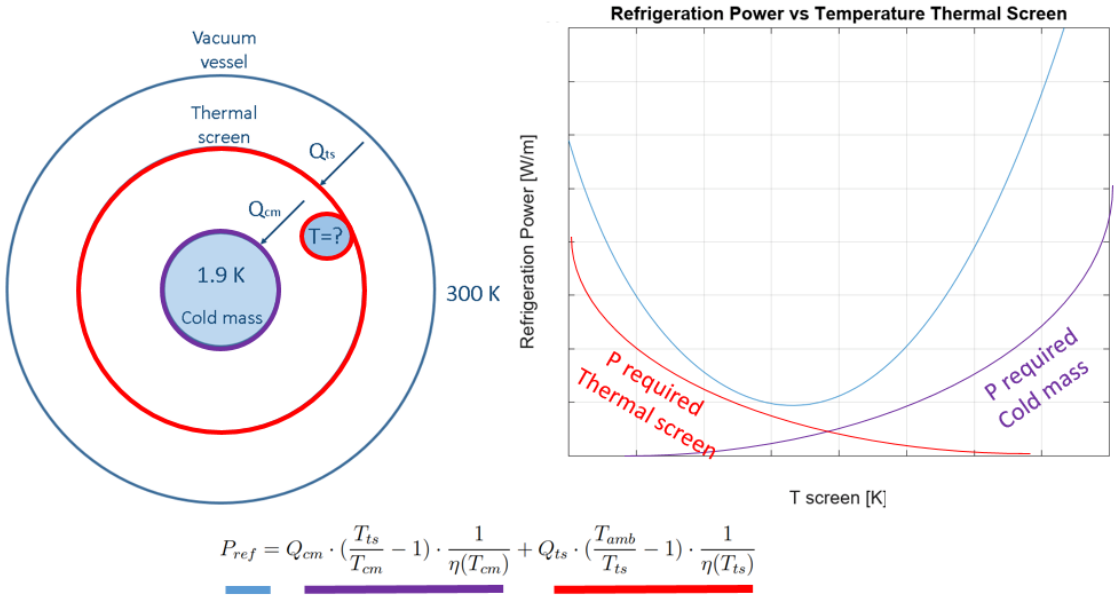

Figure 22: Refrigeration power curve in function of the thermal screen temperature

2.1 Doctoral thesis

A thermal screen for cold mass protection in a particle accelerator kept at temperatures of around 50 K could be a more efficient solution in terms of refrigeration power consumption with respect to configurations at higher or lower temperatures.

3 Development of test method

3.1 Methodologies for multilayer insulation system performance experiments

The most common methodology for measuring heat transfer performance of an insulation system in cryogenics is the boil-off method, which is also used for the purpose of this work. This methodology consist of the application of the insulation material on a test tank, where a cryogen is kept at saturated liquid conditions. Its temperature will not change during the heat transfer process. The test tank is kept normally in vacuum and the hot boundary can be either room temperature or another cryogen kept at saturated conditions in a surrounding vessel. Some methodologies could foresee also a different system for varying the outer hot boundary temperature. An example of a non-calorimetric method is an experiment done at CERN by Mazzone [16]. A copper cylinder suspended in a cylindrical vacuum vessel is cooled down with a cryogen from the top and heated up from the bottom with some heaters. The cylinder is wrapped by MLI and surrounded by a copper plate equipped with heaters and temperature sensors. By measuring the heat flux at different temperature and heat inputs they calculate the portion of heat coming only through thermal radiation.

3.2 Test campaign description

In order to find the best temperature for the thermal screen to be able to complete equation (5.3.5) tests were planned for different blankets configurations at different hot boundary temperatures. The first test were performed for blankets of 10 layers and different packing densities: 10, 20 and 30 layers/cm. A dedicated method was invented to control the layers length with a good reproducibility (see chapter 3.6). The choice of 10 layers as a start was taken in order to be able to compare results with the heat transfer measured on LHC. After seeing no big difference between the three packing densities proposed, and after having improved the system for increasing resolution, the choice was to test a bare vessel, a single aluminized foil and two extremes for the 10 layers blankets densities: 10 and 50 layers/cm, see chapter 4. All the configuration are also tested in degraded vacuum conditions to check the case of a helium accidental leak. The final tests proposed are summarized in Table 2.

Type of test	Layers density [layers/cm]	T hot [K]	T cold [K]	p [mbar]
Bare vessel	-	100 - 300	77	2E-7
Bare vessel	-	20 - 60	4.2	2E-7, 1E-5, 1E-4, 2E-4
1 aluminum foil	-	20 - 60	4.2	2E-7, 1E-5, 1E-4, 2E-4
10 layers MLI	10	20 - 60	4.2	2E-7, 1E-5, 1E-4, 2E-4, 1E-3
10 layers MLI	50	20 - 60	4.2	2E-7, 1E-5, 1E-4, 2E-4, 1E-3

Table 2: Summary of tests foreseen for the MLI test campaign

3.3 Cryostat overview

The experimental setup is based on a test cryostat, see figure 23 and 24, first developed by Wroclaw University of Science and Technology. It was previously used to measure performance of MLI between 293 K and 77 K and between 77 K and 4.2 K [27], [28], and subsequently it has been modified for the purpose of the new tests planned at CERN.

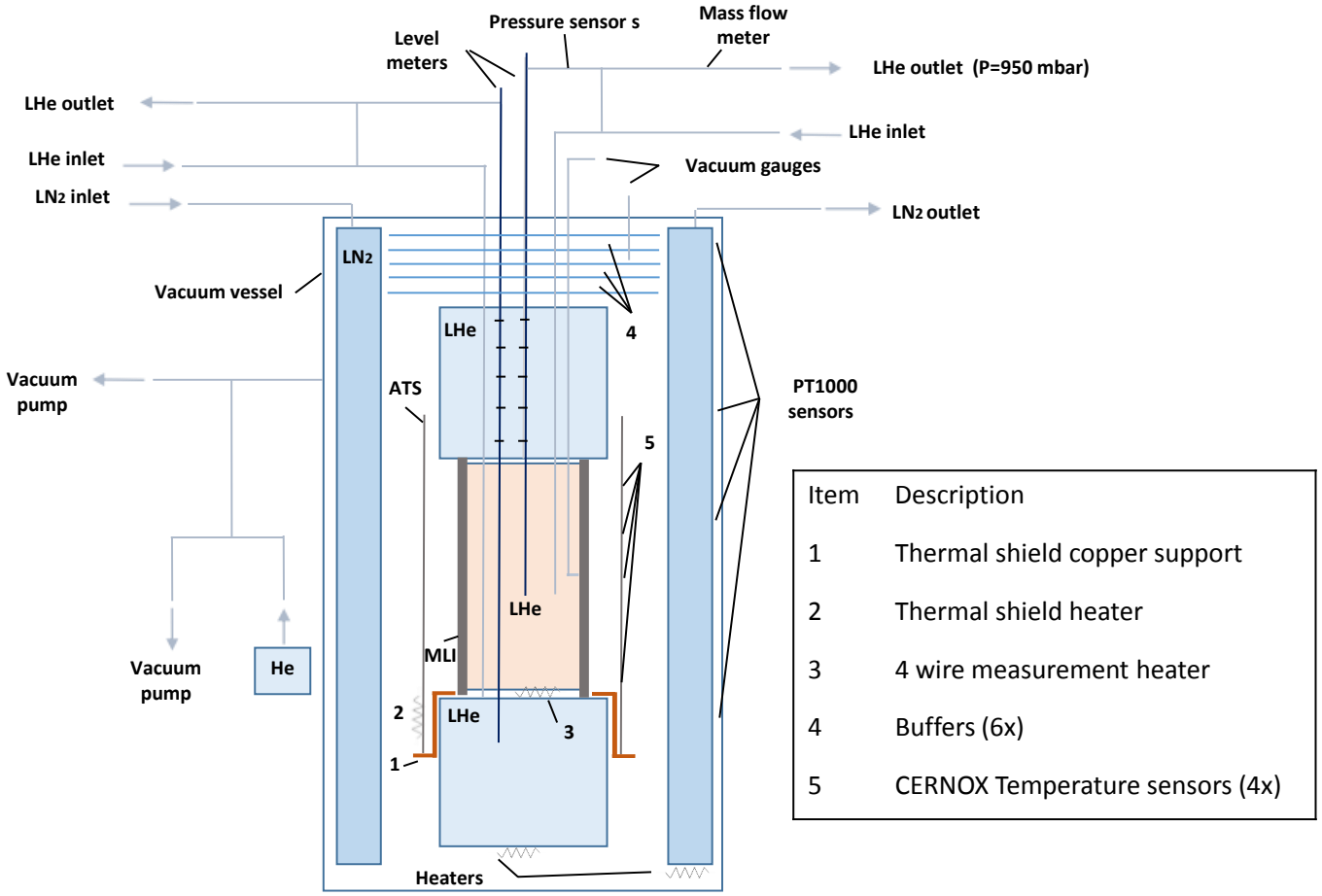

Figure 23: Test cryostat overview: the test vessel is thermally protected by a guard vessel composed by an upper and bottom tank always filled with liquid helium during the measurements. The guard and test vessels are protected by an annular vessel containing liquid nitrogen, the whole inside a vacuum vessel. A thermal screen in aluminum has been designed with its support on the lower part of the guard vessel in order to reach 20 K in steady-state in good vacuum conditions and it's heated up by a heater to reach temperatures up to 80 K - 100 K

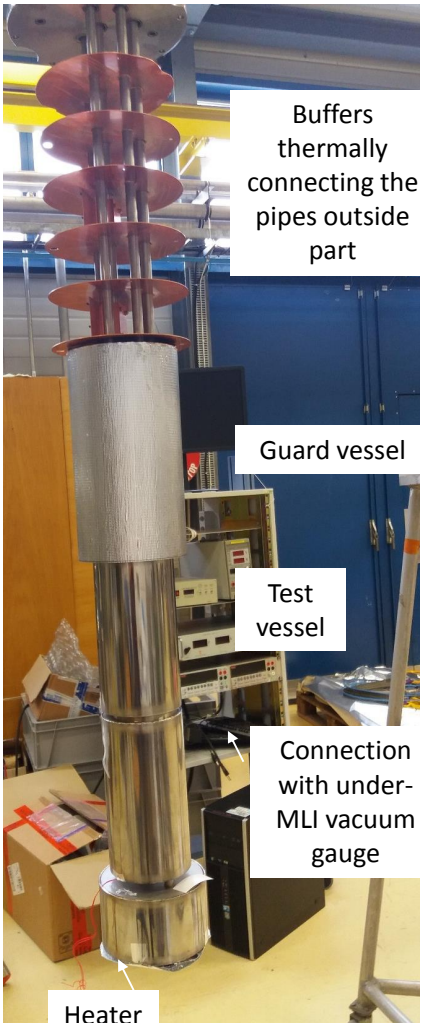

Figure 24: Test cryostat picture: the test vessel is a ylinder measuring 0.5 m with an external surface of 0.2 m^2

The cryostat is composed of an inner test vessel around which the MLI sample is wrapped, the external cylinder surface is 500 mm high with a total surface of 0.2 m^2. A double LHe guard vessel, with bigger diameter, ensures insulation from the longitudinal direction and an external LN2 tank provides shielding from room temperature thermal radiation. The pipes of the guard and test vessel are double walled to aid in insulation. On the outer wall all the pipes are welded (see figure 25) on the six buffer thermal shield insulating the cryostat from the top side thermal radiation and pipe conduction.

Figure 25: Buffer thermal shield welded on pipes, liquid Nitrogen anular vessel

A feature of the test cryostat is the measure of the pressure underneath the MLI blanket through an integrated pipe connecting the sample vessel to the outside flange. This information is important to check the residual gas pressure from out gassing of the MLI sample that is directly related to molecular conduction within its layers.

3.3.1 The aluminium thermal shield, ATS

For the purpose of this study a modification to the test cryostat was made at CERN in order to allow intermediate temperature levels for the warm boundary to be fixed between 20 K and 60 K. A 1 mm thick aluminium thermal screen (ATS) has been designed and

placed on a copper support in weak contact with the bottom guard vessel, see figure 26. The aim is to establish, in steady-state conditions, an equilibrium temperature of the ATS between the inner tank at 4.2 K and the external tank at 77 K. 20 K is reached with no additional heat applied. In order to set the temperature of the ATS, a 60 Ω electrical resistance heater, which provides power in the 5-6 W range, has been placed to provide a heat source. Four CERNOX temperature sensors are distributed along its length. Initial simulations of the system using ANSYS, see figure 27, show that the optimal position for the heater is on the bottom part of the ATS in order to minimize the temperature gradients along the ATS length. Later on tests have confirmed the good positioning of the heater.

Figure 26: ATS copper support. The ring is resting with an Iindium joint on the bottom LHe guard tank. Three arms are providing the weak thermal link where the ATS is resting by its own weight

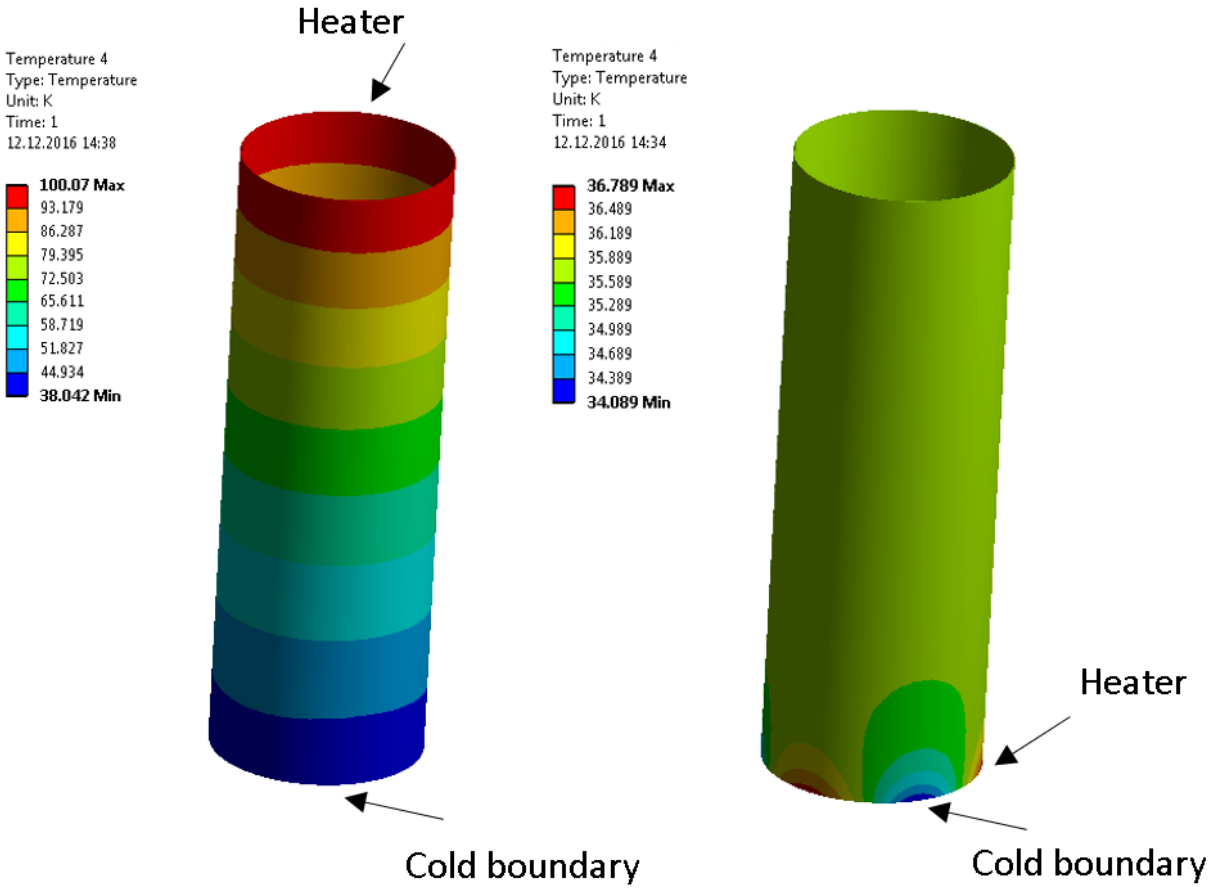

Figure 27: Simulation of the Aluminum Thermal Shield temperature distribution. The maximum temperature dgradient is present only on the bottom arrangement and it is of 2.6 K. The lower 10 cm of the ATS are not facing the test vessel and the surface of interest for the experiment has a maixmum gradient of 1 K

3.3.2 Degraded vacuum system

The heat flux through MLI in case of degraded vacuum from a helium leak in the system is tested by means of a helium injection apparatus. The vacuum vessel is connected with a small volume of 2.3 cm^3 where helium is injected at atmospheric pressure, see figure 28.

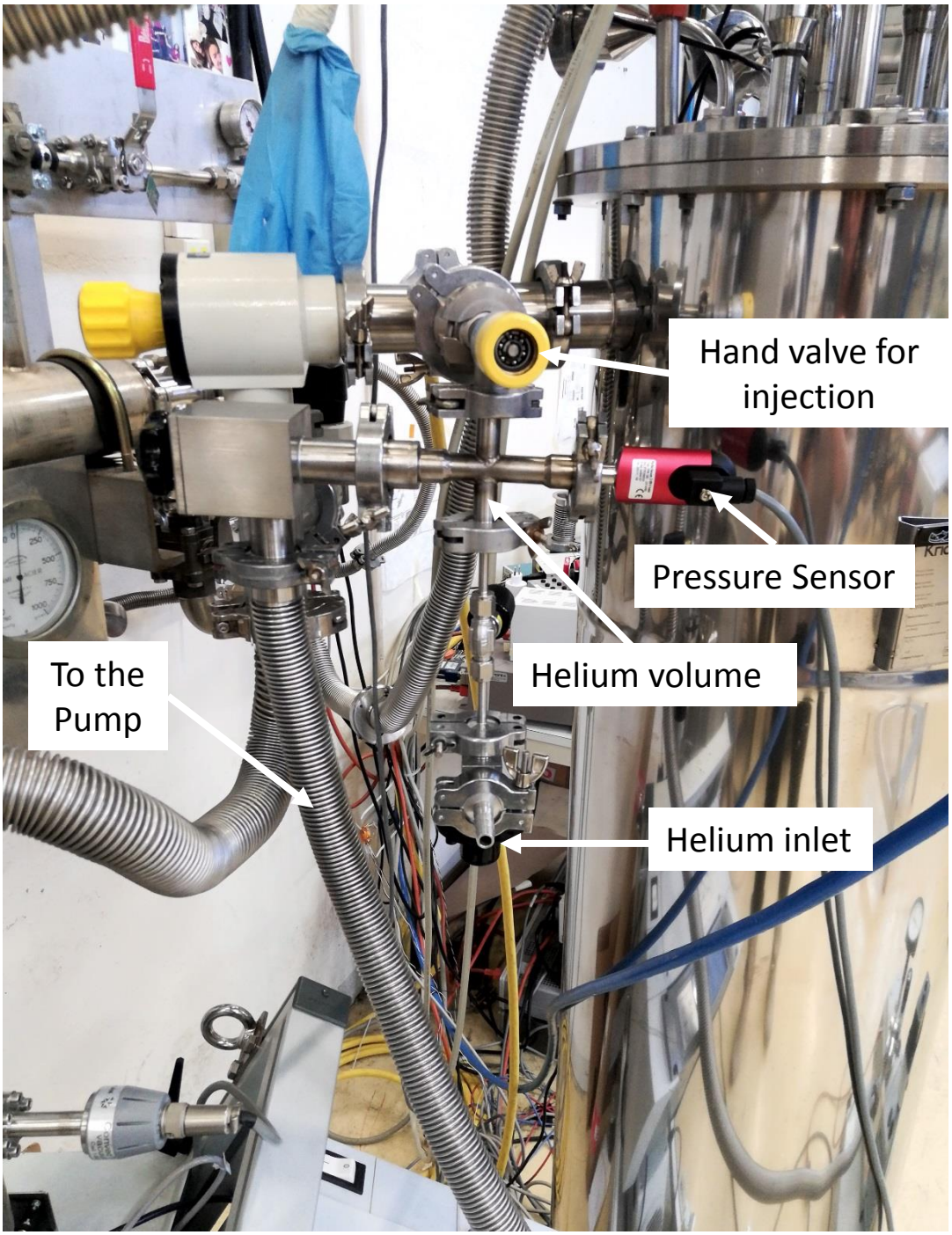

Figure 28: Degraded vaccuum system for helium injection

The pipes cross is connected to:

- The vacuum vessel through a hand valve
- The helium source through two hand valves
- The pressure gauge

- The vacuum pump with a hand valve

Helium can be transferred slowly with a hand valve till the desired degraded vacuum level in the cryostat is reached.

3.4 Instrumentation

3.4.1 Sensors and heaters

The cryostat is equipped with two Pfeiffer ITR 90 - FullRange Pirani/Bayard-Alpert vacuum gauges working at room temperature. Due to thermal transpiration [6], a conversion formula is applied, Knudsen relationship, see equation (3.4.1):

$$\frac{P_{hot}}{P_{cold}} = \sqrt{\frac{T_{hot}}{T_{cold}}} \tag{3.4.1}$$

Where P_{hot} is the pressure measured at room temperature, P_{cold} is the pressure calculated on the cold area, T_{hot} is the temperature at which the pressure is measured and T_{cold} is the temperature at which the pressure is calculated.

The first vacuum gauge is placed on the top of the upper flange, the second one is connected with a tube which goes through the upper guard vessel and half of the test vessel and it's used to monitor the vacuum level underneath the blanket.
A pressure transmitter Keller 23/8465-1.5 has been placed after the first experiments on the outlet of the test vessel.
All the cryostat vessels have been equipped with instrumentation for liquid level control: in the LN2 vessel four Pt1000 sensors have been placed outside the vessel at different heights in order to indicate different levels of the liquid phase; on the helium guard and test vessels the liquid levels were monitored by two super conducting level meters.
The aluminium thermal screen has been equipped with 4 CERNOX temperature sensors. They were distributed in a way to have a full picture of the screen temperature. Two were placed at the bottom, one on the center and another one on the top.
A thermal mass flow meter of the kind Brooks 5850 has been placed two meters far away from the test vessel's top in order for the flow of helium vapour to reach room temperature. It consists of three basic units: a flow sensor, a control valve and an integral electronic control system in order to produce a stable gas flow, which eliminates the need monitor and readjust gas pressures. The flow meter consists of two temperature sensors applied on a tube with a heater in between, see figure 29. The two temperature sensors measure zero temperature difference when there is no flow while when gas is present, the first sensor will measure the incoming flow temperature while the second sensor will measure the flow temperature after the gas has been heated up by the constant power applied. In this way it is possible to have a correlation between the temperature difference and the mass flow by considering the geometry of the tube and the heat capacity of the gas. A bridge circuit is amplifying and interpretation the signal.

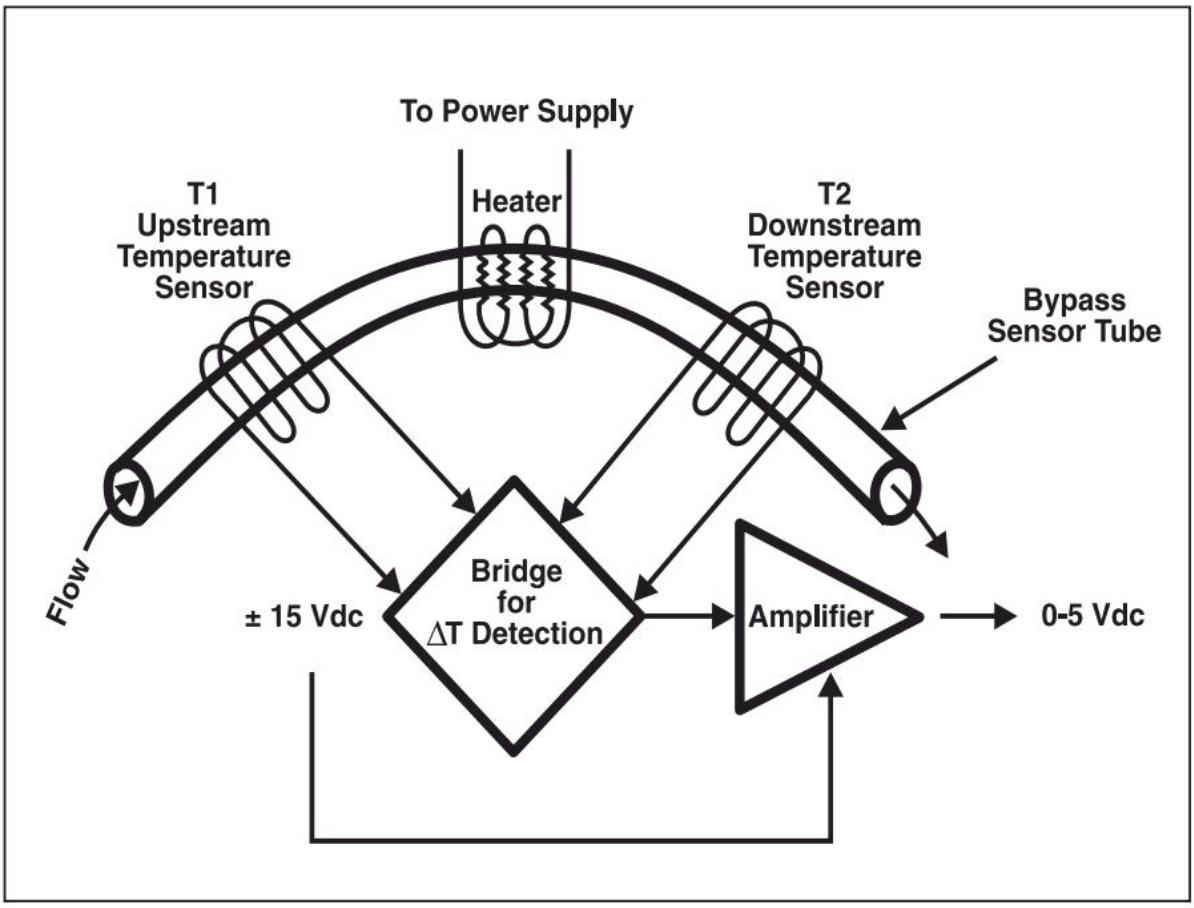

Figure 29: Mass flow meter principle from the Installation and Operation Manual Model 5850E Mass Flow Controller [12]

A low power heater has been placed on the thermal shield on the ATS for reaching different temperature levels. One heater has been placed on the test vessel instrumented in four wires configuration to allow precise calibration heat loads in the test vessel. Hence a direct calibration with stepwise increased heat load and precise fitting of the heat load on the flowmeter signal can be done. Two other heaters have been set on the guard vessel and nitrogen vessel for fast evaporation during the warm-up of the cryostat.

3.4.2 Data acquisition

The 4 temperature sensors, together with the the ATS, the guard vessel and test tank heaters have been connected to a common 24 pin fisher connector while all the instrumentation related to the nitrogen vessel has been connected to a second fisher connector. This choice was made based on how the cryostat is opened when a blanket has to be installed. The two have been connected to multimeters of the kind Keithley 2000. An interface built in LabVIEW was recording all the data together. In the program it was possible to insert all necessary data for signal conversions.

3.4.3 Safety devices

All the safety valves were dimensioned according to the ISO 4126-7 (International Standards for safety devices for protection against excessive pressure) and were placed in each tank containing cryogens and on the vacuum vessel in case of leaks. The risk analysis included a potential helium loss into the vacuum vessel which would cause the test and guards vessel to undertake a sudden heat load up to $38\,\mathrm{kW/m^2}$ [42], the value used for heat loads without MLI coverage.

3.5 Data acquisition procedure

A LabVIEW program created at CERN has been installed. It was prepared for data acquisition of different inputs from different scanner cards. Relevant data recorded during the experiments included the helium exhaust mass-flow out of the test vessel, its pressure and the temperature along the ATS. Moreover a level meters was present in both LHe vessels and temperature sensors are on the LN2 vessel to check the tanks filling. Data are recorded when the system is in steady-state. By experience it has been found that stable conditions appear less than 1 h after setting the heaters when MLI was present. A sampling rate every 20 s has been found to be sufficient for the time response of the system. For each test configuration, a measurement window of 10 minutes at steady-state condition provided a sample of 30 measurement points of which a mean value was calculated. The mass flow meter data indicated an accuracy of 1 % of the reading on the full range, but measurement campaigns have shown that a statistical error of 12 % of the mean value, was estimated over its full range. In order to enhance the precision of the measurements, for each configuration a set of measurements were taken by imposing some heat in 2 steps on the test vessel. The points are interpolated to reduce uncertainty and a new more precise point at zero additional heat applied was calculated form the fitting curve. A precision of 2.5 % is found in average. The value was then converted to heat flux through the curve at zero thermal radiation, see chapter 3.8.2. The CERN electronic pools offers Keithley multimeters with 10 channels cards and two of them has been used. The control of the heater for the shielding has to be programmed.

3.6 Sample preparation

A dedicated laboratory for MLI blanket preparation has been set up. A sewing machine and a big cutter have been set for the thesis work. The installation of MLI blankets is a critical moment as it can be easily influenced by the way the person installing it while wrapping them around the object. The parameter which can be most easily affected is the packing density, see figure 30, the number of aluminized layers per unit length through the blanket.

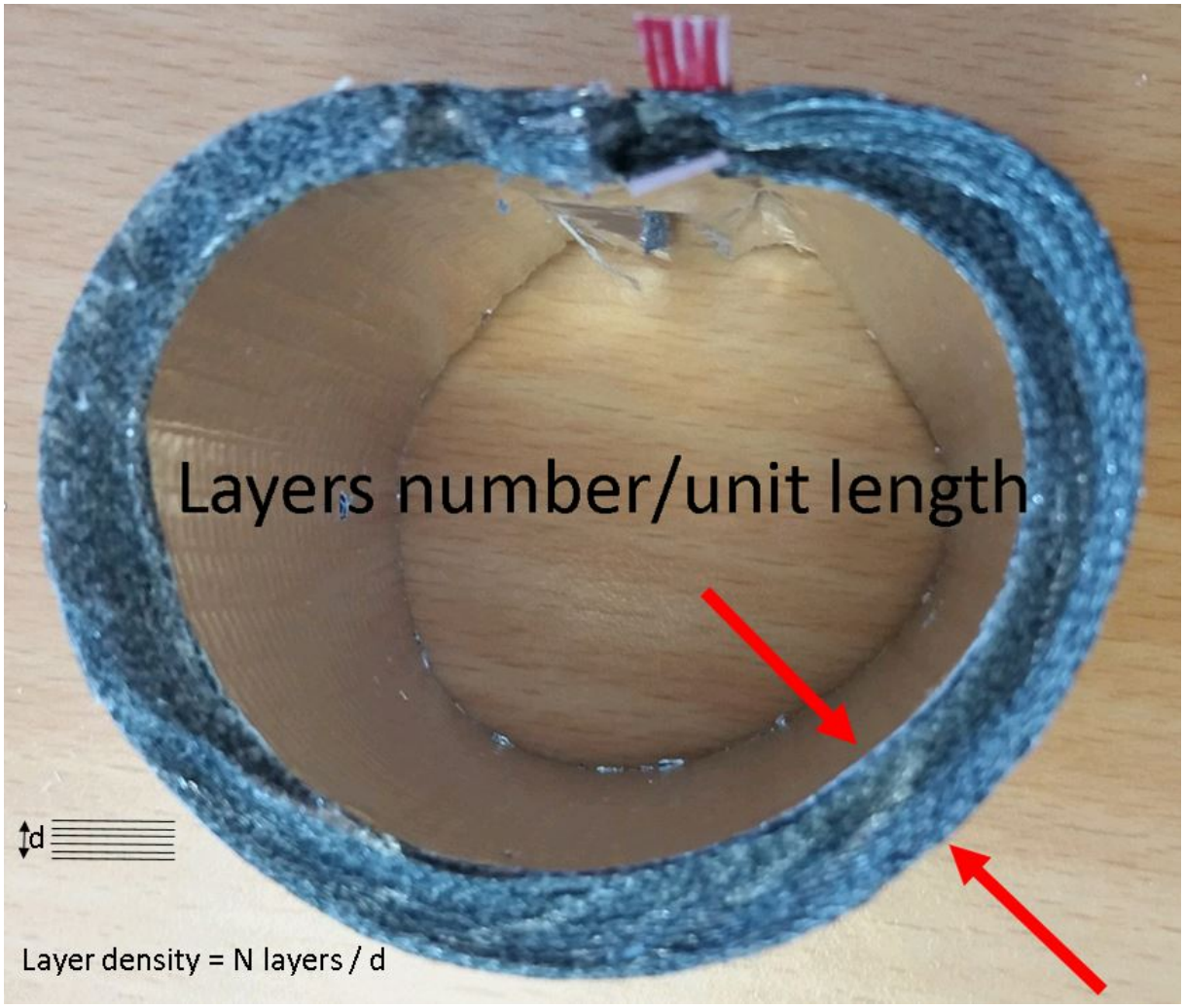

Figure 30: Layer density definition for the applied cylindrical geometry

It is common that MLI blankets are cut and sewed by the producing company before installation. An example are the blankets on LHC magnets, where the insulation material is equipped with Velcro® straps and its inner layers are shorter than the outer ones, in a fixed design. The blanket could be installed more or less tightly, and this could change the way the layers touch each other. For the experiments planned in this work it has been fundamental to find a methodology to be able to produce blankets with different layer densities after installation in a reproducible way.

Two options have been considered:

- 1) cutting the layers in the exact length to obtain different densities and wrap them around the cold mass, one by one to avoid thermal short cuts
- 2) create a seamed full blanket with a certain layer density and wrap it around the cryostat (by Velcrotextregistered or aluminium tape)

The first option would theoretically be the best in terms of insulation as the layers would

not overlap. As a drawback though the solution could be extremely time consuming and especially with low chances of good reproducibility on a vertical test vessel, especially for the contact with the spacer material. Moreover handling all the layers one by one would certainly have caused some disturbance in the emissivities. The second option would have certainly created a disturbance in the heat transfer through seams but in a reproducible way, with the advantage of an easy installation. For these reasons the second option has been chosen.

The way MLI are cut and kept with a fixed density starts with geometrical considerations about the layers and the length needed to achieve a certain distribution. The blanket comes from the company with a seam on one side only and a height equal to the one needed to cover the cryostat longitudinally, see figure 31.

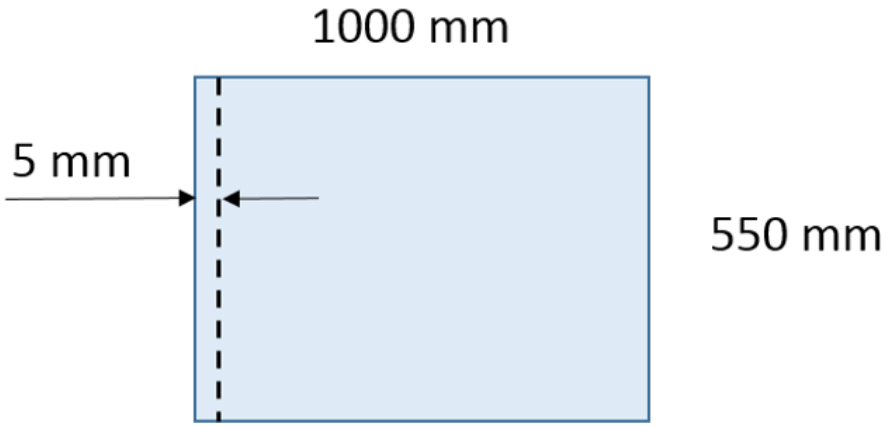

Figure 31: MLI blanket starting configuration

The first step of the process was to define the length of the innermost and outermost layer and put a mark on each of them, see figure 32.

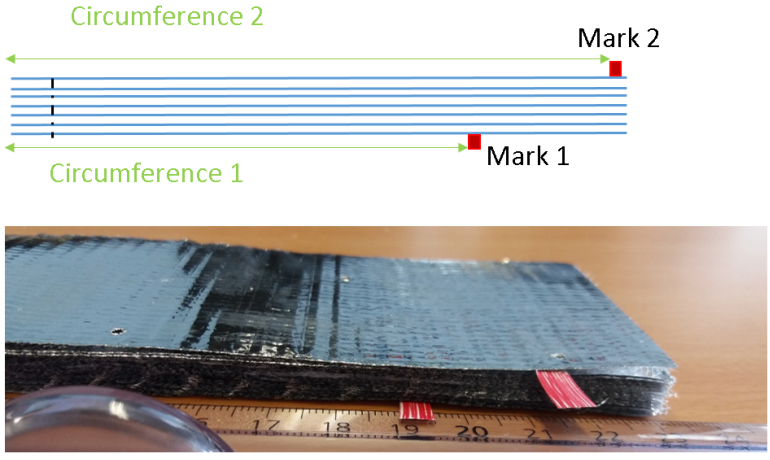

Figure 32: Schematics and photo of teh procedure to define the length of the innermost and outermost layer in the MLI blanket

The extremity of the blanket coincident with the seam was rolled in order for the layers to start sliding one on the other till the two marks would have coincided. The blanket was then first kept with a temporary fastener, then cut, and finally sewed. The layers would automatically get gradually increasing lengths between the extremes, see figure 33.

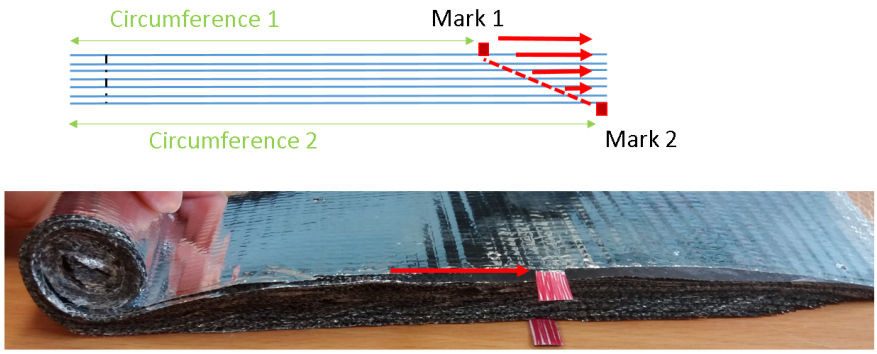

Figure 33: Rolling the MLI blanket till the marks coincide

3.7 First run for method development

3.7.1 Tests with liquid nitrogen

The first test performed with the cryostat was the one at high temperatures by filling the test vessel, the guard vessel and the external vessel all with liquid nitrogen. The aim was to check the performance of the aluminium thermal shield in terms of temperature distribution and to check the lowest possible temperature reached. After 2 days of vacuum pumping, liquid Nitrogen was inserted. The lowest temperature reached for the ATS was only 104 K after three days with a gradient of $3 - 4$ K along its length. The vacuum level reached was 10^{-6} mbar. It was decided then to take some measurements despite the screen didn't reach 77 K. The nitrogen flow measured through the level meters was directly converted in mass flow and heat flux, three measurements were taken at 104 K, 162 K and 225 K. The experiments were compared with a theoretical curve for radiant thermal heat between two concentrical surfaces with emissivities found in literature [5], see figure 34.

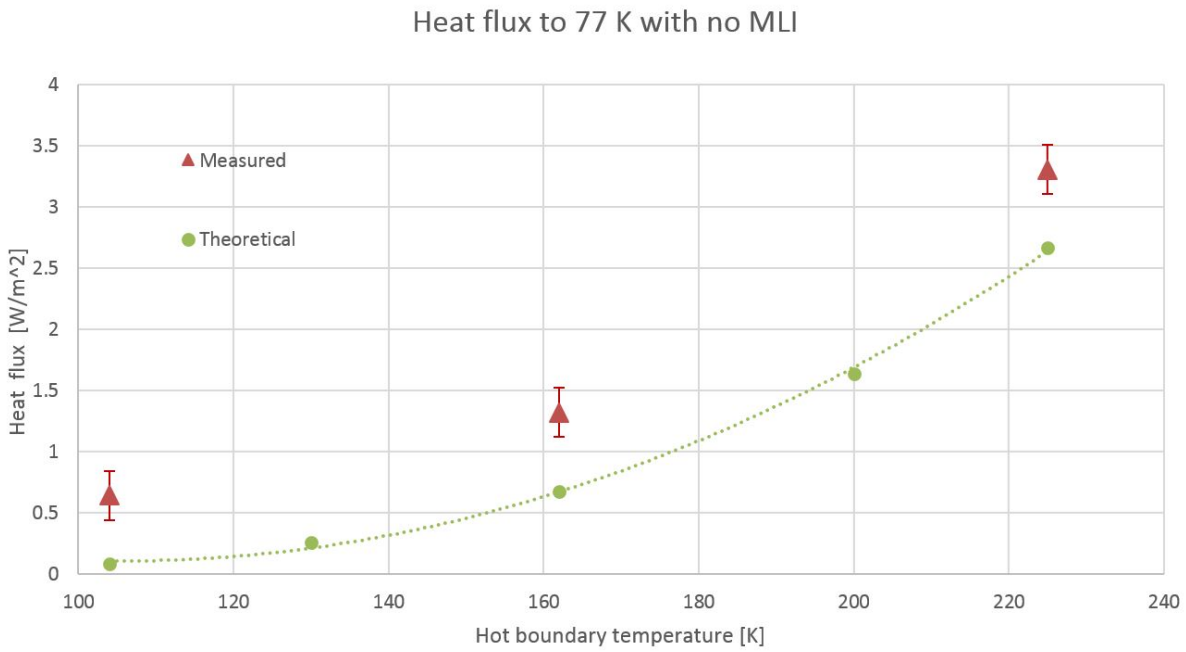

Figure 34: Heat flux to 77 K and comparison with theoretical radiant heat curve

3.7.2 Test with liquid helium and no MLI applied

During the first test using liquid helium for the test and guard vessel, the lowest temperature reached by the ATS was 150 K with a gradient of 1 K. This meant that the contact with the copper support needed to be improved in order to obtain a lower temperature. A vacuum level of 2×10^{-6} mbar was measured in the region outside the ATS. The heat transfer without MLI on the 4.2 K vessel was measured by means of the two level meters in the test and guard vessel as the flow meter bought was undersized for the flow obtained: the background heat load was not foreseen to be so high. The rate of evaporation was measure to be constant during the emptying of the test vessel, see figure 35.

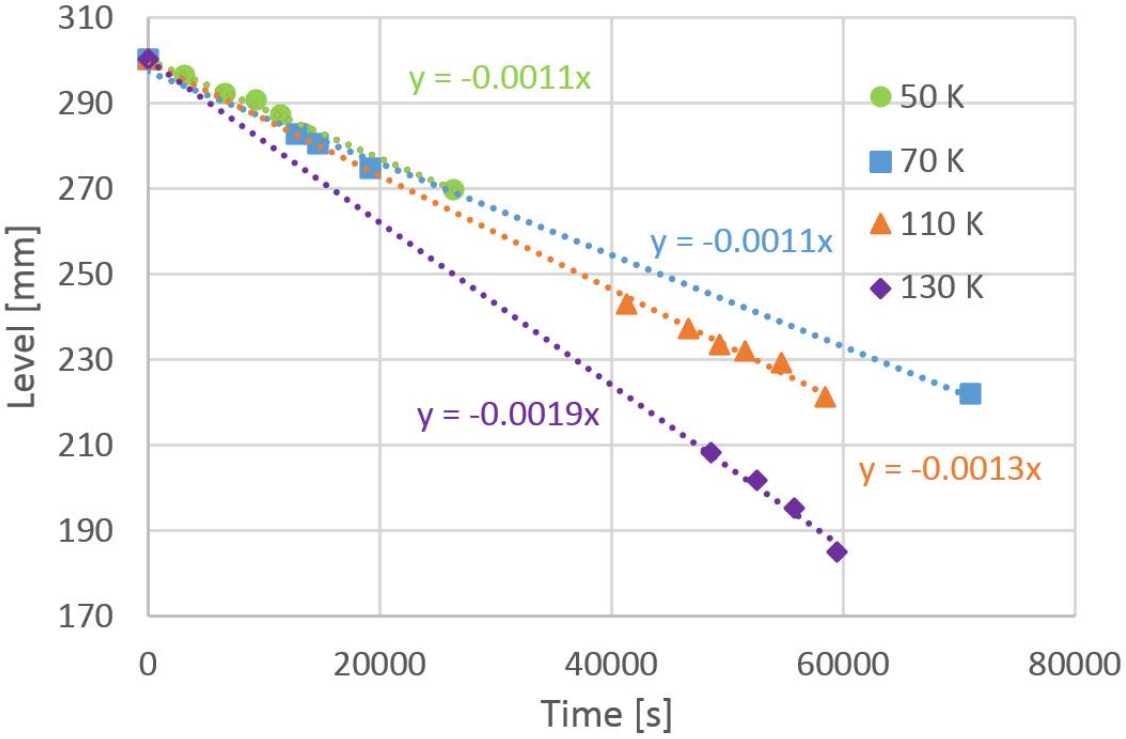

Figure 35: Evaporation of helium to 4.2 K due to heat flux vs time for different temperatures of the ATS

The corresponding heat flux calculated is shown in figure 36.

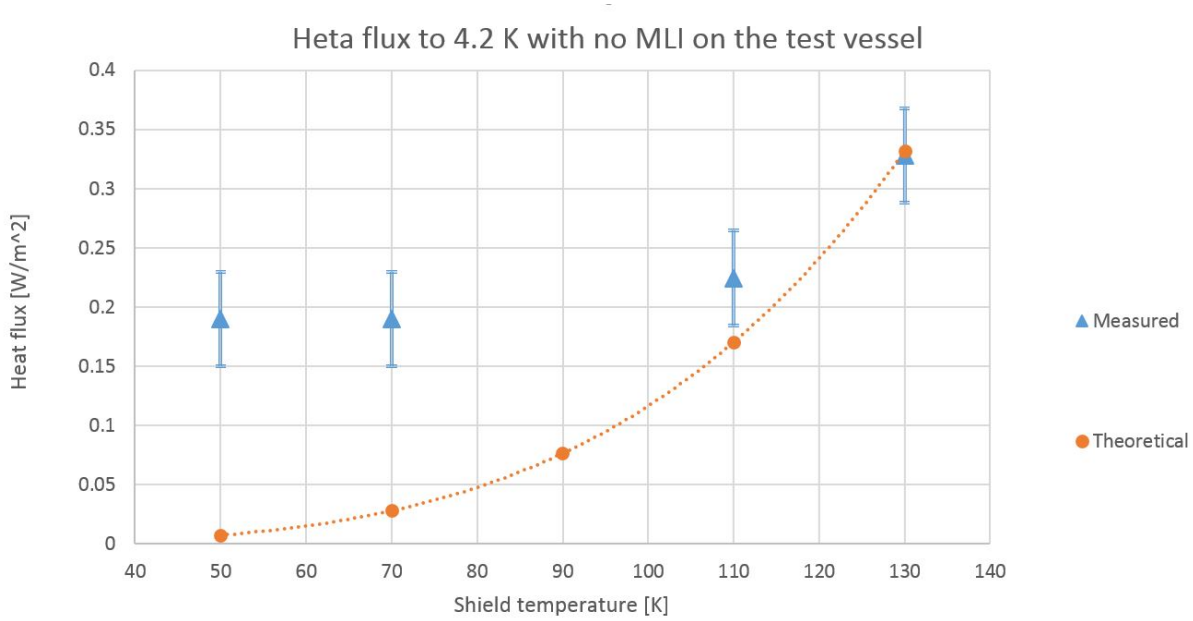

Figure 36: Preliminary measurement results by liquid level meter of heat flux to 4.2 K with no MLI on the test vessel

3.7.3 Test with liquid helium and 1 aluminized foil applied

As the temperature of the ATS in the configuration helium-nitrogen with no MLI did not reach a value lower than 50 K the decision to improve the thermal contact between the ATS and its support and between the support and the guard vessel has been made before launching the test with 1 layer MLI. For this purpose indium has been placed in between all the interfaces to increase the contact areas. The thermal screen during cool down reached successfully 19 K in steady-state with no extra heat applied. In order to reach a temperature of the ATS of 60 K a power of 6 W was applied. Being the flow of helium still out of the range of the flowmeter, the level meter was used again. At low temperatures of the screen the placement of 1 aluminized foil resulted in a decrease of the heat flux to the test vessel, see figure 37.

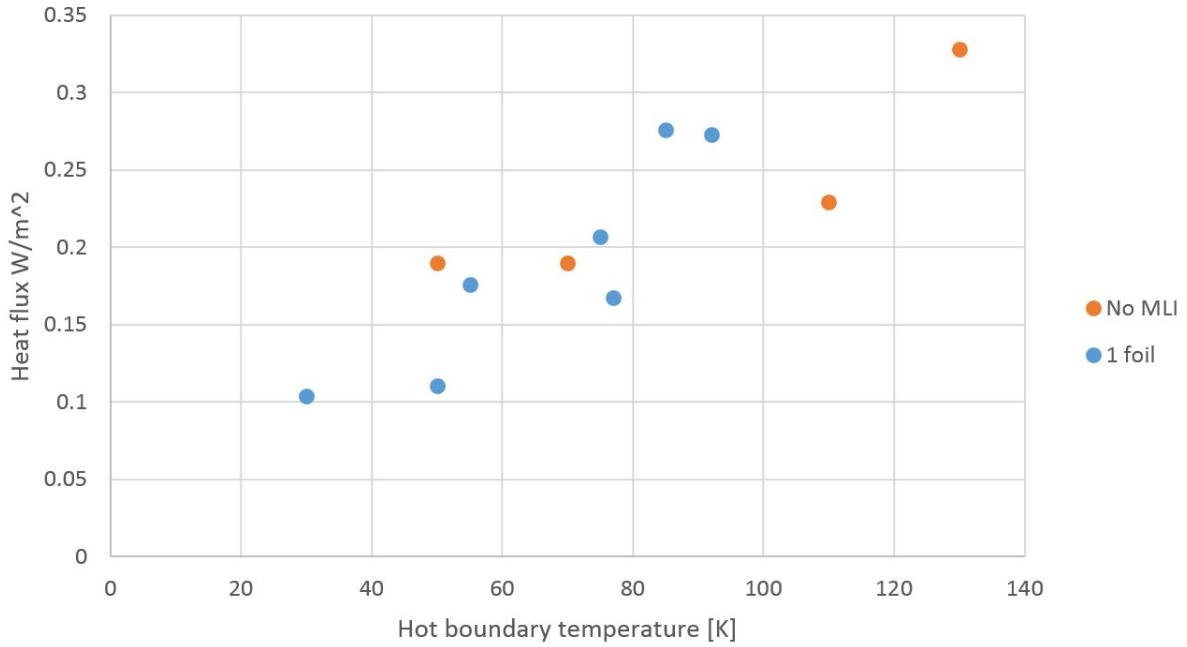

Figure 37: Preliminary measurement by level meter of heat flux to 4.2 K for the configurations bare test vessel and test vessel wrapped with 1 aluminized foil

3.7.4 Conclusions from the first run

The first test with liquid helium showed that the ATS did not reach the temperature desired so some indium was added on the support in this occasion. Measuring the heat flux by the level meter was also considered not ideal and a new flowmeter was installed. The heat probably coming from thermal radiation through the pipes and oscillations of the feeding lines was still very high and improvements were needed.

3.7.5 Improvements on the system

The level meters have been equipped with 6 foils of strong aluminized Mylar in order to cut thermal radiation from ambient, see figure 38.

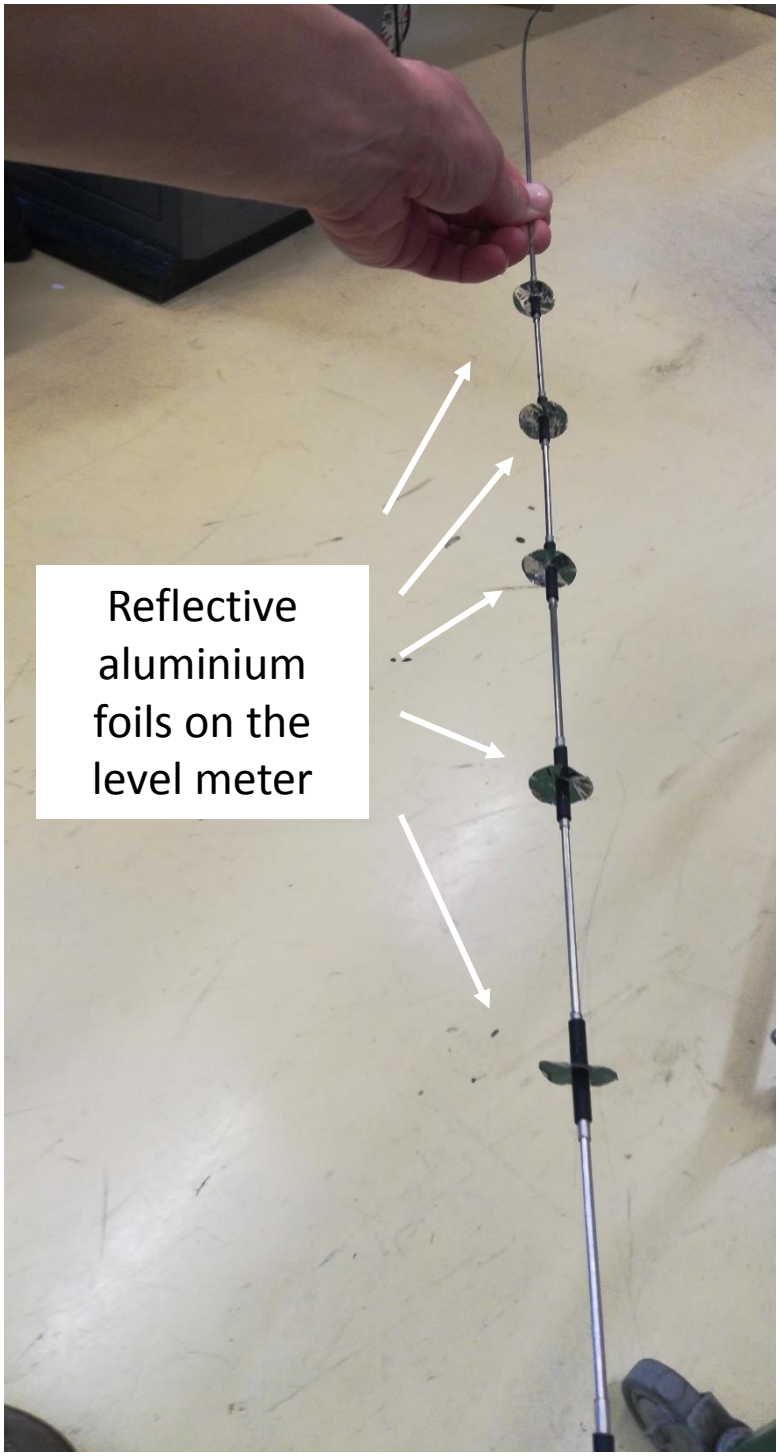

Figure 38: Aluminum foil discs inserted to cut thermal radiation in the pipe coitaining the level meters

The feeding lines of the guard vessel and test vessel have been equipped with some G10 spacers around them in order to keep them in position against oscillations during boiling. After some modification the results were still unsatisfying see figure 39

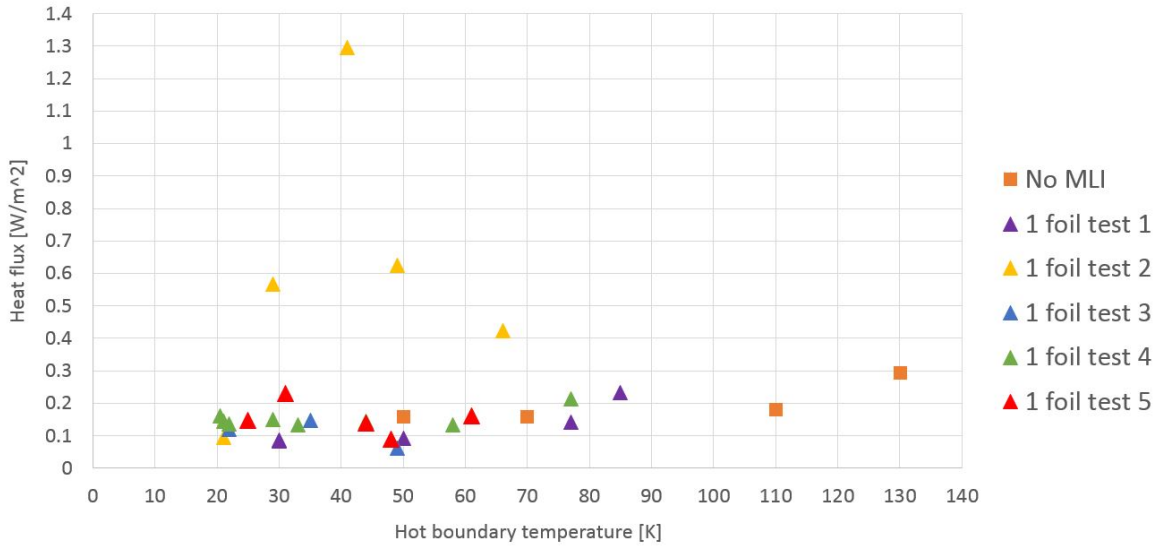

Figure 39: Preliminary measurement through level meter of teat flux to 4.2 K for the configurations bare test vessel and test vessel wrapped with 1 aluminium foil

The results showed a big uncertainty on the measuring methodology. One possible reason for having different results could be explained by a pressure fluctuation on the test vessel during measurements.

3.8 Second run for method development

3.8.1 Pressure check on the test vessel and new flow-meter

Even after trying to improve the background heat load there was an open question about why measurements differed so much one from the other. An important aspect that was not taken into consideration was the assumption that the pressure on the outlet of the test vessel was constant. The outlet of the evaporating helium was connected with a gasometer whose pressure was normally checked at distance and it was trusted to have no big excursion. The decision to insert a pressure sensor on the tests vessel's outlet was nevertheless taken. The result of such measurements were unexpected but could explain the reason of the data fluctuations. The pressure was changing over 30 mbar when any other user was doing some changes in another cryostat. An error coming from a pressure change of this magnitude was calculated to be unacceptable. The system was then connected to an external helium recovery system used only by the liquefier technicians and the pressure was monitored for a few days. Atmospheric pressure changes of $5 - 6$ mbar were noticed within a day, the time for measurements was too short to be

influenced by those changes so the result of the choice was satisfactory. The extra or released heat flux for a saturated liquid is considered in the measurements window of 10 minutes. The average changes found were of the order of 0.1 mbar which produce an extra or released heat of $0.5\,\mathrm{mW/m^2}$. Considering also the possible influence of heat coming through the level gauges, a flow meter $0-1\,\mathrm{m^3/min}$ helium belonging to the lab has also been installed.

3.8.2 Calibration curve at zero thermal radiation

With the installation of the new flowmeter covering the range $0-1\,\mathrm{m^3/min}$, a calibration curve was built.

The cryostats background heat load was measured by reducing the ATS temperature, via a special support, down to 11 K thus cancelling its thermal radiation heat contribution. The test vessel was covered with a 10 layer MLI blanket with a packing density of 20 layers/cm. A calibration curve was built in these conditions in order to directly correlate the mass flowmeter signal in volts to the external heat load coming into the tank. A four wire measurement of the electrical heating power in the test vessel allows to directly correlate the signal of the flowmeter to the heat flux. An example of the response is shown in figure 40.

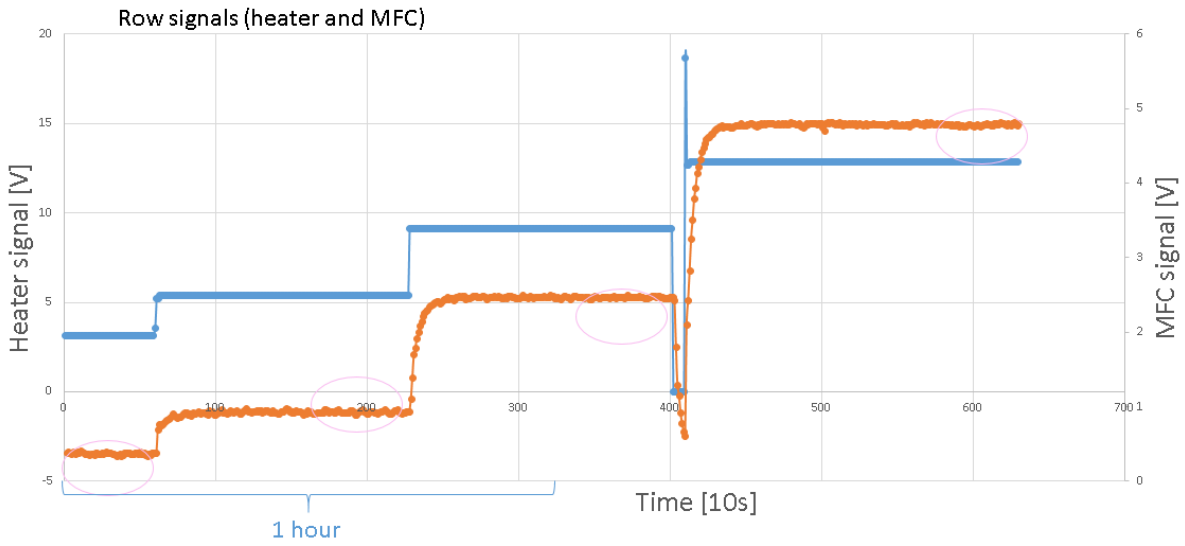

Figure 40: Typical response for the flow meter signal to the heat applied in steps. The time for a stable flowmeter signal is around 20 min

The effect of the gaseous helium filling the volume created by the evaporation of liquid is therefore taken into account as well as effects from the tubes pre-cooling by the exhaust flow. As a result, a systematic background error heat load of 20 mW was extrapolated, as can be seen in figure 41.

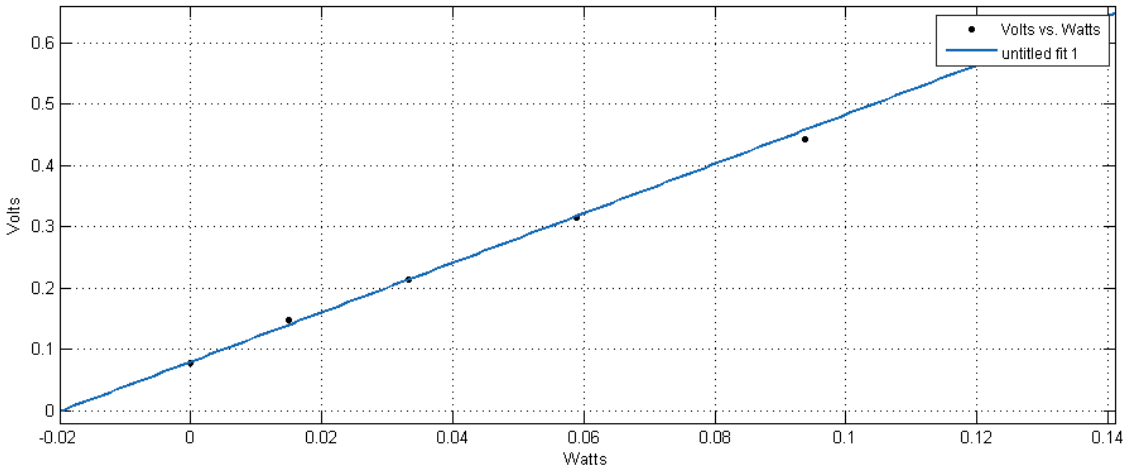

Figure 41: Calibration curve made with ATS at 11 K: several electrical heater heat loads are applied to be able to extrapolate the residual heat value of −20 mW at 0 V signal

3.8.3 Tests repeatability considerations

A study on repeatability of the test was carried out with the same blanket and repetitive measurements in different days without warming up the cryostat in order to check the errors. For each test three measurements of the flow were taken, the first one with no additional heat applied to the test vessel, the second one with 33 mW applied and the third with 133 mW applied. The test shows that the repeatability of the signal is getting better and better when the signal is in a higher range, see figure 42, 43 and 44. The deviation of the signal in the three cases goes from 17 % (no heat applied) to 4.2 K % at 33 mW applied and to 0.9 % at 133 mW applied.

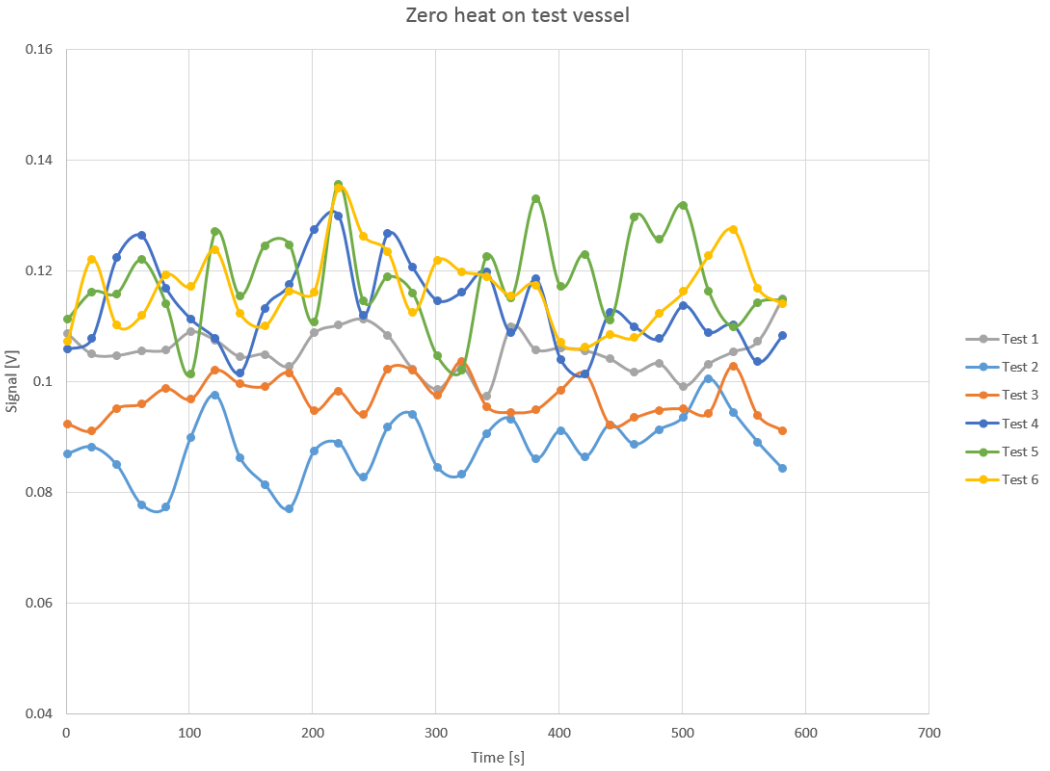

Figure 42: Repeatibility of signal for zero heat applied to the test vessel

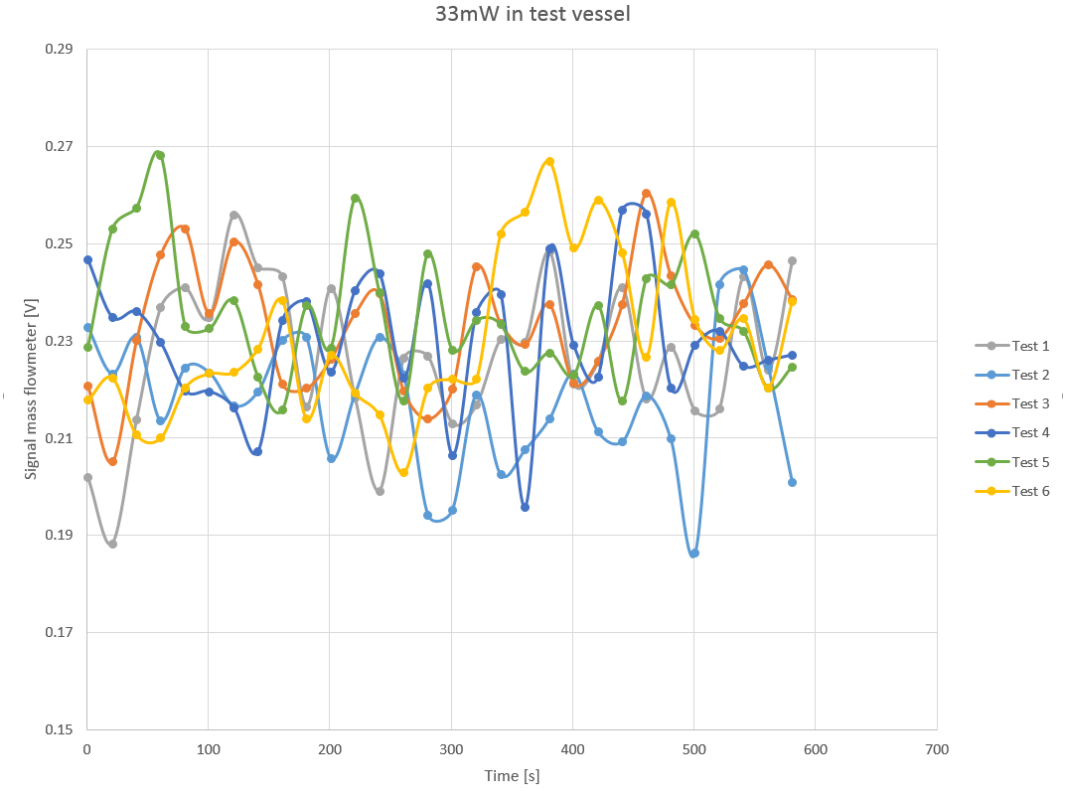

Figure 43: Repeatibility of signal for 33 mW applied to the test vessel

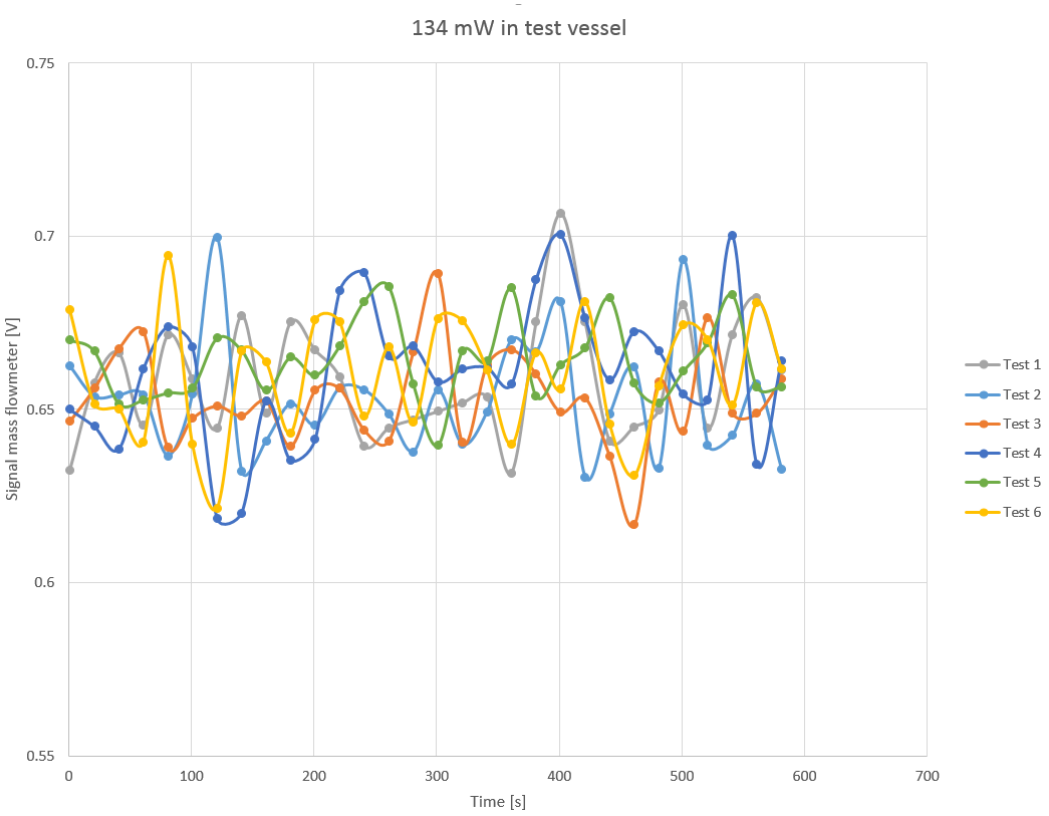

Figure 44: Repeatability of signal for 1133 mW applied to the test vessel

The test repeatability consideration lead to the decision of measuring the signal with added heat load on the test vessel for each measurement point in order to improve accuracy, see chapter 3.8.4.

3.8.4 Extrapolation method

The results on the repeatability lead to the decision of increasing the precision of each measured point by adding heat load in steps for each ATS temperature. For each temperature additional two points of measurements are taken by adding 33 and 133 mW to the test vessel, see figure 45.

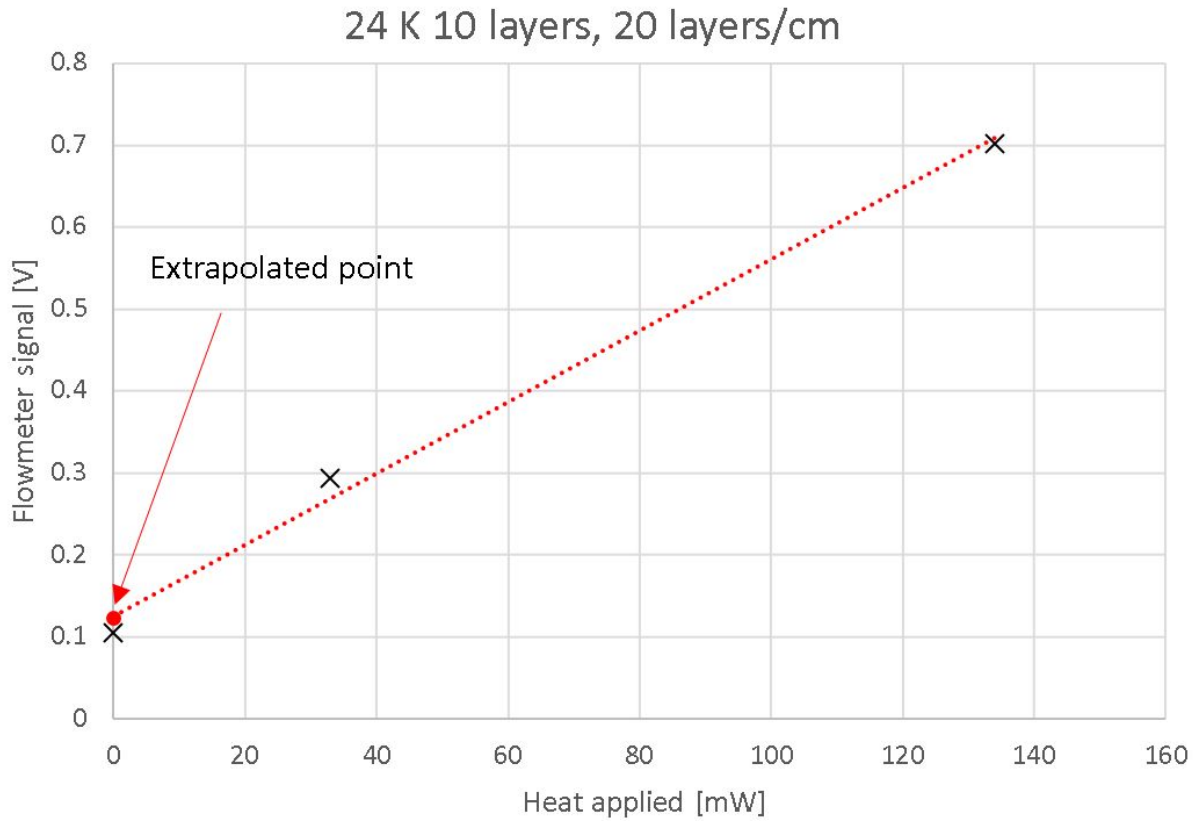

Figure 45: Methodology including interpolation and extraction of the signal based on extra heat applied on the test tank

The final interpolated signal is converted into flow using the calibration formula, see chapter 3.8.2.

3.8.5 Tests with 10 layer blankets

The second set of experiments was conducted on 3 MLI samples of 10 total layers of the kind used in LHC. The blankets have different layers density:

Sample 1: 10 layers/cm
Sample 2: 20 layesr/cm
Sample 3: 30 layers/cm

Tests have been repeated for each configuration in order to evaluate reproducibility of results and are presented in figure 46 after having corrected the systematic and statistical errors. The results seem to be uninfluenced by the temperature of the screen below 60 K.

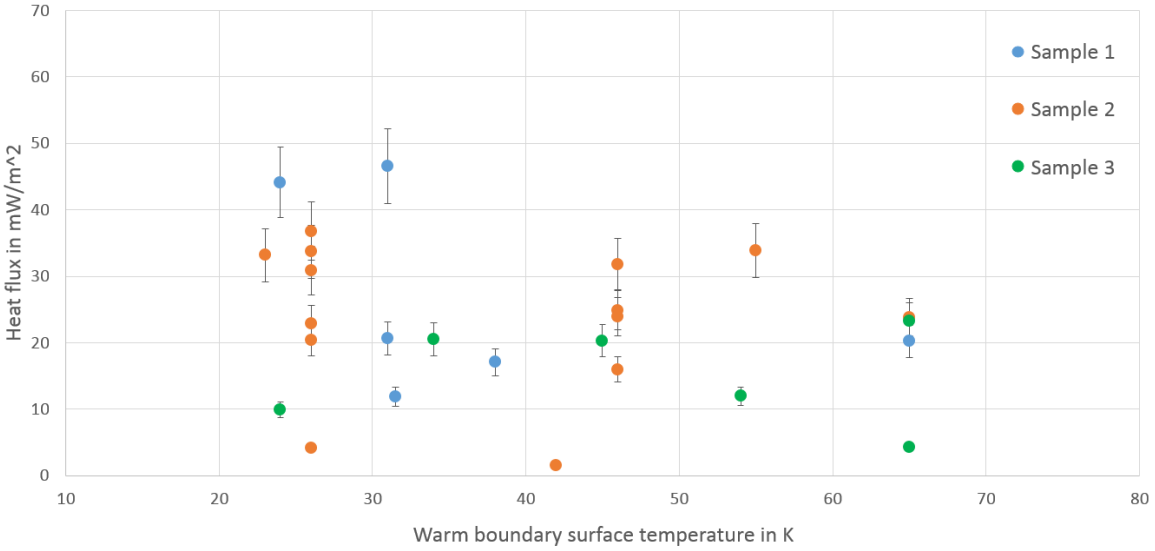

Figure 46: Results for MLI blankets with 10 layers and different layers/densities

The overall signal is too low and difficult to be reproduced for the same configurations. It seems that remaining variations are not covered in the extensive calibration procedure described in chapter 3.8.4. All the tests were performed with the bare ATS, with the hot boundary at low emissivity. It was found that the noise-to-signal ratio was too big for a direct comparison of different blankets so it was decided to increase the signal by black coating the internal part of the ATS.

3.9 Third run for method development

3.10 Black coated screen

After the first two runs of tests it was decided to black coat the ATS internally with a vacuum compatible varnish (DAG 502) in order to increase the magnitude of the signal.

No MLI insulation was applied on the test tank for a first test with the black screen. The results could be compared with a simple thermal radiation heat transfer between two cylindrical surfaces [41].

The first experiment performed with the black screen show that the temperature has an influence on the heat transfer above 60 K, see figure 47.

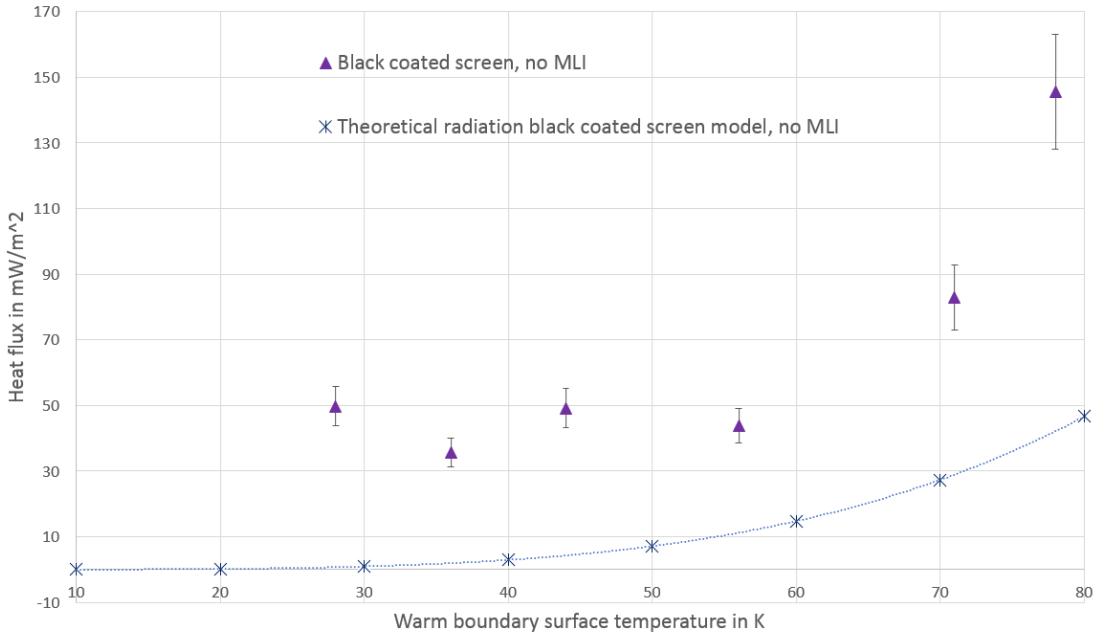

Figure 47: black coated experiments with no MLI applied on the test vessel

A second test in vacuum was performed by measuring the steady state signal with the screen at $60 - 70\,\mathrm{K}$ and then the heater was turned off and the signal was monitored till the screen reached $20\,\mathrm{K}$. It's possible to see from figure 48 that the signal was responding fast to the temperature change, which occurred in 3-4 h. It was then decided to keep this methodology as the active ATS cooling could be avoided and a lot of time could be saved.

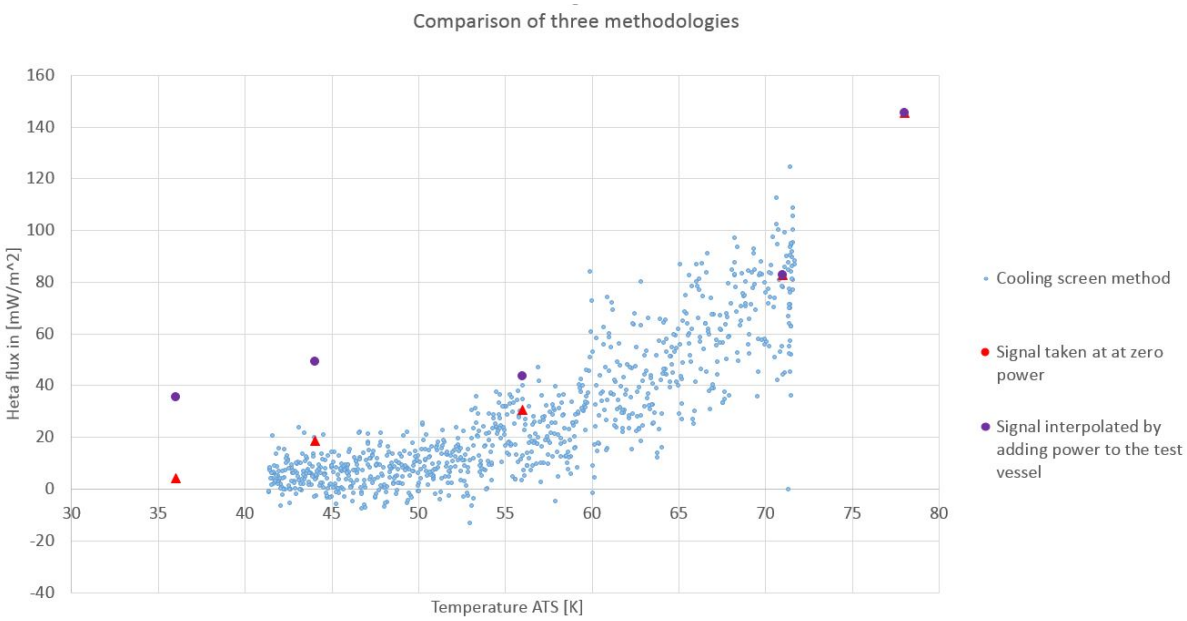

Figure 48: Comparison of three methodologies

3.11 Conclusions from the development of testing methodology

Since the first use of the test cryostat some improvements in order to minimize the background heat load have been done, including the placement of reflective layers around the level meters, spacers on the filling lines allowing for stiffness against thermo-acoustical oscillations. After performing several tests with the aluminium screen at low emissivity, it was found that the noise-to-signal ratio was too big for a direct comparison of different blankets. In order to increase the measurements sensitivity it was decided to increase the emissivity of the inner part of the shield by black coating it with a vacuum compatible varnish (DAG 502). The methodology of constructing a calibration curve for each point taken was abandoned as the intercept with the zero heat applied differs too much from the zero heat applied direct measurement. The methodology of adding heat in steps for reaching higher temperature of the thermal screen is abandoned too because causing difficult-to-control effects on the guard vessel which is thermally connected through the pipes and the baffles with the test vessel. Instead the screen is kept at a high initial temperature during cool down and is let to decrease its temperature slowly while measurements are taken. The method is used just for pressures below 2×10^{-5} mPa measured at room temperature on the test vessel. A calibration curve has been build in order to have a direct correlation for the flowmeter signal and the corresponding heat. The curve was built by setting the ATS at 11 K with a special support allowing to reach low temperatures and by applying heat loads no the test vessel with a 4 wires measurements heater with resistance 158 Ω. This method is included in order to avoid any uncertainty about the flowmeter performance.

4 Experimental results

4.1 Case 1: bare vessel

4.1.1 Tests in vacuum for case 1

Case 1 is the configuration of a bare test vessel with no insulation applied. The heat transfer is measured through the cooling screen method, see chapter 3.11. Results in good vacuum are shown in figure 49. The heat flux is considerably dropping at around 60 K with a residual pressure 7×10^{-7} mbar. The heat flux has a quite stable value of 20 $\mathrm{mW/m^2}$ below 50 K. The errorbars are found during the calibration process, especially they are described in chapter 3.5.

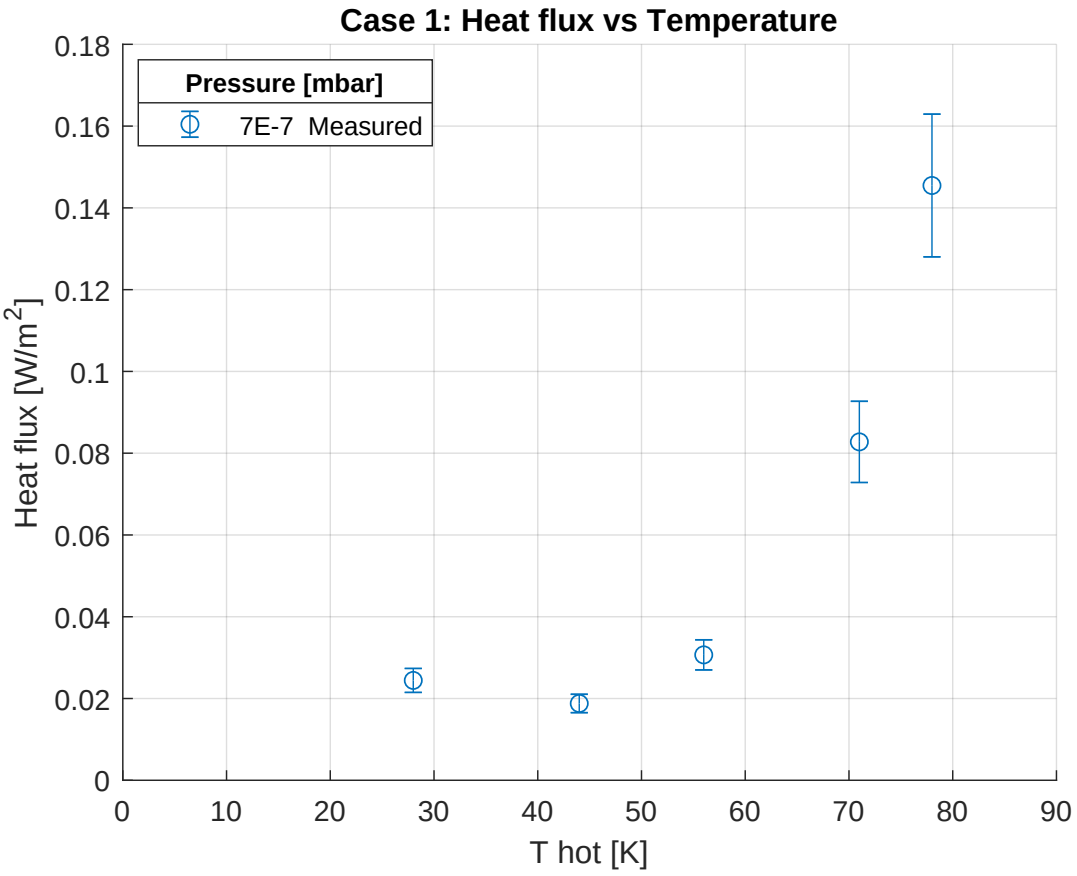

Figure 49: Heat flux to 4.2 K for bare vessel and 7×10^{-7} mbar residual pressure

The experimental results are compared with the mathematical model build for this specific configuration in chapter 4.6.2. The pressure measured in the volume inside the test vessels, which for case 2, 3 and 4 would serve to check the pressure underneath insulation, was measured to be in the one order of magnitude higher than the one measured in the vacuum vessel outside the ATS. This was interpreted as the impossibility of reaching the same vacuum level inside the pipe due to the geometry of the volume despite no insulation was present. The same result was noticed for the other configurations.

4.1.2 Tests in degraded vacuum for case 1

The tests in the degraded vacuum were performed with the introduction of helium in the vacuum chamber progressively till reaching the level desired, see chapter 3.3.2 for description of the degraded vacuum system. The results are shown for 2×10^{-5} mbar, 1×10^{-4} mbar and 2×10^{-4} mbar residual pressure in figure 50, together with the case of good vacuum. Reaching the desired vacuum level was quick (around 30 min per degraded vacuum level). The pressure measured in the volume inside the test vessels, which for case 2, 3 and 4 will serve to check the pressure underneath insulation, was measured to

be the same as in outer volume for degraded vacuum levels. The experimental results are compared with the mathematical model build for this specific configuration in chapter 4.6.2.

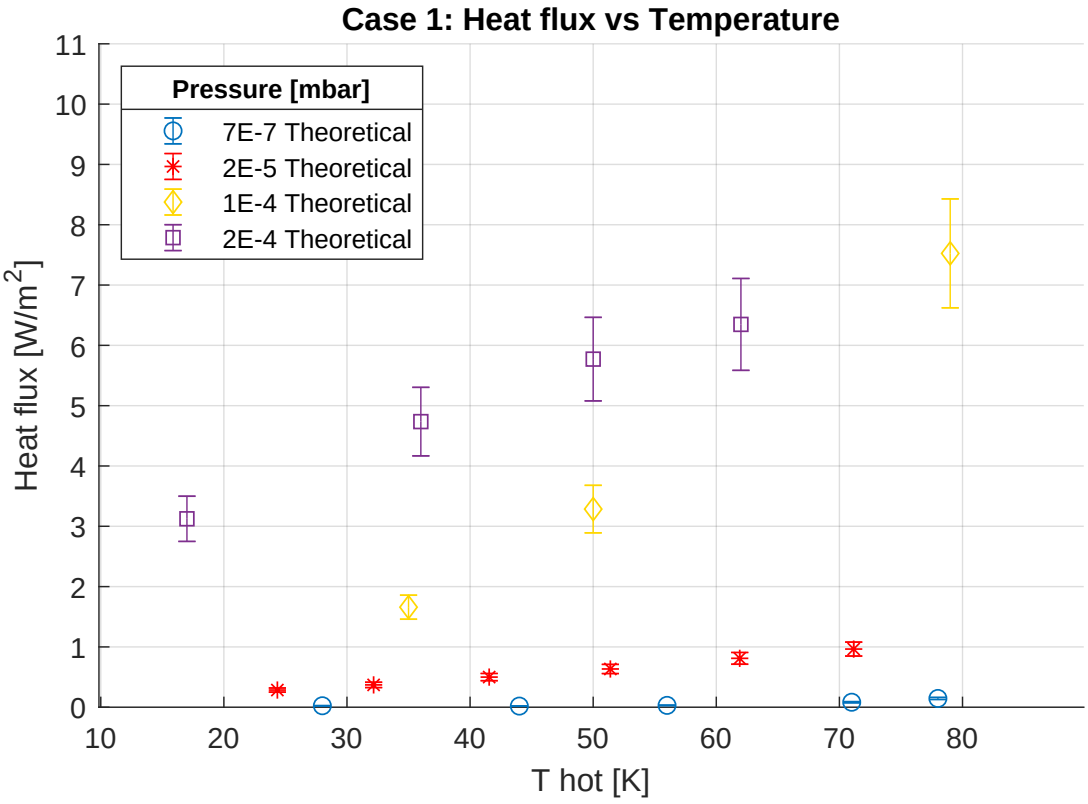

Figure 50: Heat flux to 4.2 K for bare vessel and different levels of residual pressure

The heat transfer considerably increases above $1\,\mathrm{W/m^2}$ when the residual pressure is over 2×10^{-5} mbar.

4.2 Case 2: single foil tests

4.2.1 Tests in vacuum for case 2

The second case is the one where 1 aluminized Mylar foil is wrapped around the test vessel. The foil is of the reinforced kind which are normally used for the outer or inner part of a blanket to give some strength. the aluminium foil has a spacer netting glued on its side in contact with the test vessel. Results of performance of this type of insulation are shown in figure 51. The heat flux is of the order of 0.2 mW/m^2 at temperature below 55 K.

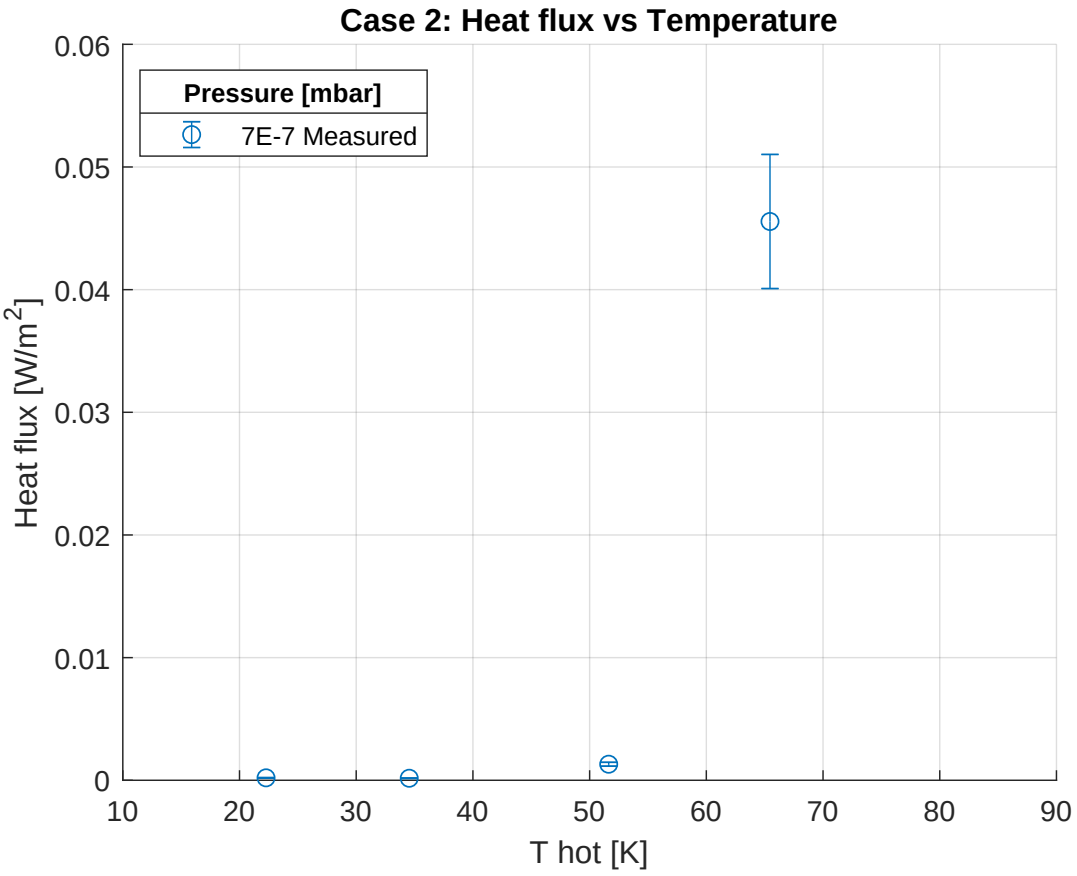

Figure 51: Heat flux to 4.2 K for single foil configuration and 7×10^{-7} mbar residual pressure

The experimental results are compared with the mathematical model build for this specific configuration in chapter 4.6.3. An comparison can be done with the case 1, configuration with a bare stainless steel vessel and the result is a dramatic decrease of the the heat flux already with one foil as insulation, see figure 52.

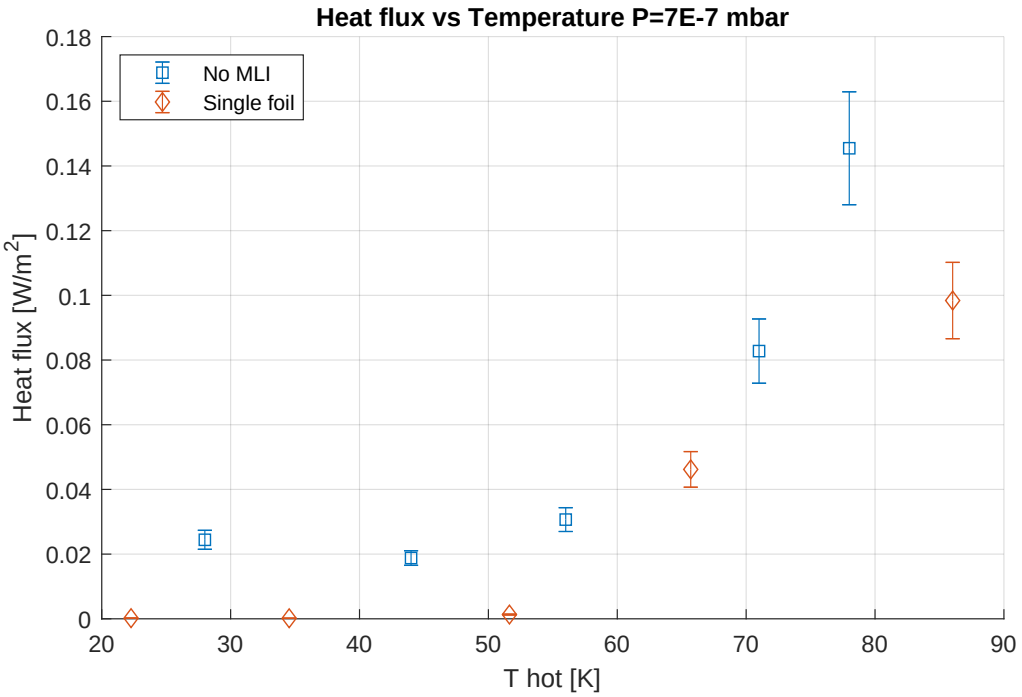

Figure 52: Heat flux to 4.2 K for single foil and bare vessel configurations configuration in the case of 7×10^{-7} mbar residual pressure

4.2.2 Tests in degraded vacuum for case 2

The tests in the degraded vacuum for case 2 were performed with the introduction of helium in the vacuum chamber progressively till reaching the level desired, see chapter 3.3.2 for description of the degraded vacuum system. The results are shown for 2×10^{-5} mbar, 1×10^{-4} mbar and 2×10^{-4} mbar residual pressure in figure 53. Reaching the desired vacuum level was quick as for case 1 (around 30 min for each point of degraded vacuum level).

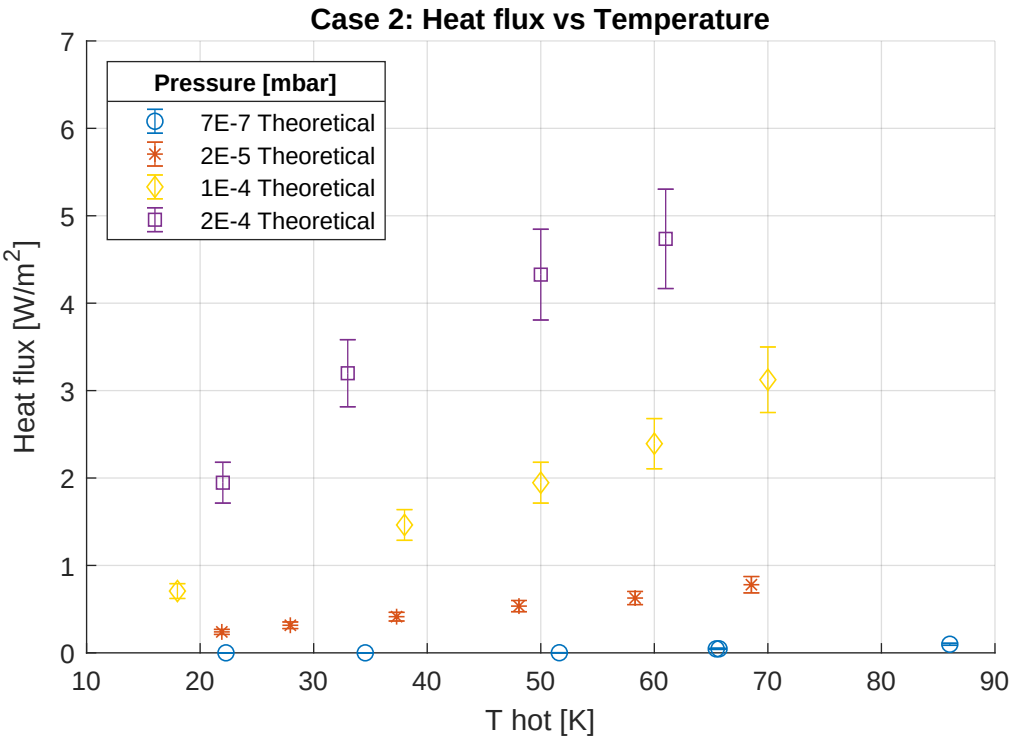

Figure 53: Heat flux to 4.2 K for single foil configuration and different levels of residual pressure

Also in this case the heat transfer is below 1 W/m^2 for residual pressures above 2×10^{-5} mbar. The experimental results are compared with the mathematical model build for this specific configuration in chapter 4.6.3.

4.3 Case 3: blanket with low layer density

4.3.1 Tests in vacuum for case 3

The case 3 is the configuration with a 10 layers MLI blanket appositely build in order to have a low layer density (see chapter 3.6). The results are shown in figure 54 and they are similar to the configuration with only one foil below 50 K but they show a better performance for the blanket at higher temperatures.

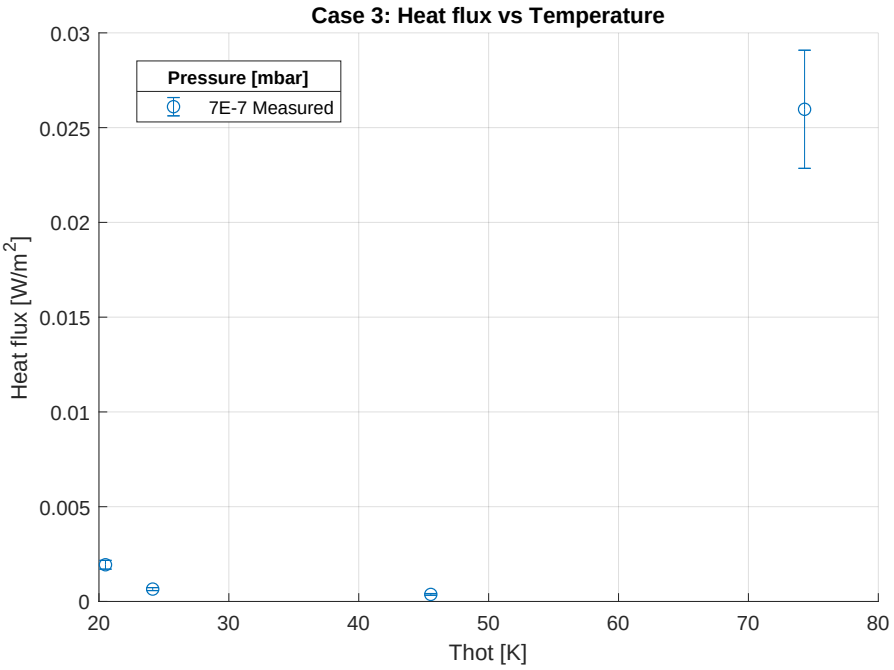

Figure 54: Heat flux to 4.2 K for a 10 layers blanket, with 10 layers/cm packing density and 7×10^{-7} mbar residual pressure

All the experimental results are compared in chapter 4.5. The experimental results for case 3 are compared with the mathematical model build for this specific configuration in chapter 4.6.4.

4.3.2 Tests in degraded vacuum for case 3

The tests in the degraded vacuum for case 3 were performed with the introduction of helium in the vacuum chamber progressively till reaching the level desired, see chapter 3.3.2 for description of the degraded vacuum system. The results are shown for 2×10^{-5} mbar, 1×10^{-4} mbar, 2×10^{-4} mbar and 1^{-3} mbar residual pressure in figure 55. The degraded vacuum takes around 1 hour to be reached in the case of a blanket.

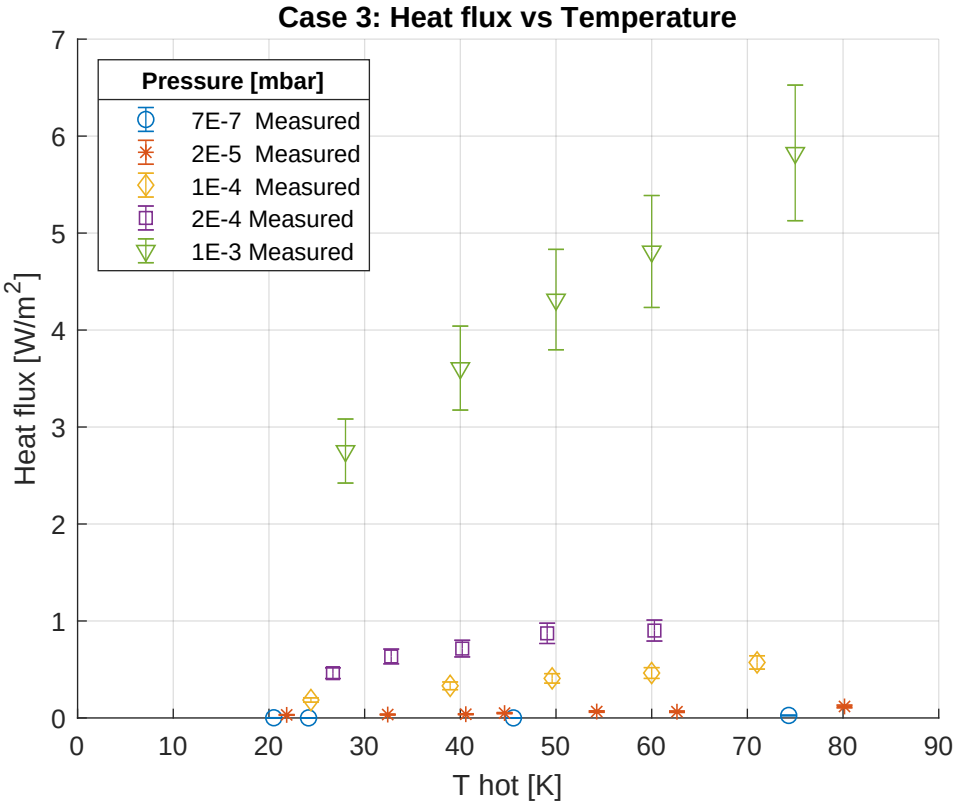

Figure 55: Heat flux to 4.2 K for a 10 layers blanket, with 10 layers/cm packing density and 2×10^{-5} mbar residual pressure

Results show an improvement of the heat flux on the test vessel compared to the case 1 and 2. The experimental results are compared with the mathematical model build for this specific configuration in chapter 4.6.4.

4.4 Case 4: blanket with high layer density

4.4.1 Tests in vacuum for case 4

The case 4 is the configuration with a 10 layers MLI blanket appositely build in order to have a low layer density of 50 layers/cm (see chapter 3.6). The results in good vacuum are shown in figure 54. The performance is degraded compared to the configuration of a blanket with the same number of layers and lower packing density. The heat flux is $10\,\mathrm{mW/m^2}$ higher in the low ATS temperature range and around $15 - 20\,\mathrm{mW/m^2}$ higher for temperatures above 50 K. All experiments are compared in section 4.5.

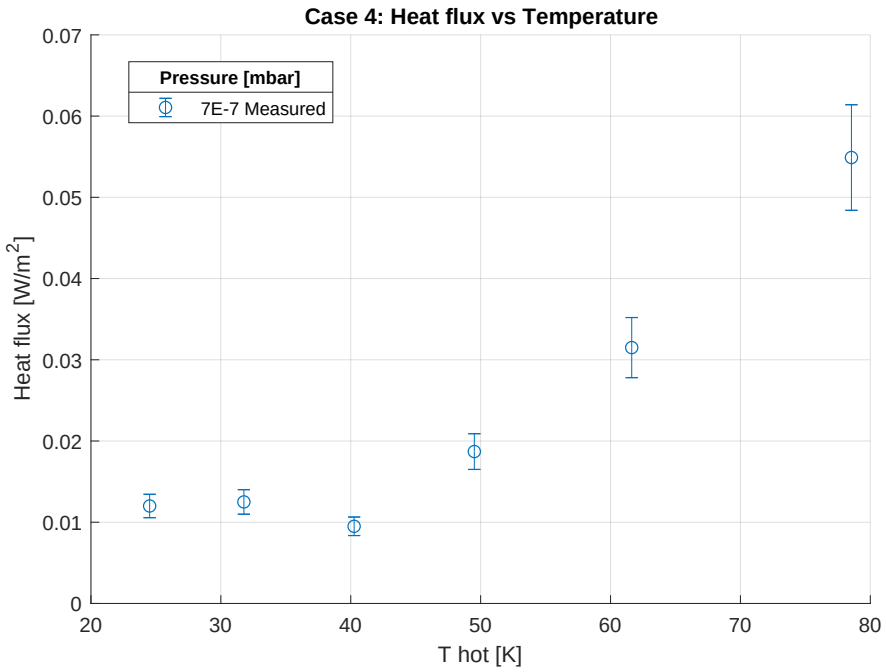

Figure 56: Heat flux to 4.2 K for a 10 layers blanket, with 50 layers/cm packing density density and different levels of residual pressure

The experimental results are compared with the mathematical model build for this specific configuration in chapter 4.6.5.

4.4.2 Tests in degraded vacuum for case 4

The tests in the degraded vacuum for case 4 were performed with the introduction of helium in the vacuum chamber progressively till reaching the level desired, see chapter 3.3.2 for description of the degraded vacuum system. The results are shown for 2×10^{-5} mbar, 1×10^{-4} mbar, 2×10^{-4} mbar and 1×10^{-3} mbar residual pressure in figure 57.

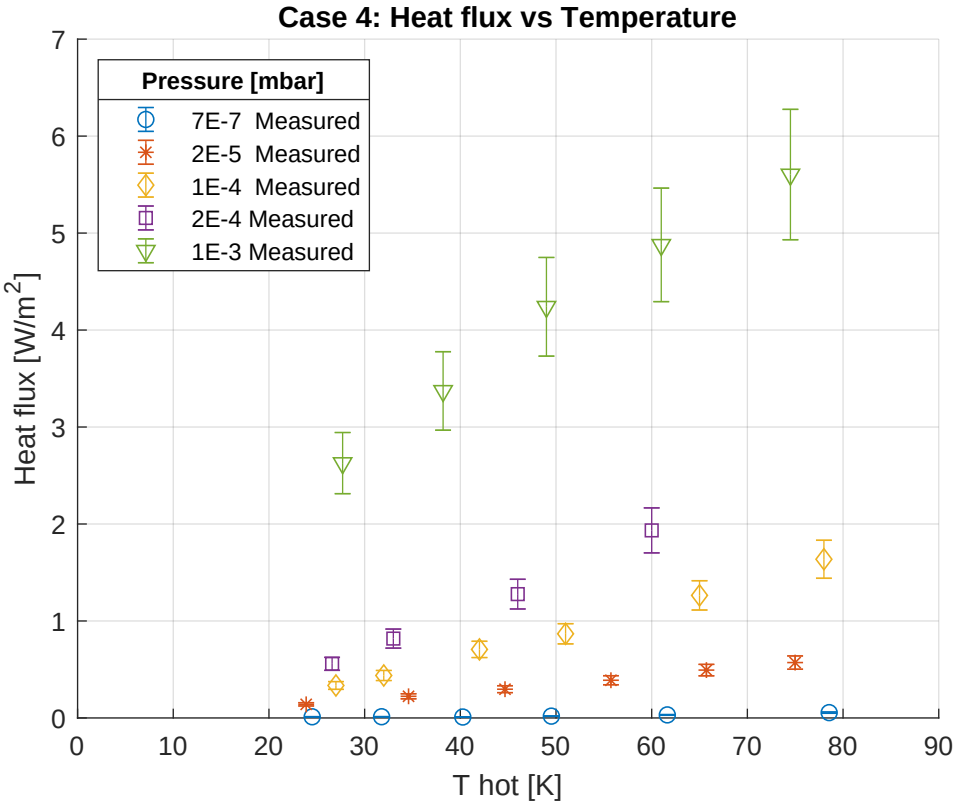

Figure 57: Heat flux to 4.2 K for a 10 layers blanket, with 50 layers/cm packing density and different levels of residual pressure

Results are more and more similar to the ones for a blanket with low packing density when the vacuum degrades, see chapter 4.5. The experimental results are compared with the mathematical model build for this specific configuration in 4.6.5.

4.5 Summary of results

4.5.1 Comparison of experiments in vacuum for the different configurations

In figure 58 all the experimental results for the various cases are shown. In case 1 the heat flux is measured for a bare vessel, in case 2 the test vessel is wrapped with 1 aluminized foil, in case 2 with a 10 layers blanket at low packing density and in case 4 with a blanket with high packing density. The heat flux vs temperature follows the trend of the radiant heat law for configurations at a vacuum level of 7×10^{-7} mbar. The heat fluxes are quite stable for each case below 50 K for all configurations. Interesting to notice that below 50 K the case with 1 aluminum foil gives better performance compared to the case of a squeezed blanket: one hypothesis could be that some gas could be still trapped in between the blankets layers and give a small heat flux contribution. At higher temperatures this

tendency inverts and the presence of the 10 layers is more efficient as the radiant heat increases.

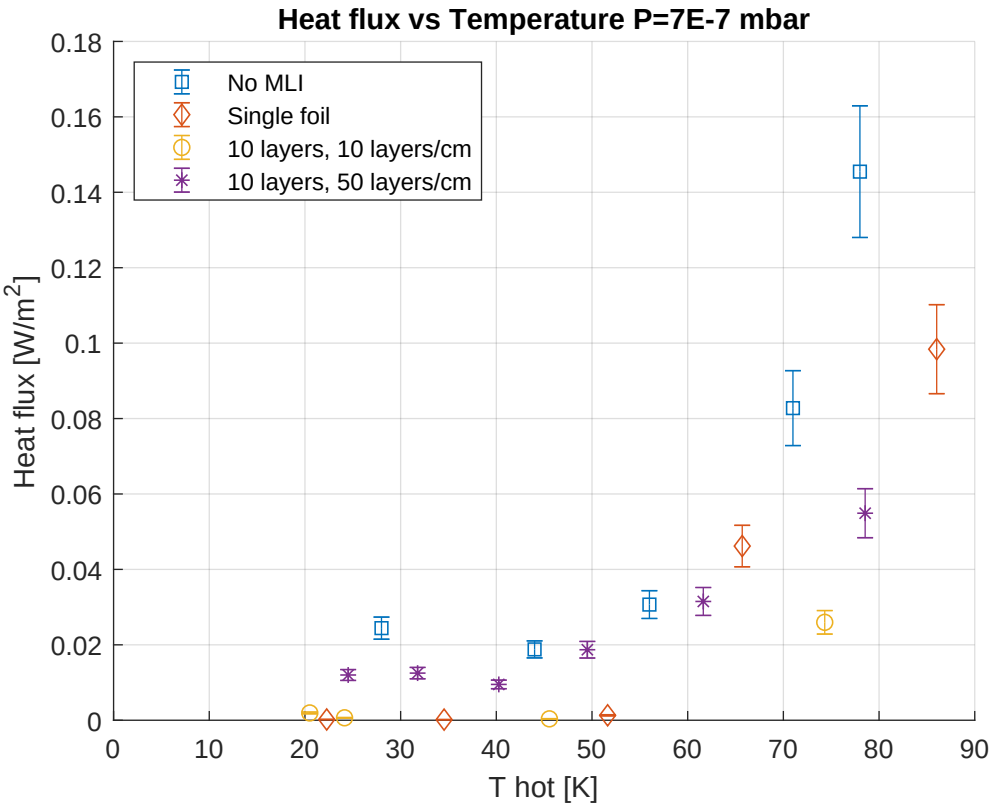

Figure 58: Heat flux to 4.2 K for different configurations of the test cryostat

4.5.2 Comparison of experiments in vacuum for the different configurations in degraded vacuum

Different levels of degraded vacuum are shown in different charts for all cases together for comparison. In figure 59 for 2×10^{-5} mbar the heat flux is below 1 W/m^2 for all cases. The behaviour looks linear with the temperature as for kinetic gas law molecular conduction formula. The heat transfer for case 1 and 2 is quite similar. Case 4 shows slightly better performance while case 3 shows a net improvement in insulation performance. The packing density plays with no doubts a key role in the performance when two blanket with same number of layers are compared.

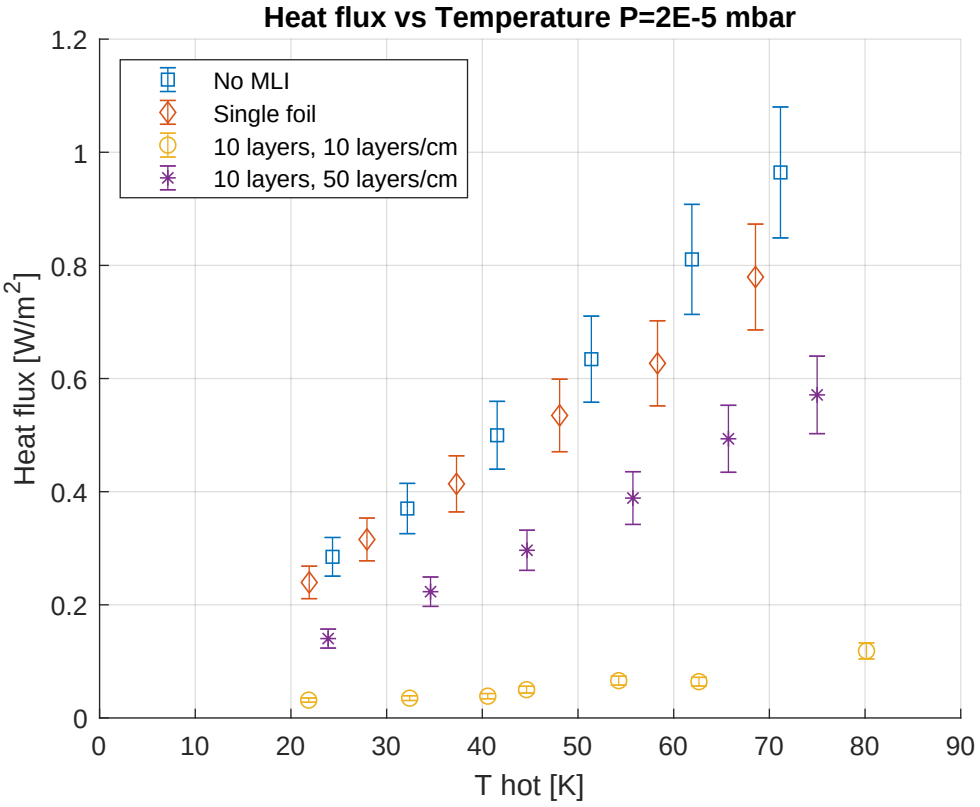

Figure 59: Comparison of heat flux to 4.2 K for different configurations at different temperatures and 2×10^{-5} mbar residual pressure

In figure 60 and 61 the performance is shown for $1^{\times}10{-}4$ mbar and 2×10^{-4} mbar residual pressure.

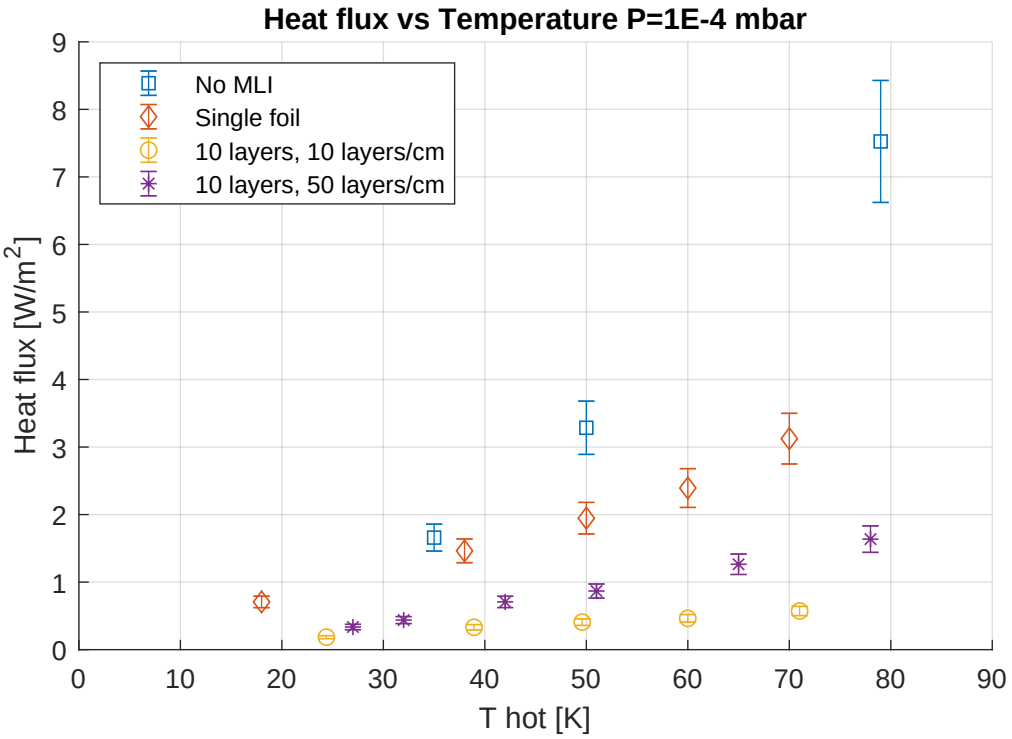

Figure 60: Comparison of heat flux to 4.2 K for different configurations at different temperatures and 1×10^{-4} mbar residual pressure

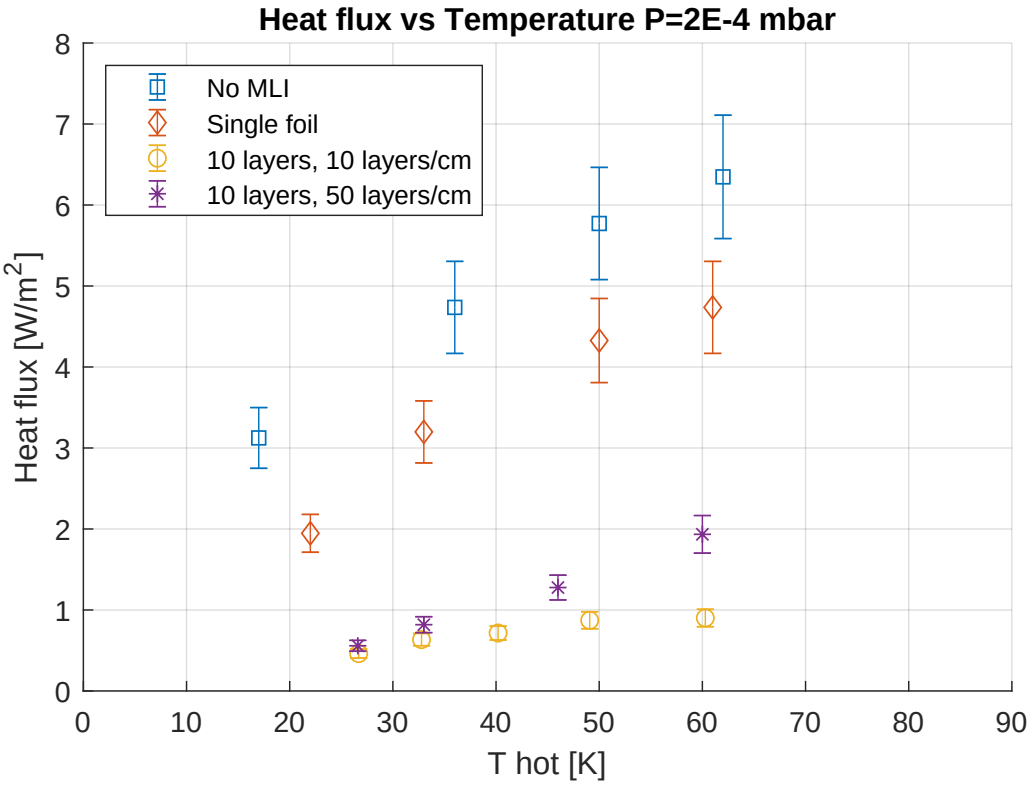

Figure 61: Comparison of heat flux to 4.2 K for different configurations at different temperatures and 2×10^{-4} mbar residual pressure

Figure 62 shows the performance of the two blankets, case 3 and case 4, for 1×10^{-3} mbar residual pressure. In this configuration the two blankets show the same performance.

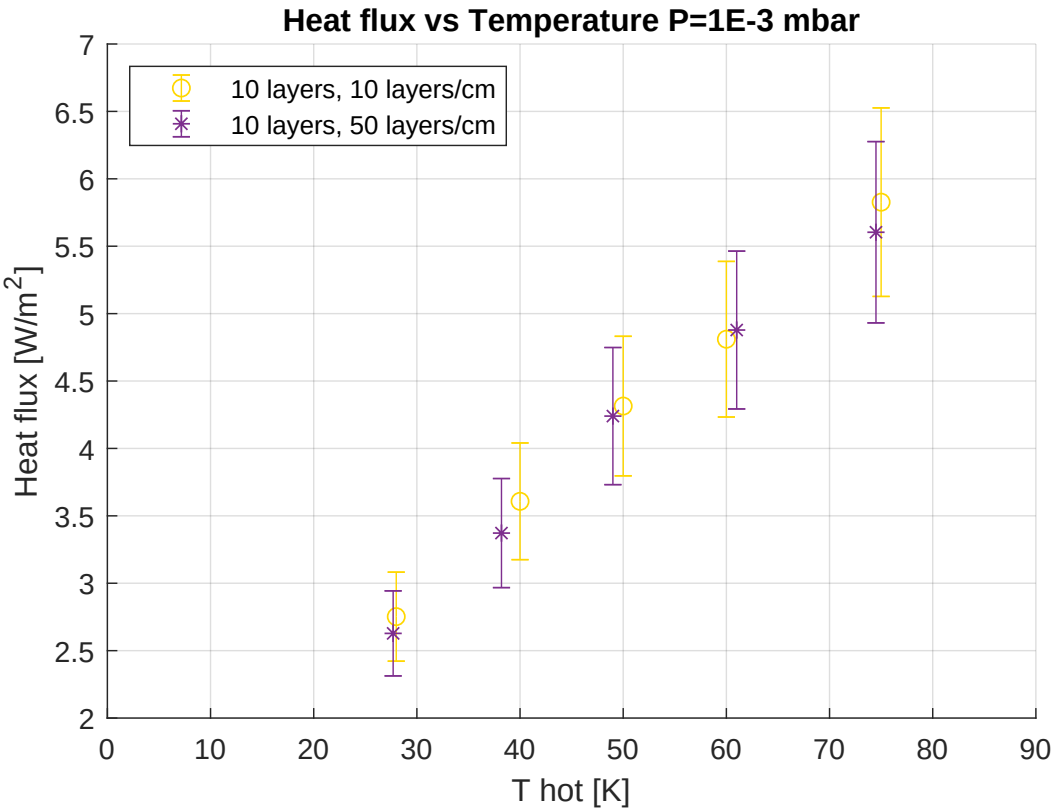

Figure 62: Comparison of heat flux to 4.2 K for different configurations at different temperatures and 1×10^{-3} mbar residual pressure

4.6 Mathematical models for MLI

The mathematical models for MLI are written for all 4 cases:

- Case 1: no thermal insulation applied on the test vessel, thermal radiation and molecular conduction are considered
- Case 2: 1 layer of aluminized Mylar applied on the test vessel, thermal radiation and molecular conduction are considered
- Case 3: a 10 layers blanket with no contact between them are present, thermal radiation and molecular conduction in between the layers are considered
- Case 4: 10 layers MLI in perfect contact are present and in contact with the test vessel, solid conduction is considered between layers, thermal radiation and molecular conduction outside the outer layer

The equations used for molecular conduction, solid conduction and thermal radiation are described in chapters 1.4.3, 1.4.4 and 1.4.5. regarding molecular conduction, figure 63 shows the comparison between the mean free path of helium at different residual pressures and different average temperatures between the cola and warm walls. The Knudsen number is higher than 1 for all temperature ranges (molecular conduction regime) from 1×10^{-7} mbar till 1×10^{-4} mbar. For residual pressure equal to 2×10^{-4} mbar the Knudsen number becomes lower than one with low boundary temperatures, and for the case at 1×10^{-3} mbar the regime is fully transient.

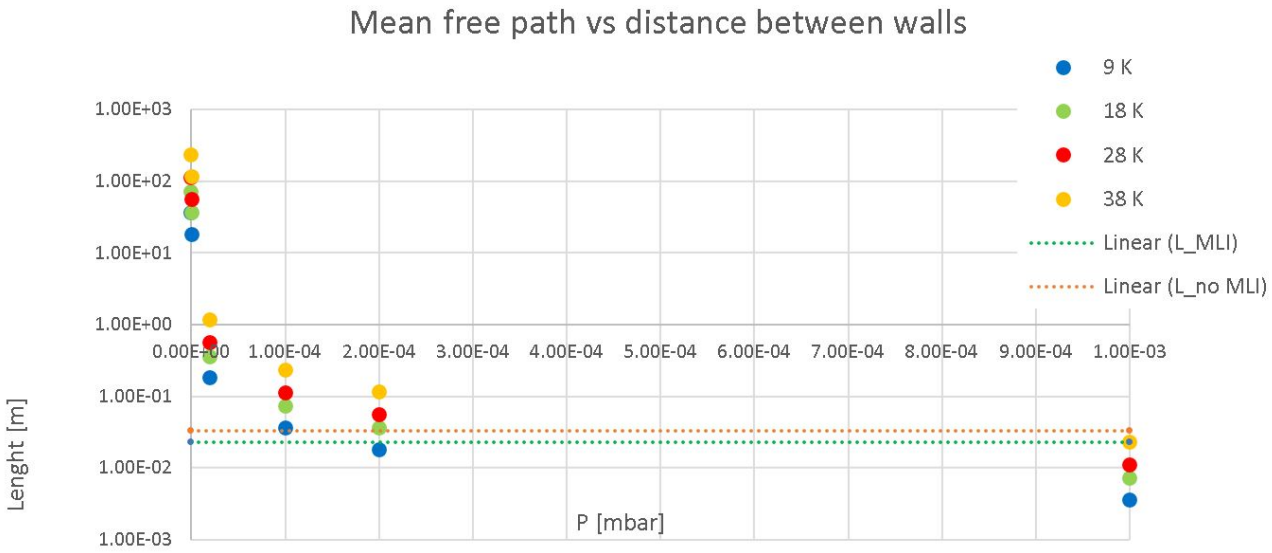

Figure 63: Free mean path for diffenet residual pressure levels and mean temperatures between walls

For the solid conduction some considerations have been made. A iterature review of thermal contact modelling in MLI systems and especially the paper from Bapat, [35] suggests that a lot of mathematical models have been introduced already in the early 90ths for all the three kind of heat transfer: solid contact, thermal radiation and molecular conduction. The complexity of the phenomenon of solid conduction between layers and the amount of work done for the prediction of the heat transfer gave the general feeling that for MLI is not easy to find a formulation that can describe any kind of MLI design working in different temperature ranges, at different pressure and packing density. This last one is probably the most unpredictable factor for the solid contact understanding. In this work, the solid contact modelling started indeed from the consideration about the contact area that exists between the layers and the polyester netting. A way to understand the total surface in contact has been found by painting of a polyester net and the insertion of it under some 10 MLI blanket, with a white paper at the bottom. The pattern of random and very heterogeneous points was uploaded on a software that can recognize the percentage of colour over the total area. The sample taken was a 20 x 20 mm^2. The total contact area found was 0.005 %, see figure 64.

Color	Color Code	Percentage
	#787878	0.723657
	#909090	0.133287
	#786060	0.121435
	#484860	0.010648
	#303060	0.005602
	#a84860	0.005046
	#903048	0.000231
	#481848	0.000093

Figure 64: Contact area found below 10 layers MLI blanket on a white surfaces with no pressure applied

4.6.1 Material properties

All material properties used in the mathematical models are summarized in Table 3

Description	Value	Unit	Reference
Aluminum foil emissivity	0.0035*T^0.5	-	Chorowski et al
Stainless steel emissivity at 4.2K	0.07	-	Obert et al
Black screen emissivity at 20-60K	0.8	-	Assumption
Polyester density	1.38	g/cm^3	Jehier
Mylar density	1.39	g/cm^3	Dupont
Polyester thermal conductivity at 4.2 K	0.00743	W/(m K)	NIST
Mylar thermal conductivity at 4.2 K	0.00743	W/(m K)	NIST
Mylar specific heat	1172	J/kg/K	Dupont

Table 3: Material properties for mathematical models

4.6.2 Mathematical model for case 1

Case 1 is a set of experiments for a bare vessel configuration in good and degraded vacuum from 7×10^{-7} to 2×10^{-4} mbar. The surface of the stainless steel test vessel is a polished one.

For the mathematical modelling of case 1, a thermal radiation model for two infinite cylindrical surfaces is used for the contribution due to thermal radiation, in addition a model from molecular kinetic theory is used for the heat exchange through molecular conduction in degraded vacuum, see chapter 4.6.1.

$$q_{12} = \frac{\sigma \cdot (T_1^4 - T_2^4)}{\frac{1}{\epsilon_1} + \frac{1-\epsilon_2}{\epsilon_2}\frac{A_1}{A_2}} + P\alpha(T_1 - T_2)\frac{\gamma+1}{\gamma-1}\sqrt{\frac{R}{8\pi} \cdot M\frac{T_1 - T_2}{2}} \tag{4.6.1}$$

Where ϵ_1 is the emissivity of the hot surface, A_1 is the area of the external surface, ϵ_2 is the emissivity of the cold surface, A_2 is the area of the internal surface, σ is the

Stefan Boltzmanns constant, P is the residual pressure, α is an averaged accommodation coefficient which is used normally in absence of detailed gas-surface interaction models it is a measure of the the efficiency of the thermal energy interchange occurring when a particle hits a surface and it is describe in chapter 1.4.7, γ is the ratio between the isentropic expansion factor for helium, R is the Boltzmann constant and M is the molecular weigh of helium. The emissivity for stainless steel is taken from [8]. The emissivity for the ATS is taken as 0.8. In figures 65 and 66 the results of experiments and the theoretical curves are shown. The prediction looks like a good one for the case of a bare vessel.

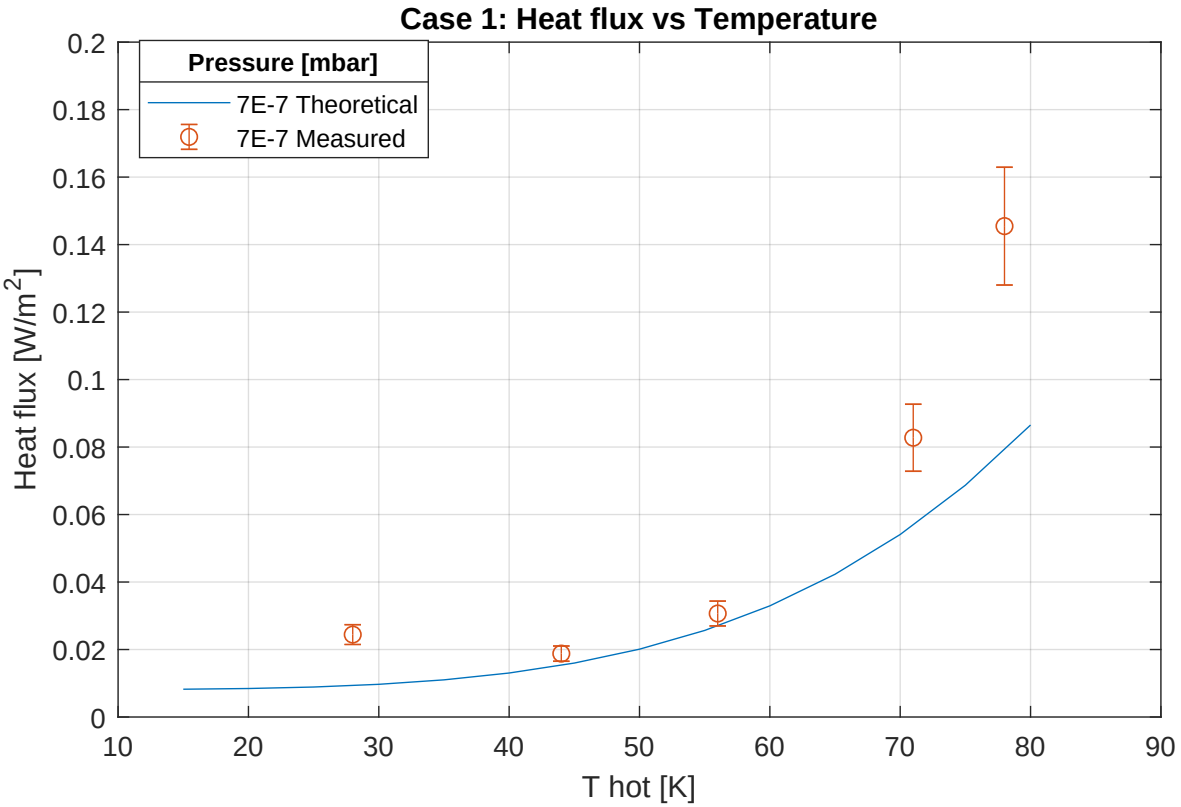

Figure 65: Mathematical model for case 1 and experimental results for good vacuum

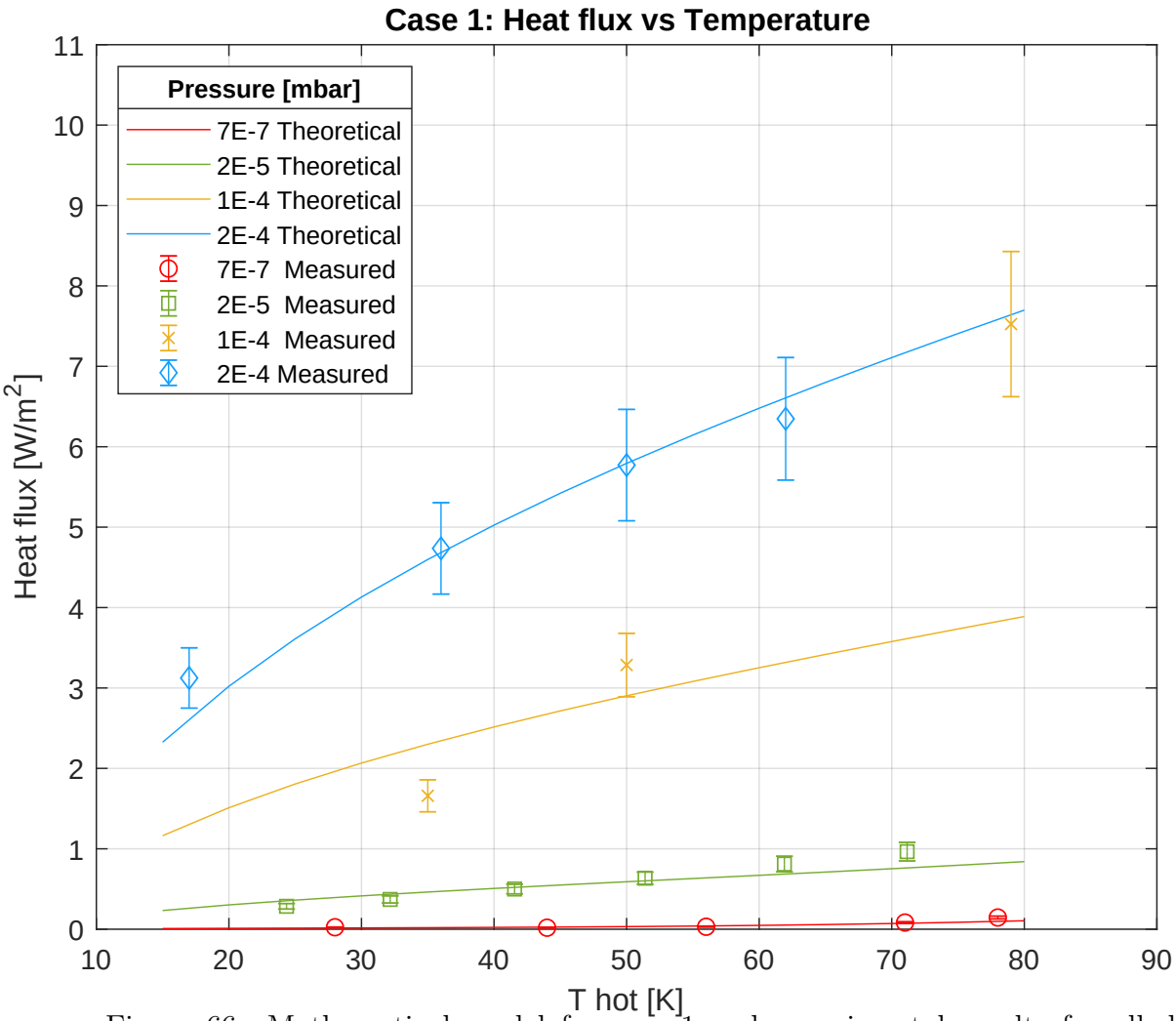

Figure 66: Mathematical model for case 1 and experimental results for all degraded vacuum levels

4.6.3 Mathematical model for case 2

For case 2, similarly as for case 1, a thermal radiation model for two infinite cylindrical surfaces is used for the contribution due to thermal radiation, and a model from molecular kinetic theory is used for the heat exchange through molecular conduction in degraded vacuum. The Cold surface is this time represented by the singe foil wrapped around the test vessel, see chapter 4.6.2.

$$q_{12} = \frac{\sigma \cdot (T_1^4 - T_2^4)}{\frac{1}{\epsilon_1} + \frac{1-\epsilon_2}{\epsilon_2}\frac{A_1}{A_2}} + P(T_1 - T_2)\frac{\gamma+1}{\gamma-1}\sqrt{\frac{R}{8\pi} \cdot M\frac{T_1 - T_2}{2}} \tag{4.6.2}$$

Where ϵ_1 is the emissivity of the hot surface, A_1 is the area of the external surface, ϵ_2 is the emissivity of the cold surface of MLI layer, A_2 is the area of the internal surface, σ is the Stefan Boltzmanns constant, P is the residual pressure, γ is the ratio between the isentropic expansion factor for helium, R is the Boltzmann constant and M is the

molecular weigh of helium. Looking at the results in figure 67, it is possible to notice that the experiments show a lower value of heat fluxes at high vacuum degradation levels. The emissivity for the aluminum foil is taken from a work by prof Chorowski [19].

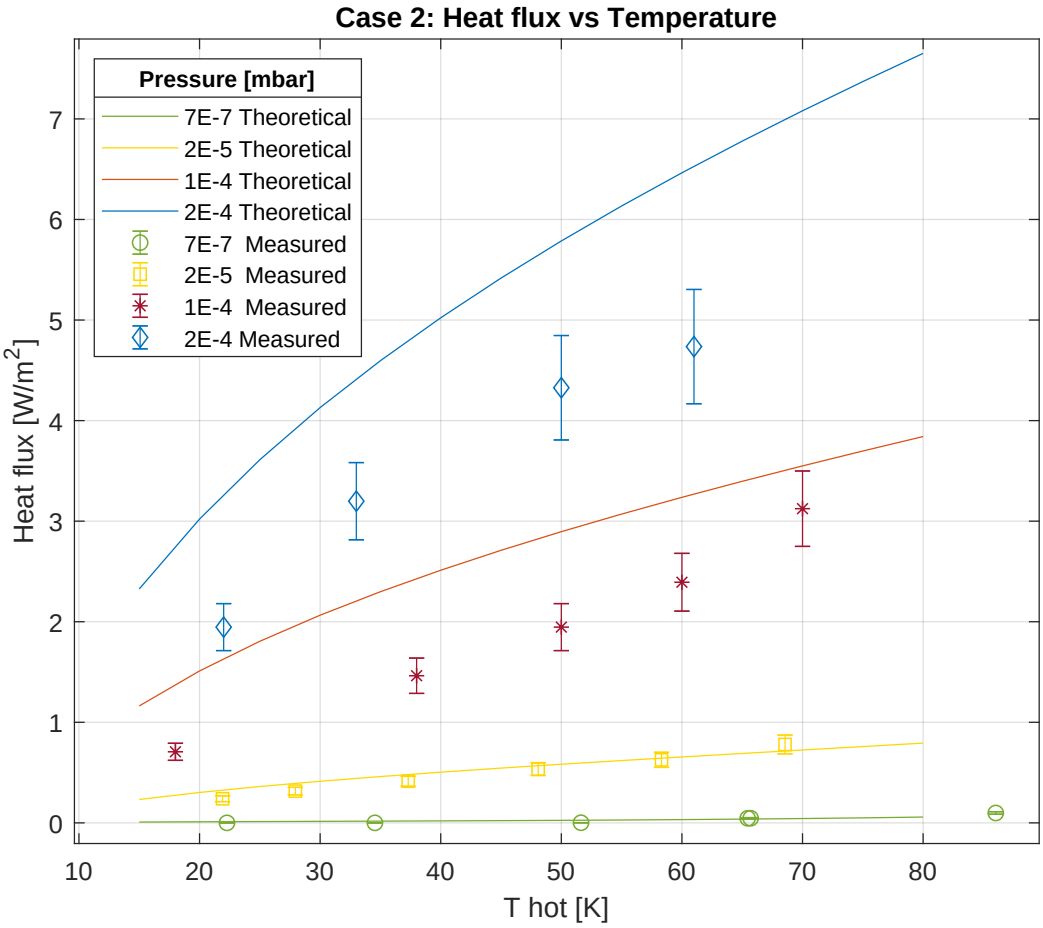

Figure 67: Mathematical model for case 2 and experimental results with correction on the residual pressure underneath MLI

By adjusting the pressure in the model, it's possible to find the residual level underneath the blanket that brings to the results see Picture 68.

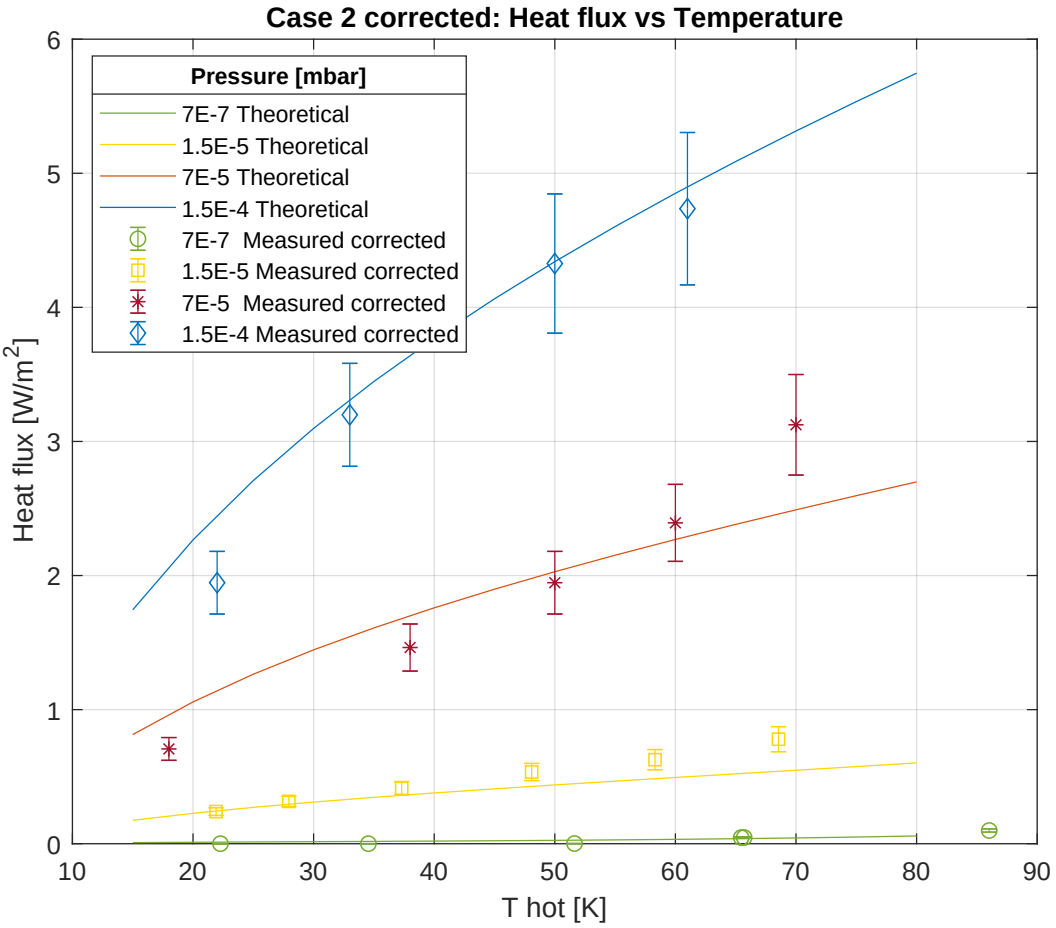

Figure 68: Mathematical model for case 2 and experimental results with correction on the residual pressure underneath MLI

4.6.4 Mathematical model for case 3

The model for Case 3 considers radiative and molecular conduction heat transfer. The blanket installed has low density so it is assumed that layers do not touch each other.

Th temperature of each layer is calculated iterating the energy balance for each layer considering its thickness and heat capacity as a Mylar body and its emissivity as an aluminum foil, see figure 69, 70, 71.

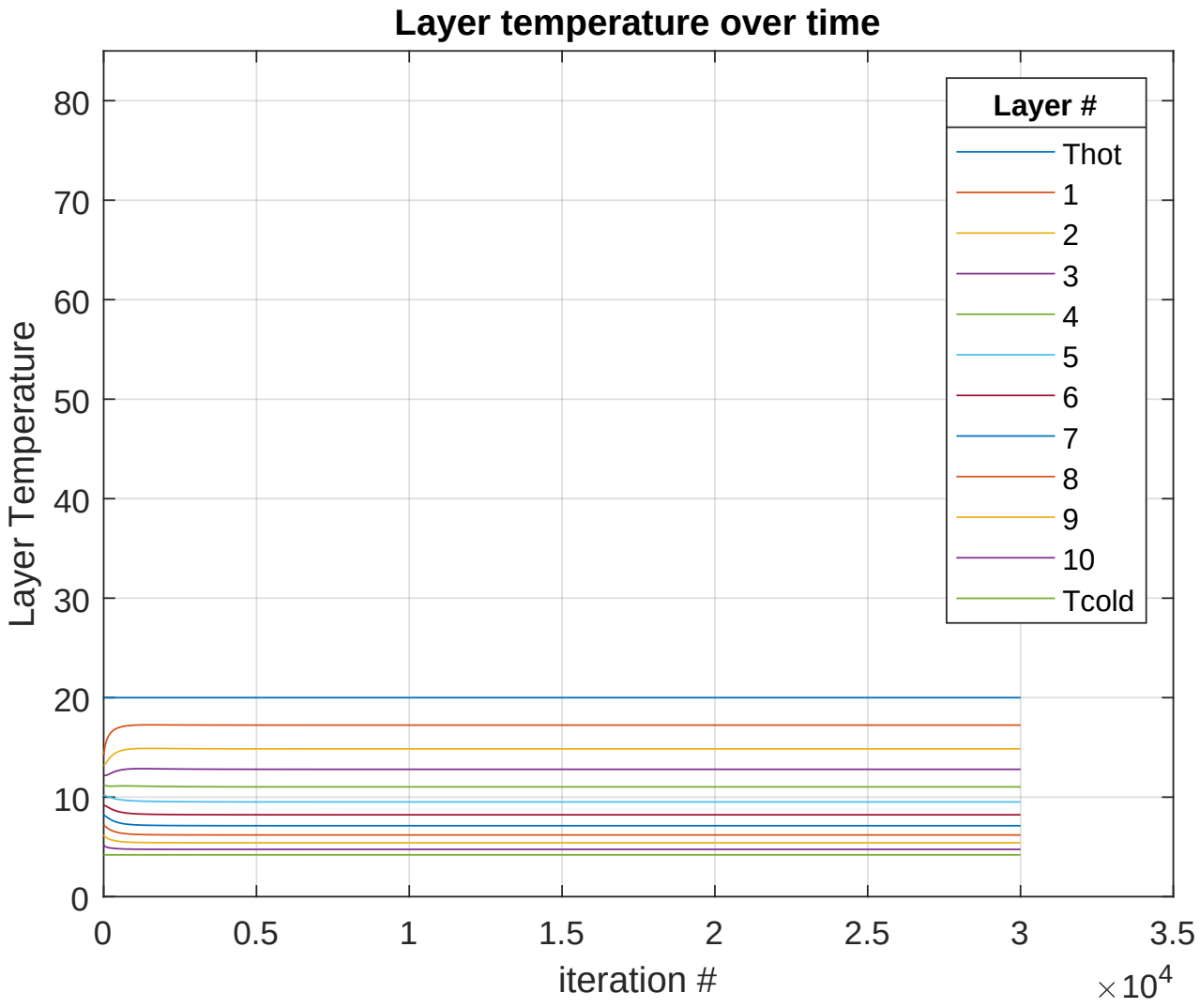

Figure 69: Layers temperature disctribution for the case ATS at 20 K

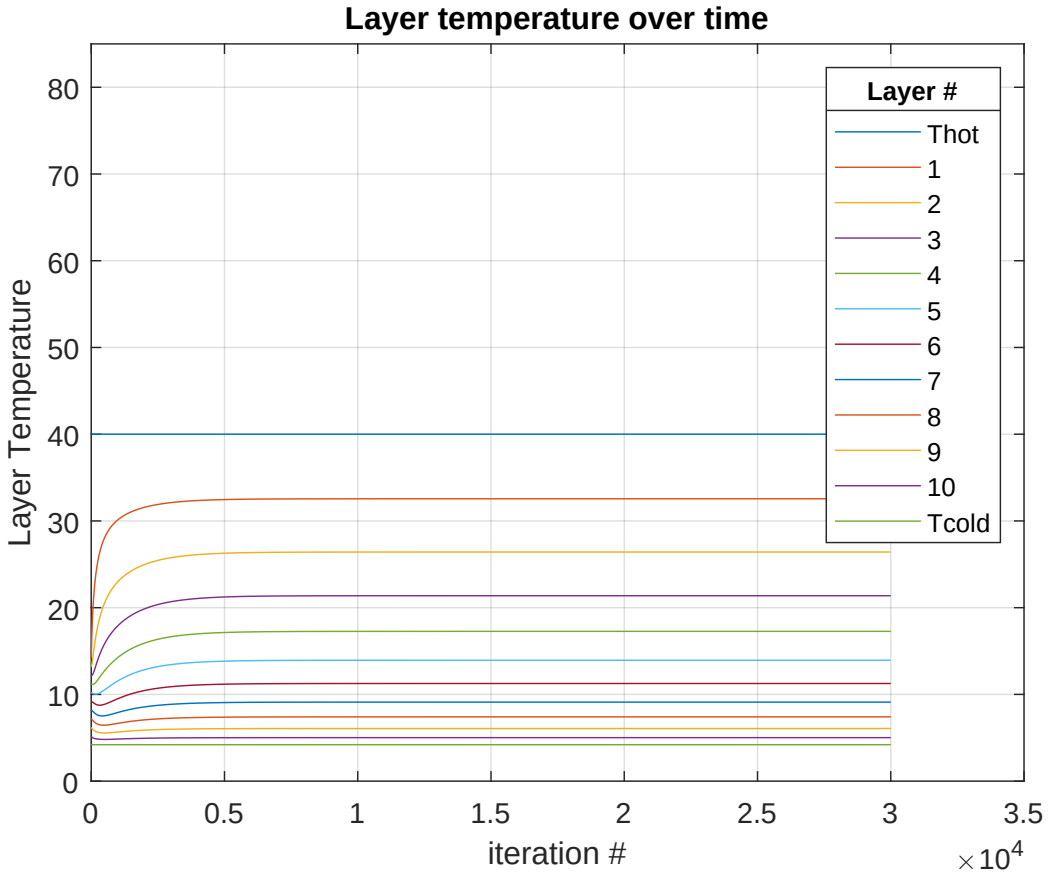

Figure 70: Layers temperature disctribution for the case ATS at 40 K

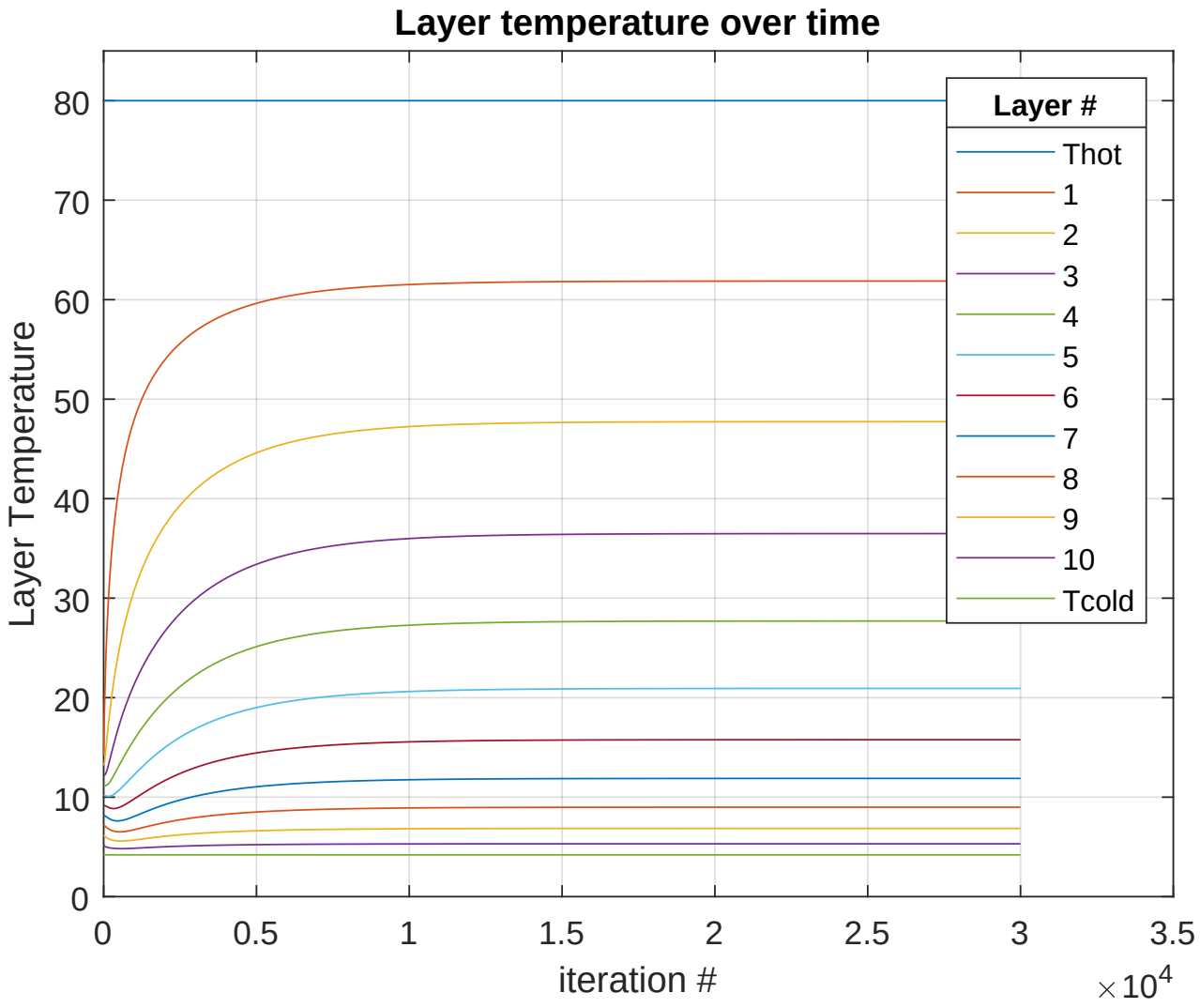

Figure 71: Layers temperature disctribution for the case ATS at 80 K

The results of the heat flux in the mathematical models are shown in figure 72, 73, 74, 75 and 76.

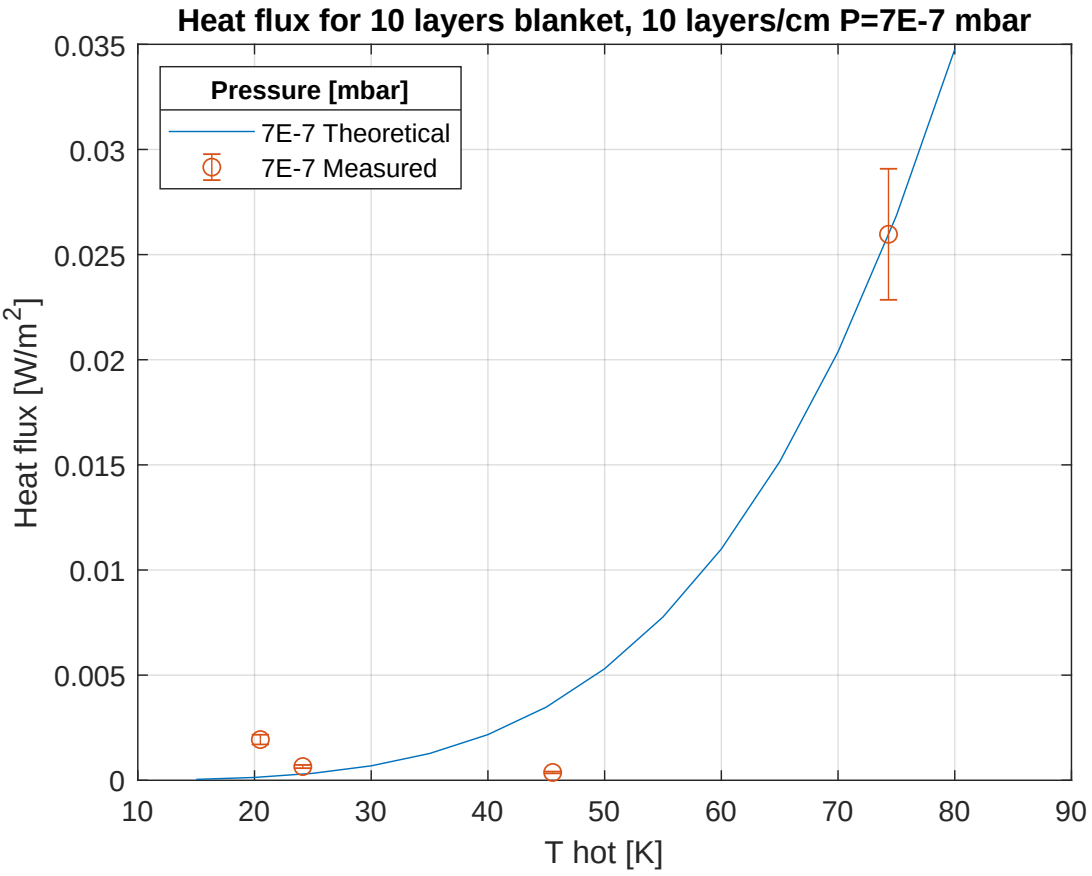

Figure 72: Heat flux to 4.2 K for a 10 layers blanket with 10 layers/cm at P= 7×10^{-7} mbar

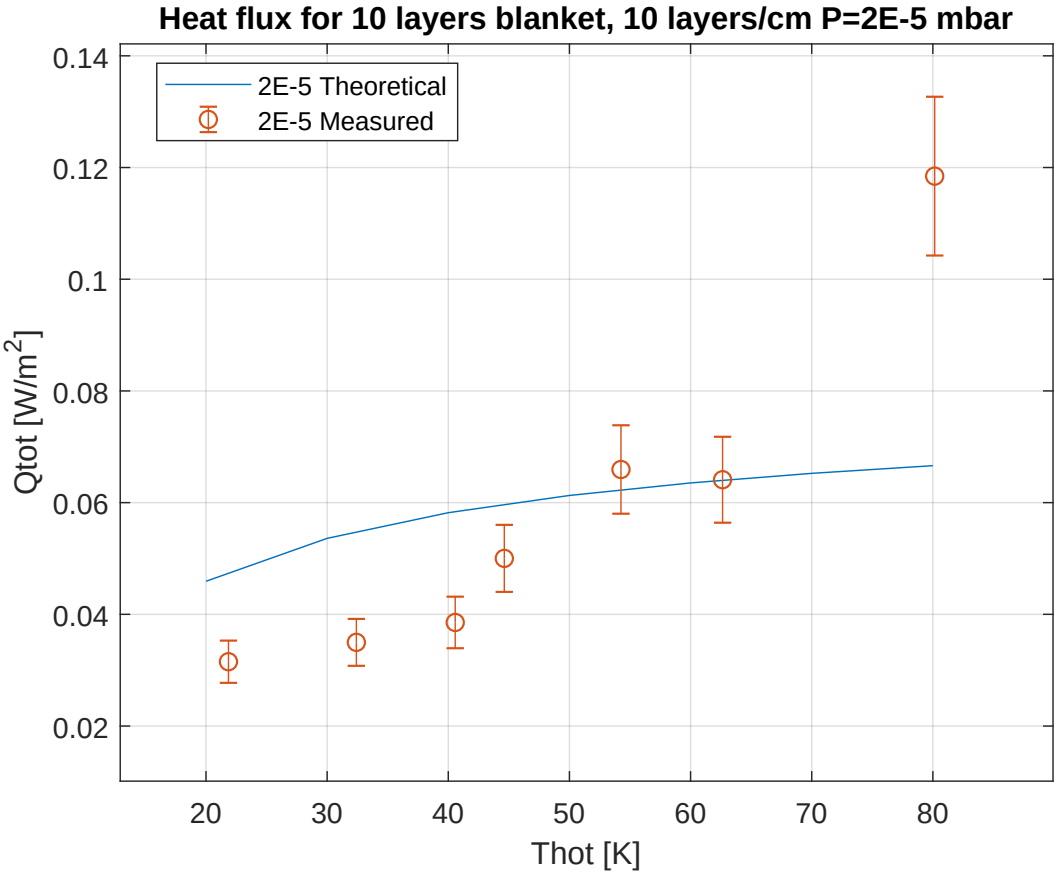

Figure 73: Heat flux to 4.2 K for a 10 layers blanket with 10 layers/cm at P= 2×10^{-5} mbar

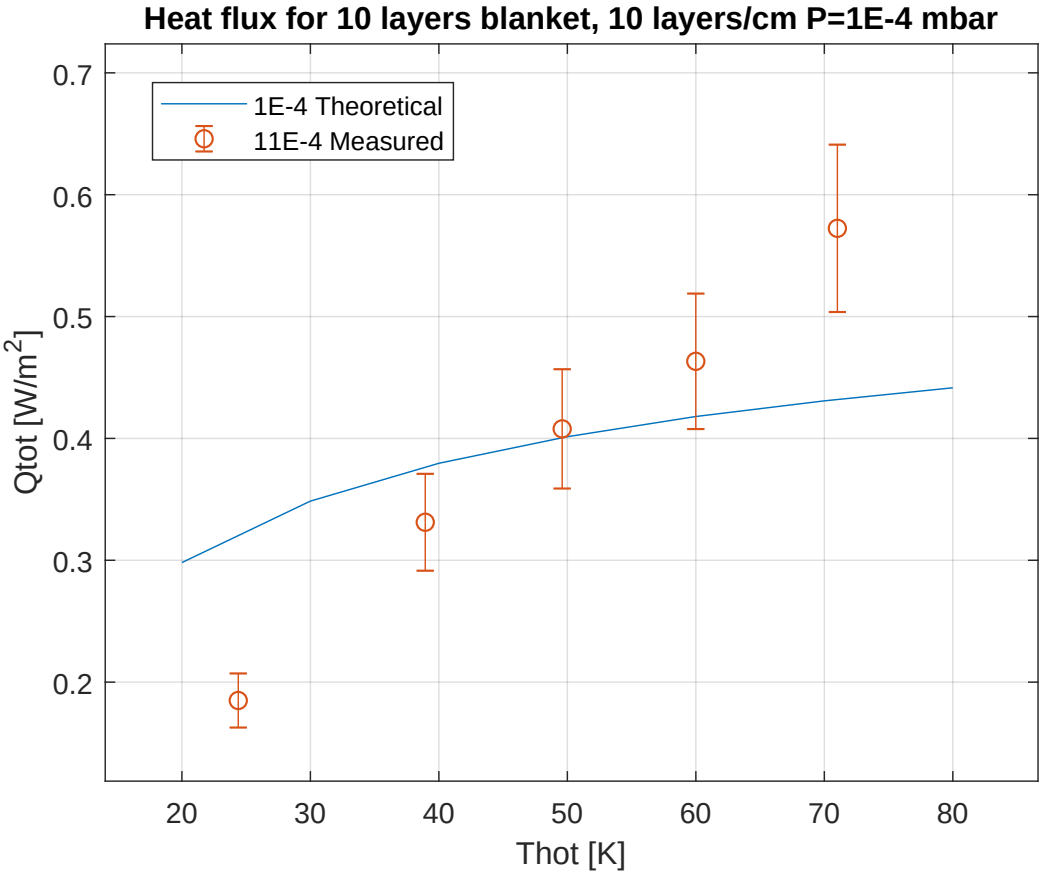

Figure 74: Heat flux to 4.2 K for a 10 layers blanket with 10 layers/cm at P= 1×10^{-4} mbar

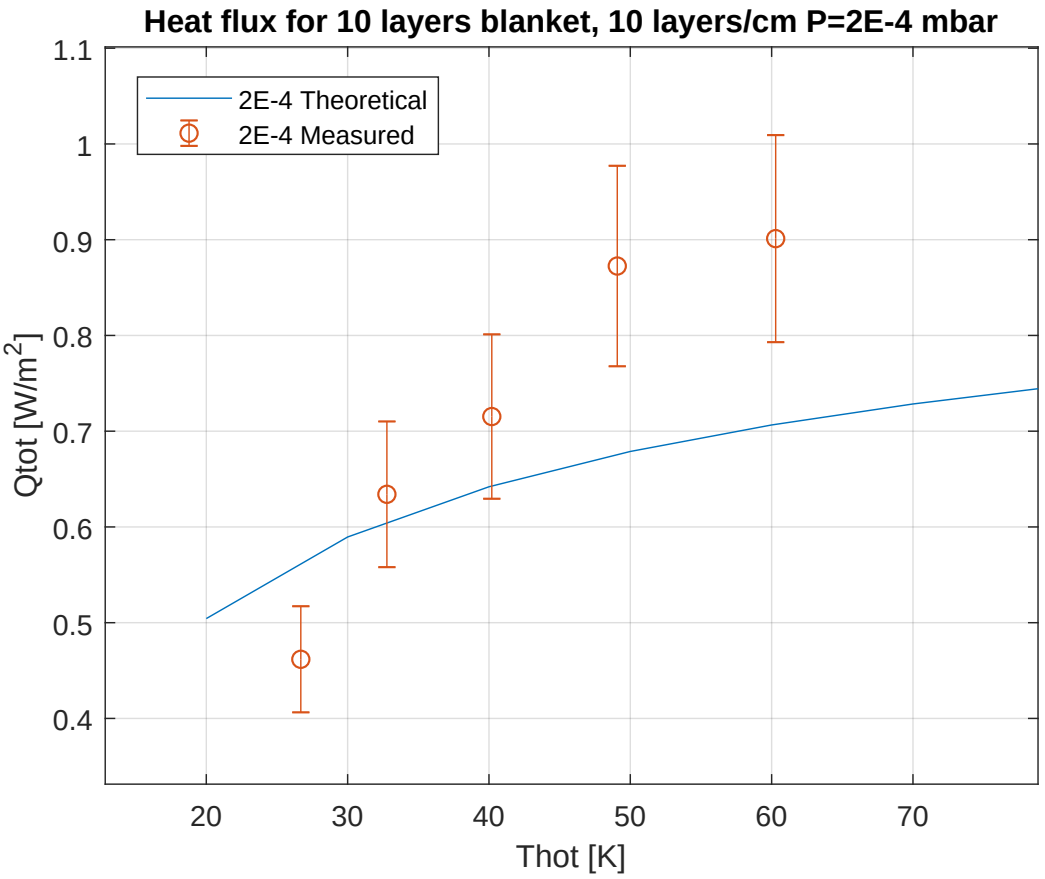

Figure 75: Heat flux to 4.2 K for a 10 layers blanket with 10 layers/cm at P= 2×10^{-4} mbar

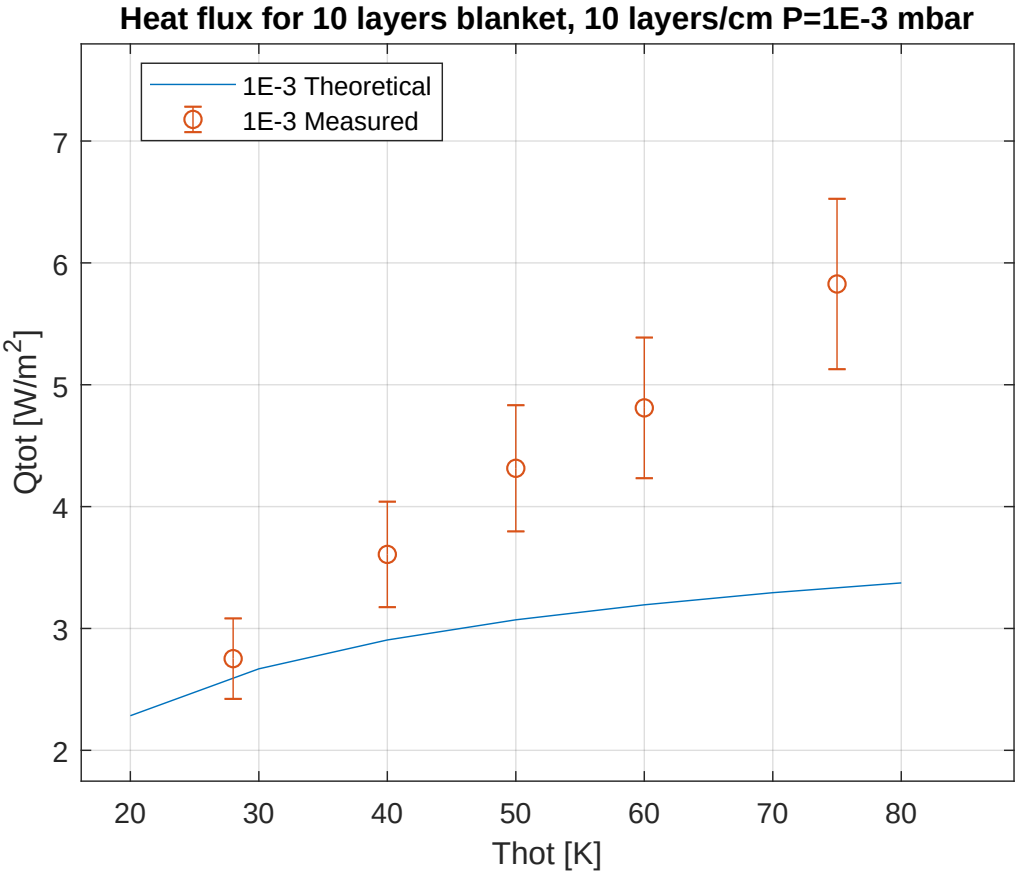

Figure 76: Heat flux to 4.2 K for a 10 layers blanket with 10 layers/cm at P=1 $\times$ 10^{-3} mbar

The mathematical model for higher pressure needs further developments.

4.6.5 Mathematical model for case 4

The model of case 4 is prepared considering full contact between layers and considering that the total area covered by the spacers.

The contact area is calculated by geometrical considerations using specification form the MLI producer. The spacer net is polyester tulle with a 7.5 g weight per square meter. The thickness is of 6 μm and its density is 1.38 g/cm^3 so the calculated total area is 0.09 m^2 for each square meter considered.

The model is does not take into account gas inside the blanket but only solid conduction through it. Residual pressure and thermal radiation are the contributions from the external part. Results are underestimating the heat transfer at good vacuum levels while they predict the experimental results better at higher residual pressures from 1 $\times$ 10^{-4}

mbar. In figure 77, 78, 79 and 80 the models for degraded vacuum levels in comparison with the experimental data are shown.

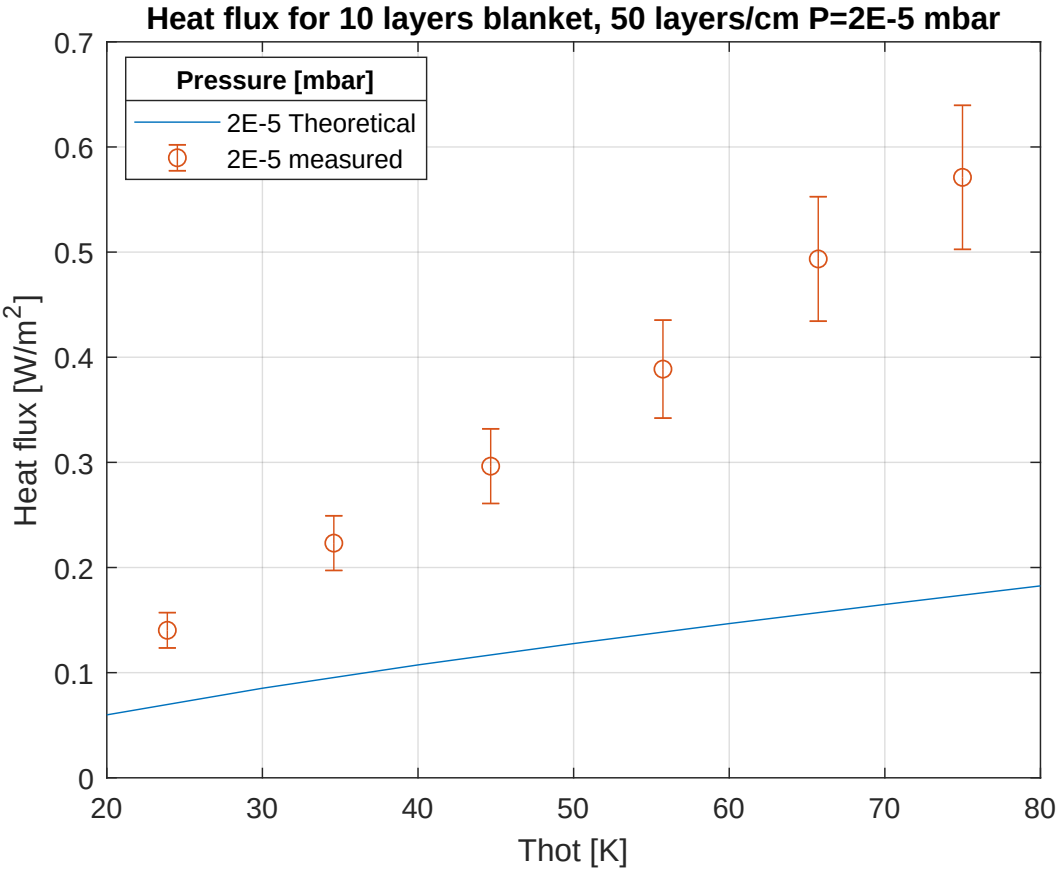

Figure 77: Heat flux to 4.2 K for a 10 layers blanket with 50 layers/cm at P=2×10^{-5} mbar

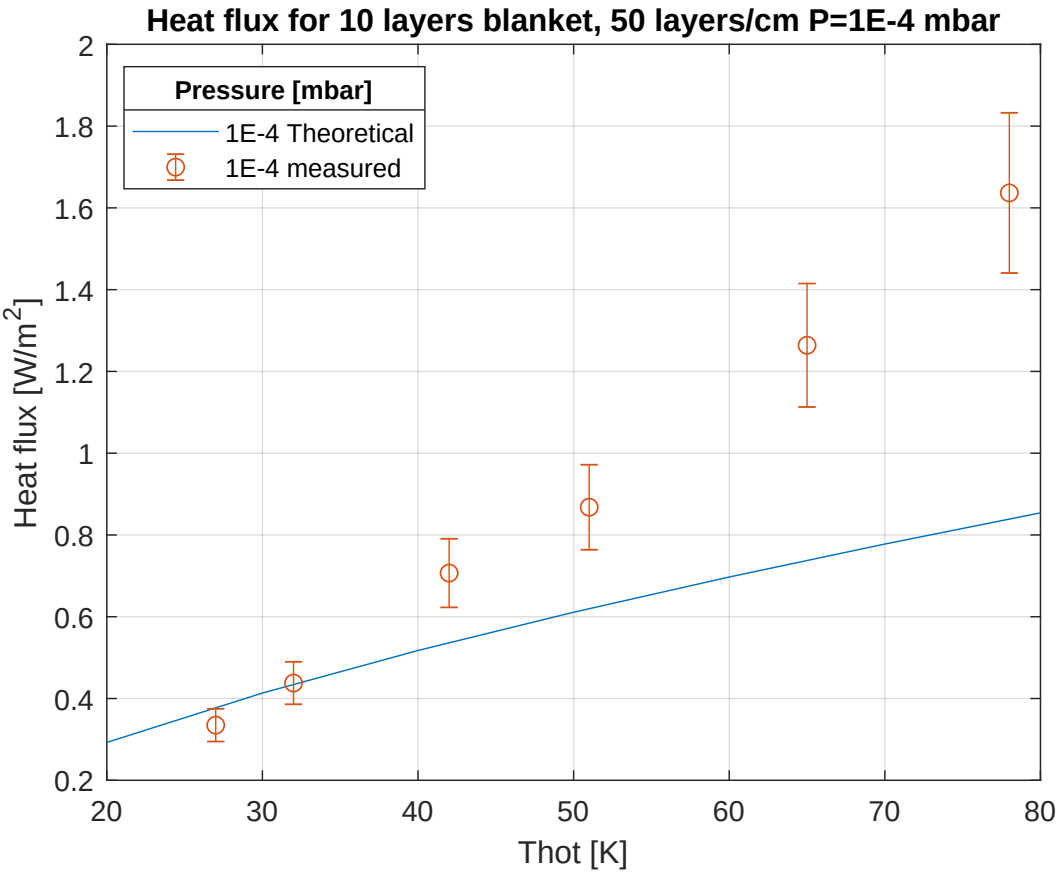

Figure 78: Heat flux to 4.2 K for a 10 layers blanket with 50 layers/cm at P= 1×10^{-4} mbar

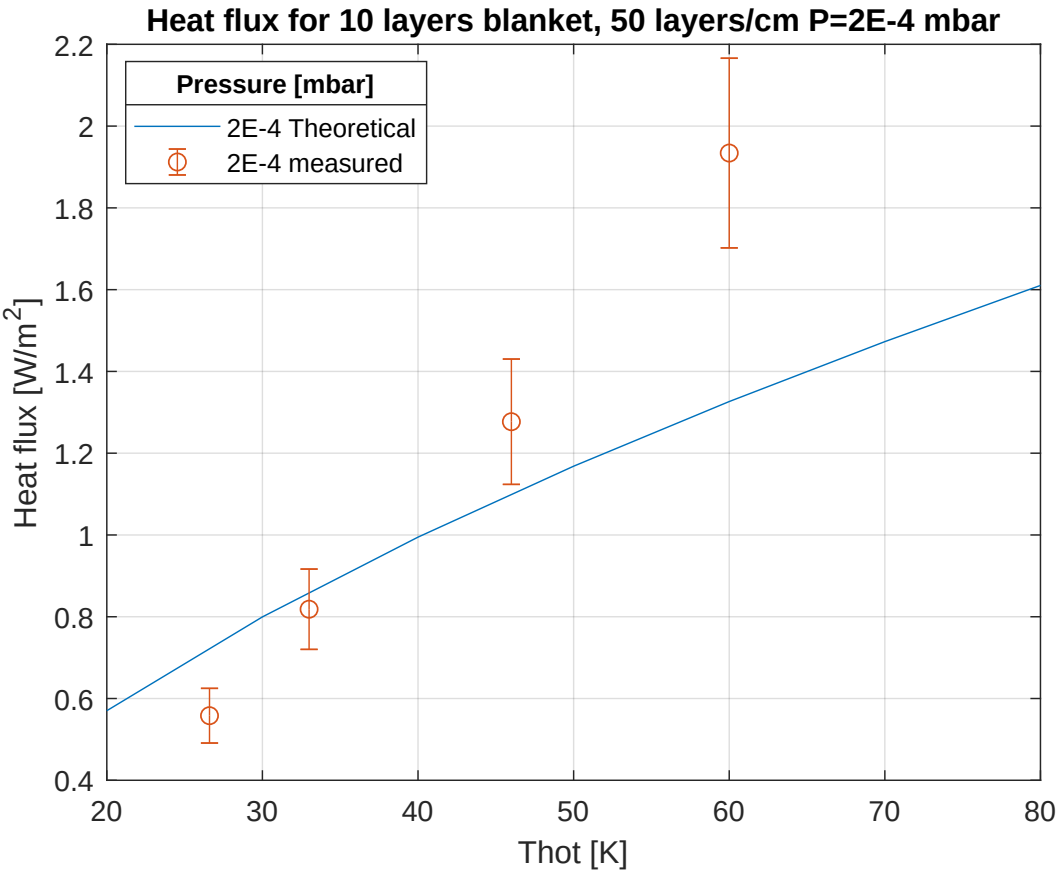

Figure 79: Heat flux to 4.2 K for a 10 layers blanket with 50 layers/cm at P= 2×10^{-4} mbar

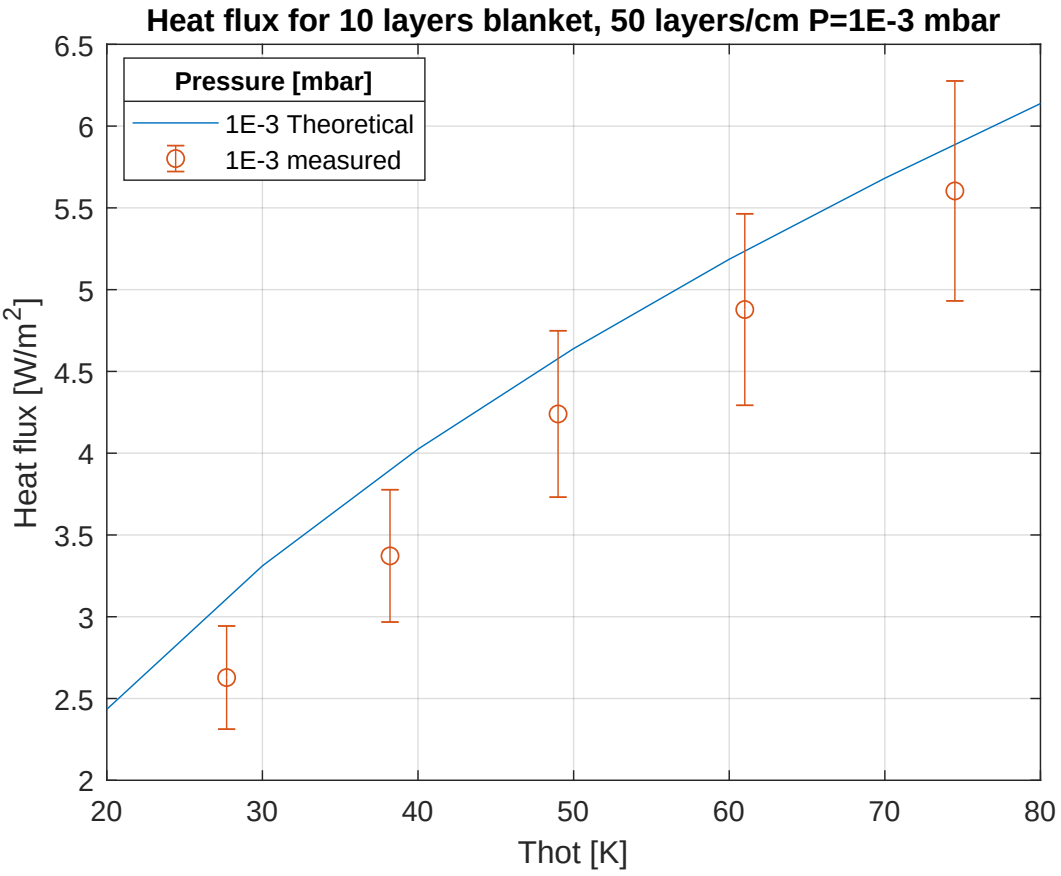

Figure 80: Heat flux to 4.2 K for a 10 layers blanket with 50 layers/cm at P= 1×10^{-3} mbar

A different model is used to predict heat transfer at 7×10^{-7} mbar. The model includes the radiation outside the MLI blanket giving heat flux to the external layer which is at a temperature of a less than 4.2 K. An offset had to be imposed to match the data, see figure 81.

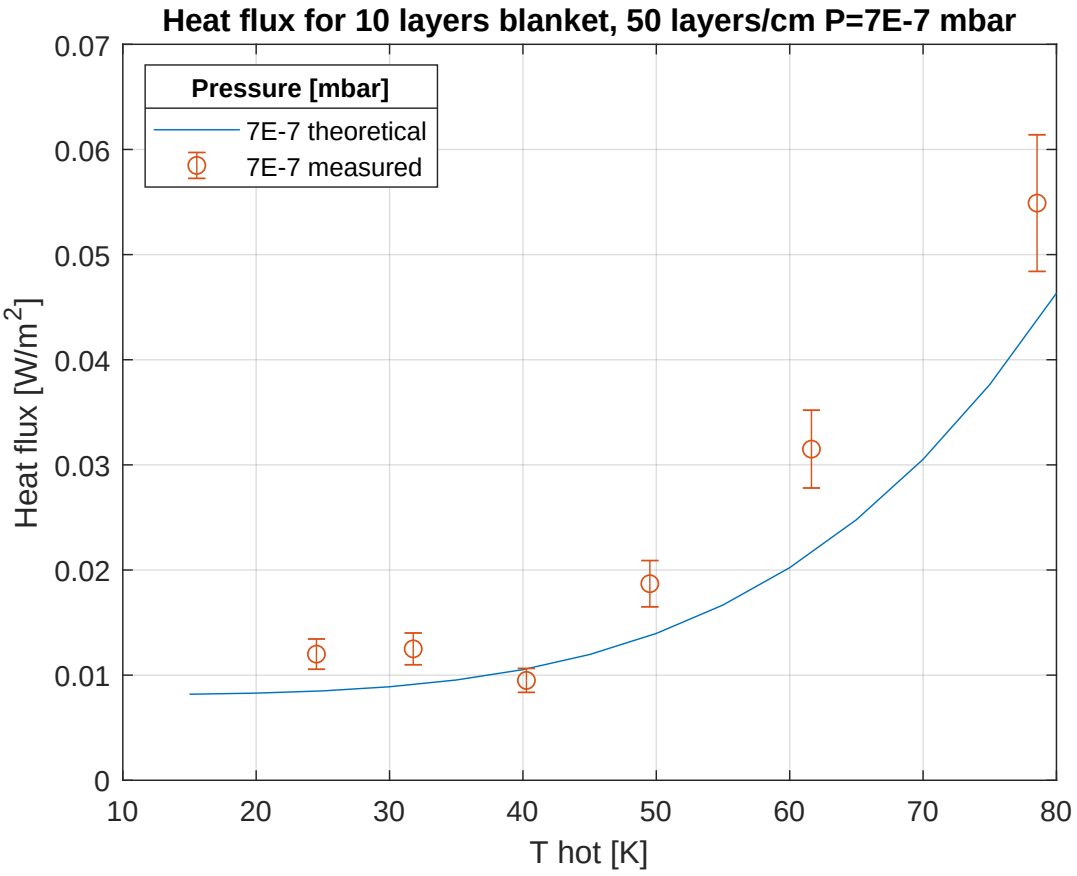

Figure 81: Heat flux to 4.2 K for a 10 layers blanket with 50 layers/cm at P=7×10^{-7} mbar

4.6.6 Mathematical model for different layer density in vacuum

If plotting the two cases where one MLI blanket with 10 layers is placed on the test vessel, case3 and 4, it is possible to notice a similar behaviour for the heat flux dependency on temperature with an offset for different layers density, see 82.

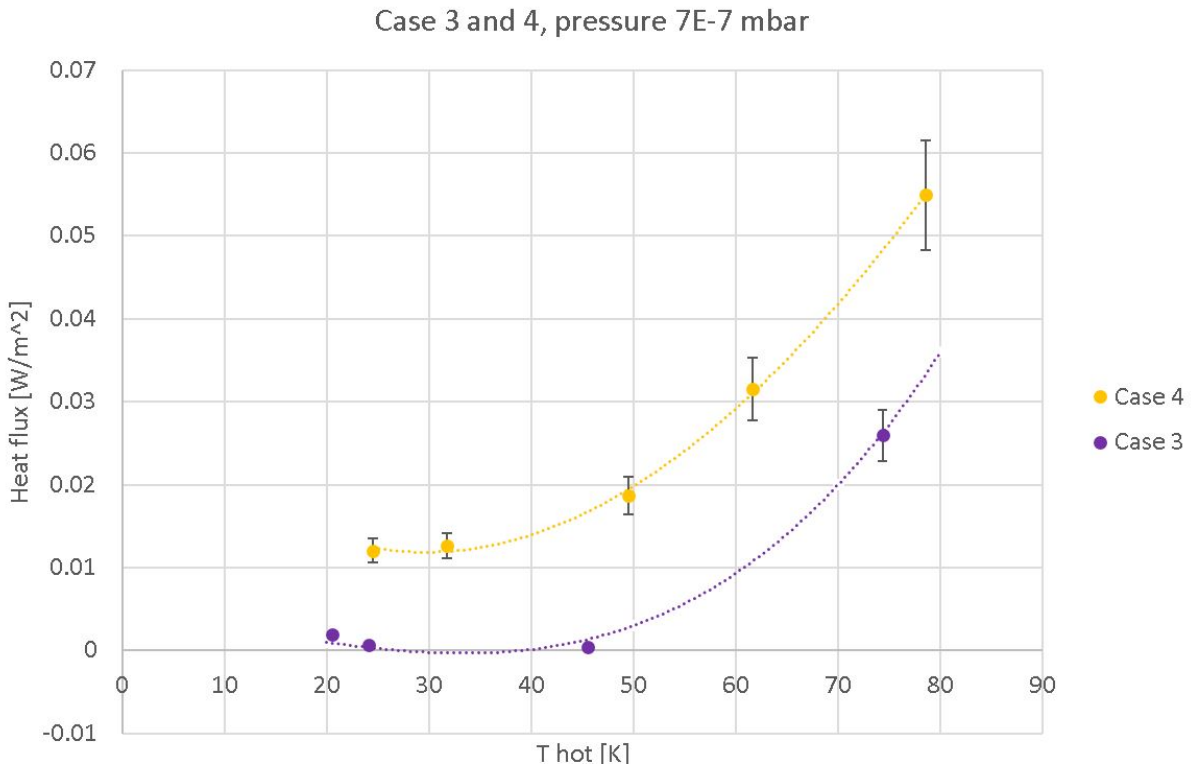

Figure 82: Heat flux to 4.2 K for two 10 layers blanket with 10 and 50 layers/cm at P=7×10^{-7} mbar

A formula has been written in function of the layer density, going from zero (no contact between layers) and 1 (full contact), see equation (4.6.3).

$$\dot{q} = 1.55E-7 \cdot T^3 - 6.11E-6 \cdot T^2 - 1.1E-4 \cdot T + 4.4E-3 + a \tag{4.6.3}$$

Where a is a is the shifting parameter depending on the temperature and the coefficient of layer density d, which goes from zero to one, assuming that the packing density percentage influences linearly the heat flux.

$$a = \frac{T}{28} \cdot 0.01 \cdot d - 1E-4 \cdot (T - 40) \tag{4.6.4}$$

The equation is plotted for different values of d as a percentage of the packing density.

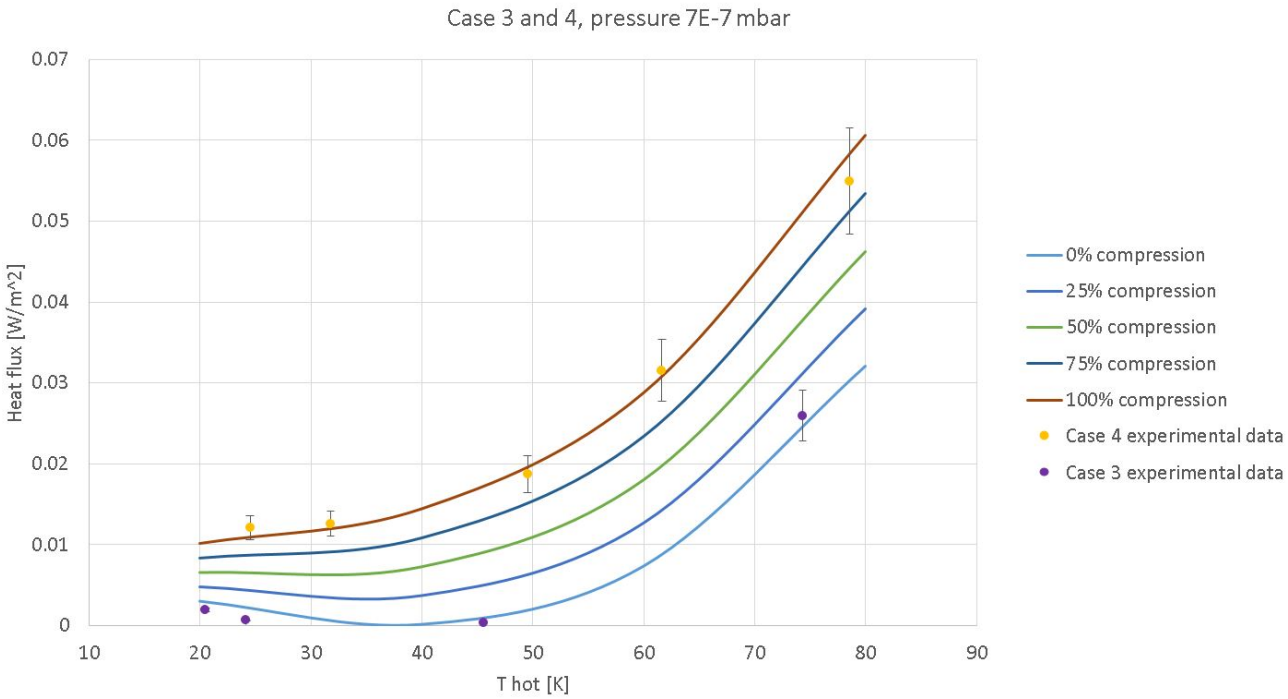

Figure 83: Heat flux to 4.2 K for two 10 layers blanket with 10 and 50 layers/cm at P=7×10^{-7} mbar and mathematical model in function of layer density percentage: 100 %

With this model, if an estimation of the layer density can be done in advance, an estimation of the heat flux in function of the screen temperature can be obtained for a good vacuum condition.

5 Mathematical model for the FCC cryostat optimisation

5.1 FCC cryostat description

The cryostat design for FCC takes into consideration a single thermal screen because the beam screen is to be cooled at the same temperature as the thermal screen. The 800 mm diameter cold mass, see figure 84, is composed of two beam screens surrounded by the superconductive coils, kept in place by non magnetic collars. The iron yokes keeps the parts in place in place when the magnetic field acts, and they are fit into an aluminium collar. The whole cold mass just described sits on three G10 support posts along the 15 m dipole length. The support posts are in contact with the vacuum vessel, in proximity of the jacks. A cooled aluminium thermal shield in between the cold mass and the vacuum vessel acts as a heat intercept.

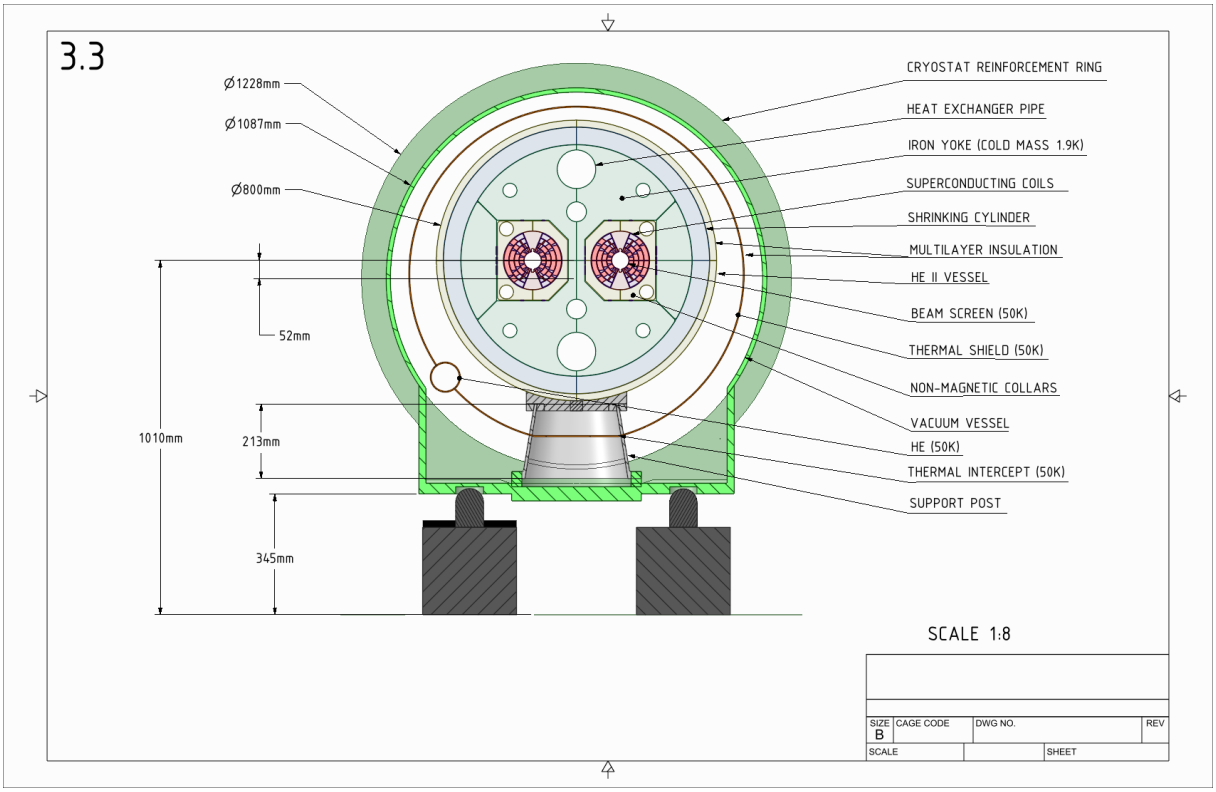

Figure 84: FCC cryostat design

5.2 Refrigeration power

5.3 Exergy approach

In the introductory chapter of the thesis chapter 1.3, an equation describing the refrigeration power to the cold mass and the thermal screen of the FCC cryostat was introduced. The approach starts from considerations on the total exergy produced by the system which should be minimized [38]. The total exergy is the sum of the one correlated to the cold mass and the one correlated to the thermal screen in ideal refrigeration, see equation (5.3.1):

$$\Delta E = \Delta E_{ts} + \Delta E_{cm} \tag{5.3.1}$$

$$\Delta E = (Q_{ts} - Q_{cm}) \cdot (\frac{T_{amb}}{T_{cm}} - 1) + Q_{cm} \cdot (\frac{T_a}{T_{ts}} - 1) \tag{5.3.2}$$

The refrigeration electrical power needed is described in equation(5.3.3):

$$P_{ref} = \frac{\Delta E}{\eta(T)} \tag{5.3.3}$$

where $\eta(T)$ is the efficiency with relation to Carnot described in equation (5.3.4):

$$\eta(T) = \frac{COP_{Carnot}}{COP_{Real}} \tag{5.3.4}$$

where COP_{real} is the coefficient of performance, indicator of the efficiency of the refrigerator system, defined by the ration between the cold capacity and the driving power. This value is normally lower than the Carnot efficiency, the COP_{Carnot}, defined as the ratio between the cooling power and the ideal driving power using the Carnot equation. The refrigeration power can be then obtain, see equation (5.3.5):

$$P_{ref} = Q_{cm} \cdot (\frac{T_{ts}}{T_{cm}} - 1) \cdot \frac{1}{\eta_{cm}(T_{cm})} + Q_{ts} \cdot (\frac{T_{amb}}{T_{ts}} - 1) \cdot \frac{1}{\eta_{ts}(T_{ts})} \tag{5.3.5}$$

The efficiency compared with the Carnot efficiency for a 4.2 K helium temperatrure level was measured for LHC and it corresponds to 0.27, the [32]. For the 1.9 K and 40 K values of 0.18 and 0.42 are respectively considered in FCC cryogenic studies [15]. The heat Q_{ts} coming to the thermal screen is calculated with the simplified formula for MLI having layers with same emissivity using 30 as number of foils as it was used in LHC, see equation (5.3.6).

$$Q_{ts} = \frac{\sigma \cdot A \cdot (T_{amb}^4 - T_{ts}^4)}{(\frac{1}{\epsilon_1} + \frac{1}{\epsilon_2} - 1)(31)} \tag{5.3.6}$$

In figure 85 the model for the refrigeration power in function of the screen temperature considering a cold mass 1.8 K and implementing the results of the experiments for the 10 layers/cm blanket with low density is shown.

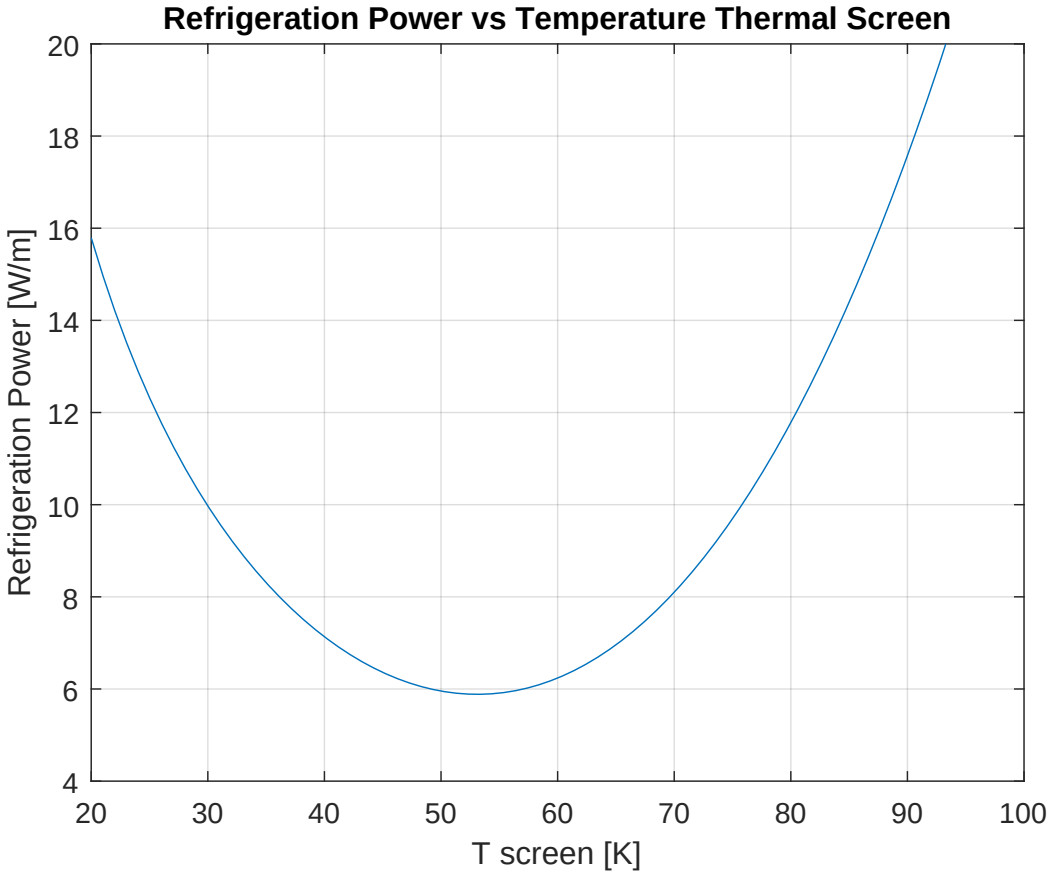

Figure 85: Refrigeration power per linear meter necessary for different temperature of the thermal screen if a blanket of 10 layers MLI with density 10 layers/cm is used

The optimal temperature found for the thermal screen is found to be 53 K.

6 Conclusions

The problematic of energy efficiency is a current global interest in any field. In cryogenics, the refrigeration power required to keep systems at specific low temperature can be reduced by optimizing the insulation systems. In this thesis work the cryostat of the Future Circular Collider is taken as an example to demonstrate that energy can be dramatically reduced by optimizing the operating temperature of an intermediate thermal screen protecting the cold mass. The optimal thermal screen temperature is found by the equation describing the energy balance of the systems in terms of refrigeration power. One very important term appearing in the equation is the heat load on the cold mass in function of the screen temperatures. For temperatures lower than 77 K there are no data available about the efficiency of the thermal insulation systems MLI, used on the cold

masses. Therefore experimental results have been produced in this thesis work. Multilayer insulation system efficiency was measured at different hot temperatures boundaries for heat flux to 4.2 K. Different configurations of MLI and different degraded vacuum levels were also tested. The boil-off cryostat used in previous experiments was modified with an original method in order to create a variable temperature hot boundary. An aluminum thermal screen has been designed to be in weak contact with the lower guard vessel to have a uniform equilibrium temperature of 20 K. Extra heat was applied to warm it up at higher temperatures. Results were found after a time consuming calibration of the system due to the very low heat fluxes to be measured. Now data on heat transfer through MLI at low temperatures are available for low ranges of temperatures and five different level of degraded vacuum. The performance of two different blankets with same number of layers and different packing densities were also explored and compared. The efficiency of the systems seems to depend on the higher boundary temperature above 50 K, lower temperatures do not have any longer influence on the performance in vacuums of the order of 1×10^{-6} mbar. Mathematical models have been proposed for the cases studied but there is still margin for improvement for those for degraded vacuum cases in presence of blankets. Results were implemented in the model for finding the minimum refrigeration power for a typical FCC dipole cryostat design. A temperature of 53 K is found to be optimal for the operation of thermal screen protecting the cold mass. Temperature such as 77 K would double the overall refrigeration power required. The data and mathematical models produced in this work are available to the cryogenic community.

References

[1] Standard guide for thermal performance testing of cryogenic insulation systems. *ASTM International*, 2013.

[2] Terminology relating to thermal insulation. *ASTM International*, 2013.

[3] S. Jacob S. Kasthurirengan A. S. Kumar, M. K. Murthy. Thermal performance of multilayer insulation down to 4.2 K. *Advances in Cryogenic Engineering*, 2000.

[4] J. L. Caron. Cross section of LHC dipole. Dipole LHC: coupe transversale. 1998.

[5] F. Barron D. Randall. Cryogenic Heat transfer. *ISBN-1-56032-551-8*, 1999.

[6] S. Dushman. Scientific foundations of vacuum technique.

[7] H. L. Hart J. R. Heim E. M. W. Leung, R. W. Fast. Techniques for Reducing Radiation Heat Transfer Between 77 K and 4.2 K. *Adv. Cryog. Eng.*, 25, 1980.

[8] W. Obert et al. Emissivity measurements of metallic surfaces used in cryogenic applications. *Advances in Cryogenic Engineering*, 1982.

[9] J. E. Fesmire. Standardization in cryogenic insulation systems testing and performance data. *Physics Procedia*, pages 1089 – 1097, 2015.

[10] M. A. Green. Radiation and gas conduction heat transport across a helium Dewar multilayer insulation system. 1994.

[11] U. Wagner H. Gruehagen. Measured Performance of Four New 18 kW @ 4.5 K Helium refrigerators for the LHC Cryogenics System. *20th International Cryogenic Engineering Conference*, 2004.

[12] Brooks instruments. Installation and operation manual model 5850e mass flow controller. 2009.

[13] C. Darve J. Fesmire, S. D. Augustynowicz. Performance characterization of perforated multilayer insulation blankets. *Advances in Cryogenic Engineering*, 2008.

[14] S. Augustynowicz J. Fesmire. Cryogenic thermal Insulation Systems. *16th Thermal and fluids analysis workshop*, 2005.

[15] C. Kotnig. Analysis and design of the cryogenic system of the future circular collider. *http://cds.cern.ch/record/2628165/files/CERN-THESIS-2018-085.pdf*.

[16] J. M. Rieubland G. Vandoni L. Mazzone, G. Ratcliffe. Measurements of multi-layer insulation at high boundary temperature, using a simple non-calorimetric method. 2002.

[17] T. P. Lukose. Performance prediction and experimental investigation on multilayer insulation, phd thesis, indian institute of technology. 1986.

[18] N. Bourcey T. Colombet V. Parma I. Slits J. P. G. Tock M. Canetti, F. Gangini. Design, manufacturing and integration of LHC cryostat components: An example of

a collaboration between CERN and industry. *Particle accelerator. Proceedings, 10th European Conference, EPAC 2006, Edinburgh, UK, June 26-30, 2006*, 2006.

[19] C. Parente G. Riddone M. Chorowski, P. Grzegory. Optimisation of multilayer insulation: an engineering approach.

[20] D. Delikaris P. Duda C. Haberstroh F. Holdener S. Klppel C. Kotnig F. Millet J. Polinski H. Quack L. Tavian M. Chorowski, H. Correira Rodriguez. Towards the conceptual design of the cryogenic system of the Future Circular Collider (FCC). 2017.

[21] N. Martin. Superconductive Magnets. *Oxford University Press, ISBN 0-19-854810-9*, 1987.

[22] P. Lebrun S. Myers R. Ostojic J. Poole P. Proudlock O. Brning, P. Collier. LHC design report. 2004.

[23] H. K. Onnes. The resistance of pure mercury at helium temperatures. *Commun. Phys. Lab. Univ. Leiden*, 1911.

[24] L. Tavian P. Lebrun. Beyond the Large Hadron Collider: a first look at cryogenics for CERN future circular colliders. *25th International Cryogenic Engineering Conference and the International Cryogenic Materials Conference*, 2014.

[25] L. Tavian P. Lebrun, V. Parma. Does One need a 4.5 K Screen in Cryostats of Superconducting Accelerator Devices Operating in Superfluid Helium? *CERN Document Server*, 2013.

[26] V. Sergo B. Vullierme P. Lebrun, L. Mazzone. Investigation and qualification of thermal insulation systems between 80 K and 4.2 K. *Cryogenics Vol 32 ICMC Supplement 44-47*, 1992.

[27] J. Polinski. Cryostat for thermal measurements of Cryogenic Insulation with Evaporative Method. *Proceedings of the Twenty First International Cryogenic Engineering Conference*, 2006.

[28] J. Polinski. Modeling of the heat transfer mechanisms through the cryogenic vacuum insulations. *Wroclaw Uiversity of Science and Technology, PhD thesis*, 2006.

[29] H. L. Hart Q. S. Shu, R. W. Fast. Heat flux from 277 to 77 K through a few layers of multilayer insulation. *Cryogenics*, 1986.

[30] K. R. Leonard G. E. McIntosh R. J. Stochl, P. J. Dempsey. Variable density mli test results. *Advances in Cryogenic Engineering*, 1996.

[31] F. Millet L. Tavian S. Claudet, G. Ferlin. 1.8 K Refrigeration Units for the LHC: performance Assesment of Pre-series Units. *20th International Cryogenic Engineering Conference*, 2004.

[32] L. Tavian U. Wagner S. Claudet, P. Lebrun. Exergy Analisys of the cryogenic helium distribution system for the Large Hadron Collider (LHC). *Cryogenic Engineering Conference*, 2009.

[33] I. Vladimir S. D. Augustynowicz, A. Johnatan. Analisys of multilayer insulation between 80 K and 300 K. *Advances in Cryogenic Engineering*, 1994.

[34] T. P. Lukose S. L. Bapat, K. G. Narayankhedkar. Experimental investigations of multilayer insulation. *Elsevier*, 1990.

[35] T. P. Lukose S. L. Bapat, K. G. Narayankhedkar. Performance prediction in multilayer insulation. *Cryogenics*, 1990.

[36] S. W. Van Sciver. Helium Cryogenics. *Springer*, 2012.

[37] T. Pletzer A. Halm L. J. Koduvelikulathu C. Comparotto R. Kopecek H. Kurz U. A. Yusufoglu, T. H. Lee. Simulation of Energy Production by Bifacial Modules with Revision of Ground Reflection. *Energy Procedia*, 2014.

[38] L. Tavian R. van Weelderen V. Baglin, P. Lebrun. Cryogenic Beam Screens for High-Energy Particle Accelerators. (CERN-ATS-2013-006), 2013.

[39] L. Mazzone V. Sergo B. Vullierme V. Benda, P. Lebrun. Qualification of multilayer insulation systems between 80 K and 4.2 K. *Proc. 3rd. Int. Conf. Kryogenika'94*, 1994.

[40] R. D. McCarty V. D. Arp. Thermophysical properties of helium-4 from 0.8 K to 1500 K with pressures to 1000 mpa. *NIST Tech Note 1334*, 1989.

[41] M. Chorowski J. Polinski V. Parma A. Kopczynski V. Venturi, T. Koettig. Qualification of a vertical cryostat for MLI performances tests between 20 K and 60 K to 4.2 K. 2018.

[42] G. Zahn W. Lehmann. Safety Aspects for LHE Cryostats and LHE Transport Containers. *ICEC7, London.*

[43] Wikipedia. Black-body spectrum for temperatures between 300 K and 10000 K in a log-log diagram. 2006.